Utrecht University and the British Antarctic Survey

Master Thesis

Climate Physics and Marine Sciences

Oceanic and Atmospheric Controls on Decadal Ice Shelf Basal Melt Variability around the Amundsen Sea

Author
G.W. Janzing
5634911

Supervisors
Dr. K.A. Naughten
Dr. P. Dutrieux
Prof. dr. R.S.W. van de Wal
Second Corrector
Prof. dr. S.S. Drijfhout

November 20, 2022

Contents

Abstract

Warm ocean waters are driving the rapid ice loss around the Amundsen Sea, Antarctica. Decadal variability in melt and on-shelf heat transport is thought to be controlled by zonal shelf break winds and Pacific sea surface temperatures, leading to the hypothesis that a strong El Niño in the 1940s initiated the present-day glacier retreat. This report investigates the controls on decadal melt variability by analysing simulations from a regional ocean model for the Amundsen Sea. This model was forced by an ensemble of 20 global climate model simulations for the years 1920 until 2014.

Ice shelf basal mass loss has a strong connection with heat advection in seabed troughs in the simulations. Averaged over the ensemble, zonal shelf break winds and the El Niño Southern Oscillation (ENSO) are weakly correlated with basal mass loss. Individual members show a large spread, likely related to regional factors such as the Amundsen Sea Low and local factors such as sea ice and shelf water properties. Variability in baroclinic flow and salinity at the western shelf break suggest that melt could be sensitive to freshwater fluxes from ice shelves and sea ice. The occurrence of a large melt event in the 1940s depends on these factors. Finally, simulations with an advanced grounding line have minimal influence on decadal variability. Since ocean boundary conditions are fixed, the internal variability in the model is thus atmospherically forced.

The results underscore the importance of using a model ensemble and long time scales when modelling this system. Furthermore, the limited influence of large scale atmospheric forcing on melt makes accurate future projections more difficult. Further research is necessary to disentangle internal feedbacks and forcings.

Preface

The report before you is the result of research conducted as part of a combined Master's degree in Climate Physics and in Marine Sciences at Utrecht University. This project included a 4.5 months visit to the British Antarctic Survey (BAS) in Cambridge, UK.

Before we start, it is important to indicate clearly which part of the work was performed by other researchers and which parts by me, although this is also repeated concisely in the method section. The main part of the thesis is based on my analysis of output from published model runs previously performed by Kaitlin Naughten (BAS). A few additional model runs were performed by myself, which used a new ice shelf geometry provided by Jan de Rydt (Northumbria University) and used the model set-up provided by Kaitlin Naughten. I interpolated the new ice shelf geometry by adapting code from Paul Holland (BAS), changed the configuration and ran the simulations on an HPC facility myself. For the analysis of all the data I wrote most of the code myself, but I used time series and adapted some code provided by Kaitlin Naughten.

The one thing that remains is to thank everyone who contributed to this project. During my project, I also collaborated with Alessandro Silvano (Southampton University) and I got to be a co-author on his paper. I want to thank him for his suggestions and this opportunity. Furthermore, I want to thank Jan de Rydt for supplying me with the new ice shelf geometry and for his help via email. I really enjoyed the months that I spend in the UK, especially since it was such a clear change from the Covid years before. I thus want to thank everybody at BAS and in Cambridge who made my visit a memorable experience.

Finally, I want to thank my supervisors, Kaitlin Naughten and Pierre Dutrieux from BAS and Roderik van de Wal (Utrecht University). I welcomed their genuine interest in my results and their help and suggestions have been very useful in guiding me throughout this project and structuring my thoughts. Furthermore, I have very much enjoyed our collective meetings and I appreciated that each of them invested the time to discuss on a weekly basis, be it in person or remotely. In particular, I am thankful to Kaitlin for making me feel welcome among the staff at BAS, for her suggestion of this project and for the helpfulness with the recurring issues with MITgcm. I want to thank Pierre for the often long extended meetings (even from New Zealand) and his hospitality in Cambridge. I am thankful to Roderik for his long term investment in helping me in finding a suitable project and in navigating the rules at the University, as well as for his advice and availability throughout the year.

Last but not least, I am also grateful for all of their help and advice in finding a PhD position.

1 Introduction

The West Antarctic Ice Sheet (WAIS) has experienced rapid mass loss over the observational record. In recent decades the WAIS has been the main contributor in Antarctica to sea level rise, responsible for roughly half (Rignot et al., 2019) to more than 80 per cent (Shepherd et al., 2018) of the continent's total contribution. The WAIS, which contains sufficient ice to raise global sea levels by 3.4 m (Fretwell et al., 2013), will likely contribute to future sea level rise according to models (Seroussi et al., 2020). The size of its future contribution depends on the occurrence of ice sheet instabilities and potential WAIS collapse (Bulthuis et al., 2019).

The Amundsen Sea is one of the critical regions for the future evolution of the WAIS. It is among the regions that have dominated Antarctic mass loss in recent decades (Rignot et al., 2019) and some observations suggest that ice sheet instabilities might already have been triggered (Rignot et al., 2014). Increased ocean melting is the dominant factor in the observed mass loss here (Shepherd et al., 2004). It is related to warm Circumpolar Deep Water (CDW), which is observed to be present on the continental shelf (e.g. Jacobs et al. (1996); Walker et al. (2013); Dutrieux et al. (2014)). The subsequent high melt rates are not constant, however, but show strong decadal variability related to oceanic conditions (Jenkins et al., 2018).

One of the first modelling studies focusing on the delivery of CDW on the Amundsen continental shelf was (Thoma et al., 2008). Their model showed that CDW was transported via deep seabed troughs, which intersect the continental shelf. Furthermore, they were the first to point out the relevance of the shelf break region, as they found a connection between decadal variability in shelf break zonal winds and CDW influx. Additional importance was given to the shelf break region with the discovery of an undercurrent, which was observed to transport CDW along the shelf break (Walker et al., 2013). The undercurrent is related to ocean density gradients at the shelf break that cause vertical shear, which leads to a depth-dependent or baroclinic flow structure. Where the undercurrent encounters the seabed troughs, it is deflected and flows into the troughs, bringing the CDW onto the continental shelf.

How would surface winds influence this undercurrent? Ocean flow is not directly affected by the wind but by surface stress and curl. This consists of both a wind stress component and a sea ice stress component. At the Amundsen shelf break, the zonal components are all highly correlated, which is why surface winds are often studied in literature (Steig et al., 2012; Holland et al., 2019). It is generally thought that shelf break wind anomalies drive the currents in the troughs near the shelf break via a depth-independent or barotropic mechanism (Wåhlin et al., 2013; Dotto et al., 2020). Assuming that meridional winds show less variation, it is the zonal wind stress anomalies that influence the sea surface slope over the shelf break. In turn, the associated pressure differences affect barotropic flow, which is also the dominant mode of southward transport for CDW near the shelf break (Webber et al., 2019). Since heat anomalies are thought to build up gradually when the undercurrent is strengthened, cumulative wind anomalies are also studied aside from direct anomalies (Dotto et al., 2020).
After the study of Thoma et al. (2008), newer studies have added more details to this story, but many reconfirmed the relevance of wind forcing in the shelf break region (Kimura et al., 2017; Webber et al., 2019; Dotto et al., 2020). Furthermore, Naughten et al. (2022) inferred a connection between the shelf break zonal winds and ice shelf basal mass loss on centennial time scales.

Investigation of the shelf break winds revealed that they were influenced by tropical sea surface variability in the Pacific Ocean (Steig et al., 2012; Holland et al., 2019). Observations indeed showed a decrease in melt of Pine Island Glacier in 2011, attributed to a strong La Niña (Dutrieux et al., 2014). The discovered link between tropical variability and the dynamics in the Amundsen Sea region has led some to speculate that historical observations from the tropics could be used to infer past ocean and ice behaviour. In particular, there is the idea that the exceptionally strong ENSO event in the early 1940s could have initiated the present-day glacial retreat observed in the basin (Steig et al., 2012). Some lines of observational evidence support this claim: ice cores have shown strong isotope excursions around the 1940s related to exceptionally strong air temperature anomalies (Schneider & Steig, 2008) and sediment cores taken beneath the Pine Island Glacier ice shelf suggest that a sub-ice shelf cavity opened up in the 1940s, followed by the retreat of the glacier

from a submarine ridge (Smith et al., 2017). There is, however, still uncertainty about this idea, since other observations indicate that the Amundsen Sea region was still in balance in the 1970s (Rignot et al., 2019).

The mechanism described so far will henceforth be referred to as the **shelf break wind hypothesis**. It schematically depicted in Figure 1A and can be simplified as follows: eastward zonal wind anomalies, affected by warm SST anomalies in the tropical Pacific, accelerate the eastward shelf break undercurrent, leading to an increased CDW flux onto the continental shelf and eventually to more basal melt.

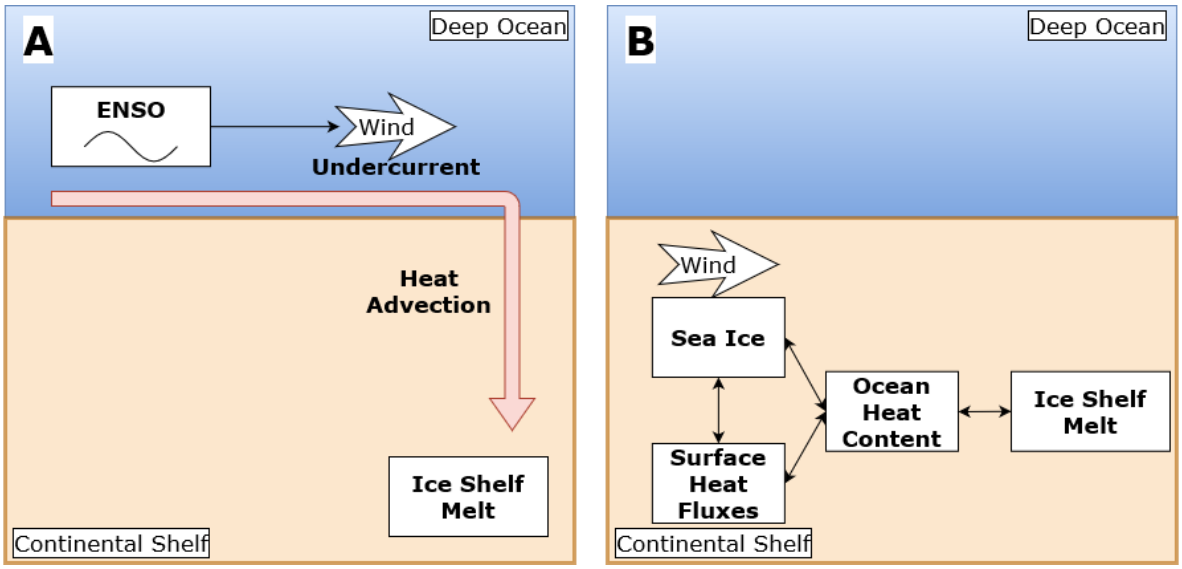

Figure 1: Schematic illustration of Shelf Break Wind Hypothesis (A) and the Surface Buoyancy Hypothesis (B).

However, this hypothesis does not have unequivocal support and other studies disputed aspects of it. Observations could not find a clear link between conditions at the shelf break and ocean conditions on the shelf (Wåhlin et al., 2013; Webber et al., 2017). Instead, they pointed towards local forcing related to surface buoyancy, such as surface heat fluxes and sea ice related processes, especially near coastal polynyas (i.e. areas with low sea ice cover), as having a large influence on the conditions in the Amundsen Sea (St-Laurent et al., 2015; Webber et al., 2017). Figure 1B presents this in a simplified way. It can be summarized that on-shelf surface heat fluxes and sea ice production lead to local changes in heat content and density, affecting the temperature of water flowing into the ice shelf cavity and thus basal melt.
Recent modelling studies have further challenged the shelf break wind mechanism. There is renewed attention to the mechanism of wind forcing, with the suggestion that wind anomalies change density structures and thus affect the baroclinic component of the undercurrent (Silvano et al., submitted). Also the role of freshwater fluxes (Bett et al., 2020) and the distribution of salinity (Planchat et al., submitted) in modulating the ocean currents and CDW influx is discussed. Besides, there is new uncertainty about the connection of basal melt with the tropical Pacific (Silvano et al., submitted; Planchat et al., submitted).

A complicating factor in the study of decadal variability in the Amundsen Sea is the limited number of observations and the short time span that they cover. At present, the observational record spans roughly three decades with limited coverage of observations, making it difficult to determine the dominant mode of variability (Jenkins et al., 2016). Even an analysis over the full satellite era, which started from the 1970s, would only contain a handful of oscillations, potentially obscured by natural variability, and would therefore have limited statistical power. A possible way to tackle this problem is the use of an ensemble of model simulations, which increases the number of realisations of decadal oscillations. This is thus the approach used in this study.

The main aim of this report is to investigate which oceanic and atmospheric controls are driving the decadal melt variability of the ice shelves in the Amundsen Sea. This is done by using a regional ocean model, forced by an ensemble of 20 simulations from a global climate model to increase the statistical power when looking at decadal variability. The results show that the shelf break wind forced mechanism can not explain the model variability by itself, but they suggest that sea ice freshwater fluxes and water properties on the continental shelf also play an important role.
The structure of the report is as follows. After a discussion of the methods used in Chapter 2, the local oceanic and atmospheric processes driving the ice shelf variability are studied in Chapter 3. Relevant remote influences such as ENSO are discussed in Chapter 4, followed by an evaluation of the effect of ice shelf geometry on the results in Chapter 5. A case study is conducted for the 1940s to see how all these processes act together in Chapter 6. Finally, there is a general discussion in Chapter 7 and a conclusion in Chapter 8.

2 Methods

2.1 Model

2.1.1 Model Configuration

This report provides further analysis on simulations with the Massachusetts Institute of Technology general circulation model (MITgcm; Marshall et al. (1997)), adapted to study the Amundsen Sea, which were performed by Naughten et al. (2022). While the focus of Naughten et al. (2022) was on longer term trends, this current report studies decadal variability. The full model description can be found in the original paper, but here the most important aspects are briefly mentioned.

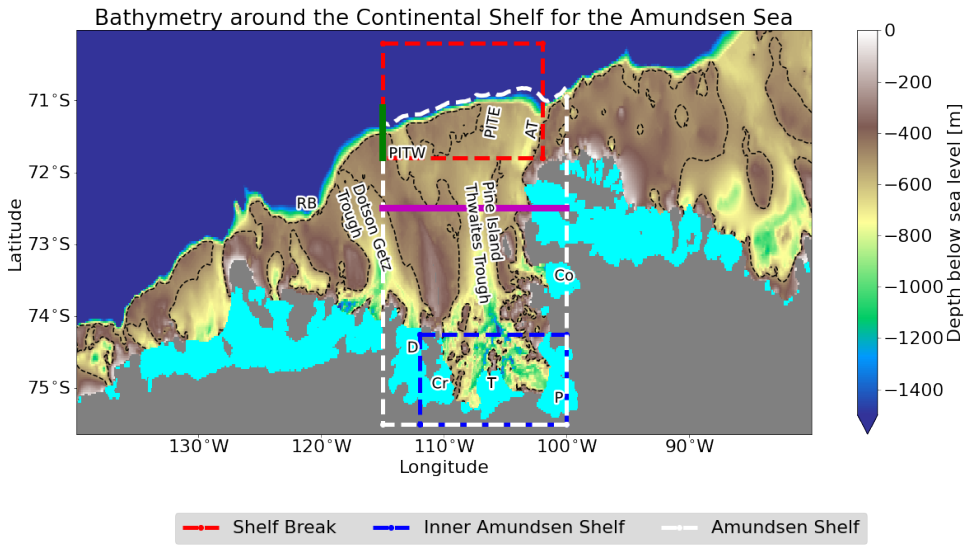

Figure 2: Bathymetry on the continental shelf for the Amundsen Sea. The grey area indicates grounded ice or land, the cyan regions floating ice shelves. The black dotted line indicates the 500m contour of the bathymetry. The green and magenta lines show cross sections taken at 115 °W and at 72.5 °S, respectively. The shelf break region is defined between 115 and 102 °W and 71.8 and 70.2 °S. The Amundsen Shelf is the open ocean region between 115 and 100 °W up to the -1745m isobath at the shelf break. The Inner Amundsen Shelf is the ocean area between 74.25 °S in the north and 112 °W in the west. Explanation of abbreviations: PITE=Pine Island Thwaites East trough; PITW=Pine Island Thwaites West trough; AT=Abbot trough; D=Dotson Ice Shelf; Cr=Crosson Ice Shelf; T=Thwaites Ice Shelf; P=Pine Island Glacier Ice Shelf; Co=Cosgrove Ice Shelf; RB=Russel Bay.

MITgcm is a numerical ocean model that solves the incompressible Navier-Stokes equation (Marshall et al., 1997). In the set-up of Naughten et al. (2022), sea ice is implemented in the model following Losch et al. (2010), using a viscous-plastic rheology. Furthermore, the model includes circulation in ice shelf cavities following Losch (2008), with basal melting and freezing parameterized by the three-equation model (Hellmer & Olbers, 1989; Jenkins et al., 2001). Melt is applied as a freshwater flux and a heat flux at the base of the ice shelf. Tides are not included in the model.

The model domain over the Amundsen Sea is derived from earlier studies (Assmann et al., 2013; Kimura et al., 2017; Bett et al., 2020). Figure 2 shows the continental shelf in the domain. The full domain extends between 80 and 140 °W and 62 and 75.5 °S. The horizontal resolution is 1/10 degree and the model uses 50 levels in the vertical with thicknesses ranging between 10 and 200 meters. The open ocean boundaries are fixed with the present-day climatology (derived from Verdy & Mazloff (2017); Locarnini et al. (2018);

Zweng et al. (2019)). The ice shelf geometry is fixed on the present-day situation. This geometry and the bathymetry were taken from MEasUREs BedMachine Version 2 (Morlighem, 2020; Morlighem et al., 2020).

2.1.2 Model Validation

The model validation by Naughten et al. (2022) is briefly summarized. Forced by historical atmospheric forcing from ERA5 (Copernicus Climate Change Service, 2017), the results showed general agreement with observations. Mean melt rates for Dotson and Pine Island Glacier are within the range of uncertainty compared to in-situ observations, though Pine Island Glacier may have a reduced range. However, melt rates at Pine Island Glacier, Thwaites and Dotson are underestimated compared to long term satellite observations. Oceanic conditions generally do not deviate strongly from the range in observations. The model does show a convective event not observed in reality, suggesting that the model might have a potential bias to convection on the continental shelf.

We have sufficient confidence in the model performance and for the analysis in this report the model is assumed to be adequate to study the processes at hand.

2.1.3 Forcing

The regional model was forced by atmospheric output of the Pacific Pacemaker Ensemble (PACE; Schneider & Deser (2018)). This ensemble consists of 20 simulations of the global Community Earth System Model version 1 (CESM1), constrained by historical external forcing and sea surface temperature (SST) anomalies in the eastern and central tropical Pacific. All members thus contain historical El Niño and La Niña events. Model runs are performed for the years 1920 to 2014, following a 30 year spin-up period forced with a repetition of the 1920-1949 PACE input. Naughten et al. (2022) applied a bias correction to thermodynamic atmospheric variables in the whole domain and to the winds near the coast east of 90 °W.

2.2 Data Analysis

This study focuses on the eastern part of the Amundsen Sea, since the region has most of the observed mass loss (Rignot et al., 2019) and is well studied, already since the 90s (Jacobs et al., 1996).

2.2.1 Time Series

Naughten et al. (2022) calculated time series by averaging over specific regions. Figure 2 shows the areas used in this analysis, which include:

- **The shelf break region**: mainly used for zonal surface winds and defined following Holland et al. (2019).
- **The Amundsen Shelf**
- **The Inner Amundsen Shelf**

Basal melt rates were integrated over all ice shelves from Dotson up to and including Cosgrove and converted to a mass flux, referred to as **ice shelf basal mass loss** or **Dotson to Cosgrove mass loss**. Additionally, an index for the undercurrent is created at 115 °W, by taking the average over the zonal flow between 71.40 and 71.45 °S and -300 and -550m depth. Depth averaged heat advection within the Pine Island Thwaites (PIT) trough is sampled at 73°S and averaged between 107 and 105 °W to create an index.

2.2.2 Climate Indices

Climate indices differ between each individual PACE member, except when sampling SSTs in the eastern Pacific, and had to be computed separately. The spatial domains used for their computation is shown in Figure 27 in Appendix A. The indices used are:

- **The Interdecadal Pacific Oscillation (IPO) index**: the Tripole Index following Henley et al. (2015). As a reference period, 1971-2000 was used.
- **The Southern Oscillation Index (SOI)**: computed following National Centers for Environmental Information (n.d.), using coordinates found in Harrison & Larkin (1996) and a reference period of 1981-2010.
- **The Southern Annular Mode (SAM)**: derived from Gong & Wang (1999) and Physical Sciences Laboratory (n.d.), using a reference period of 1981-2010.
- **'West-Pacific Sea Surface Temperatures' (WPSST)**: a sea surface temperature anomaly in a region defined by Thomas et al. (2015) was used, with 1971-2000 as reference period.

Furthermore, we use three indices for the Amundsen Sea Low, following Hosking et al. (2016).

- **Amundsen Sea Low Central Pressure (ASL CP)**: the absolute lowest pressure of the Amundsen Sea Low.
- **Amundsen Sea Low Latitude (ASL lat)**: the latitude of the location of the ASL CP.
- **Amundsen Sea Low Longitude (ASL lon)**: the longitude of the ASL CP location.

2.2.3 Spatial Maps

Several 2D spatial maps are read from the MITgcm output. Three types of ocean velocity fields are used:

- **Bottom 100m flow**: to study currents following the bathymetry, the flow in the 100m above the seafloor is averaged. When there are no grid cells within this range, the lowest cell is taken. This can happen for example because ocean velocities are taken at the edges of the grid cells. When the bathymetry has a step-wise slope, the elevation of the velocities is sometimes not in this 100m interval.
- **Barotropic flow**: for this, the depth-averaged velocity is taken.
- **Baroclinic flow**: this component is constructed by taking the bottom 100m flow and subtracting the depth-averaged velocity.

2D fields within the ocean are averaged over a specific depth interval (e.g. temperature), whereas surface fields are taken directly from the model output (e.g. wind).

Finally, cross sections were taken at 115 °W (following Silvano et al. (submitted)) and at 72.5 °S (see Figure 2).

2.2.4 Processing

The output of the model is monthly averaged data. The report mainly focuses on decadal variability and 12 or 60 month running means are applied to smooth shorter term variability. To remove longer term trends and variability, a 25 year running mean is removed from the data, similar to Jenkins et al. (2016). Cumulative anomalies are also computed from detrended data, followed by applying a running mean.

Density is computed following McDougall et al. (2003) with a reference pressure of 0 bar. This is the same as the model does online.

2.2.5 Correlation Maps

The main tool of analysis used in this report is the correlation map. A 2D field (evolving in time) is correlated with one separate time series. For each location in the 2D field an individual correlation is performed. To study lag, the 2D field and time series are shifted in time with respect to each other. These shifts are up to 24 months in both directions, unless specified otherwise. For each point, the best absolute Pearson correlation coefficient and the corresponding lag are determined. When the associated two-sided p-value in the individual member is larger than 0.05, the correlation is set to 0 and no lag is taken.

Correlations are performed for each member individually and then averaged over the ensemble. A one sampled t-test is performed to see if this mean is significantly different from 0 and p-values larger than 0.05 are rejected. The average over the correlation of individual ensemble members is not the same as the correlation of the ensemble mean. In the ensemble mean only the signal related to the constrained tropical variability in PACE should be present, generally increasing the correlation coefficients. In our approach internal variability is preserved in the correlation.

A second map is produced, showing the lag or lead between the time series and 2D field that corresponds to the optimal correlation. Lags are rejected when the standard deviation between ensemble members is larger than 8 months. This is done to still preserve a spatially coherent image, but to remove uncertain locations. To preserve the clarity of the text, this second map is sometimes moved to Appendix A.

2.2.6 Composites

Composites are created using a 60 month running mean is applied to the ice shelf basal mass loss. The time and ensemble mean of a 2D field is taken when this running mean is above its 90th percentile or below its 10th percentile.

2.2.7 Selection of High Melt Members

For the case study on the 1940s, ensemble members showing the highest melt are selected, based on the mean melt anomaly over a 2 year period from 01-1940 until 12-1941.

2.3 Simulations with a Perturbed Ice Shelf Geometry

Chapter 5 is dedicated to the effect of ice cavity geometry. The idea of this experiment is to study the sensitivity of the results to ice shelf geometry, not to provide a realistic reconstruction of the early 20th century.

A more protruded geometry for the Dotson, Crosson, Pine Island Glacier and Thwaites ice shelves was created by Jan de Rydt with the Úa ice-flow model (Gudmundsson et al., 2012). A fixed ice front was imposed and the basal melt rates were set arbitrarily to 0. The ice flow model was then run until an equilibrium was found.

Linear interpolation was used to grid the provided ice draft and floating mask on the ocean model grid. To maintain consistency with the original procedure used by Naughten et al. (2022), Matlab code provided by Paul Holland was adapted for this. During this process, the following assumptions were made:

- The same ice front was used as in the runs by Naughten et al. (2022). The protruded geometry was created with a slightly different prescribed ice front. It was decided to cut off the ice shelf to the previous front, because we are mainly interested in ice cavity geometry. With an extended ice shelf front the location of sea ice formation would also change, as well as the atmospheric forcing, which would complicate the analysis and would be beyond the scope of this project.

- Newly ungrounded ice is regrounded. In a few locations, the new geometry shows ungrounded ice in locations where the ice was grounded in the old geometry. This is probably a consequence of the interpolation to the model grid and since the main focus is looking at smaller ice cavities, it was decided to reground the ice in these positions.

The bathymetry from Bedmachine v2 was used again, except when the water column was less than 3 grid cells deep, in which case the bathymetry was dug out, following Naughten et al. (2022). This was done to maintain numerical connection between adjacent water columns given the finite vertical resolution and has its main effect near the grounding line. The old ice shelf geometry was used for other ice shelves outside Dotson to Pine Island Glacier. Figure 3 shows the protruded geometry and the differences with the geometry used by Naughten et al. (2022). The grounding line has clearly advanced and the new ice draft is generally deeper, but there are exceptions, especially to the east of Thwaites.

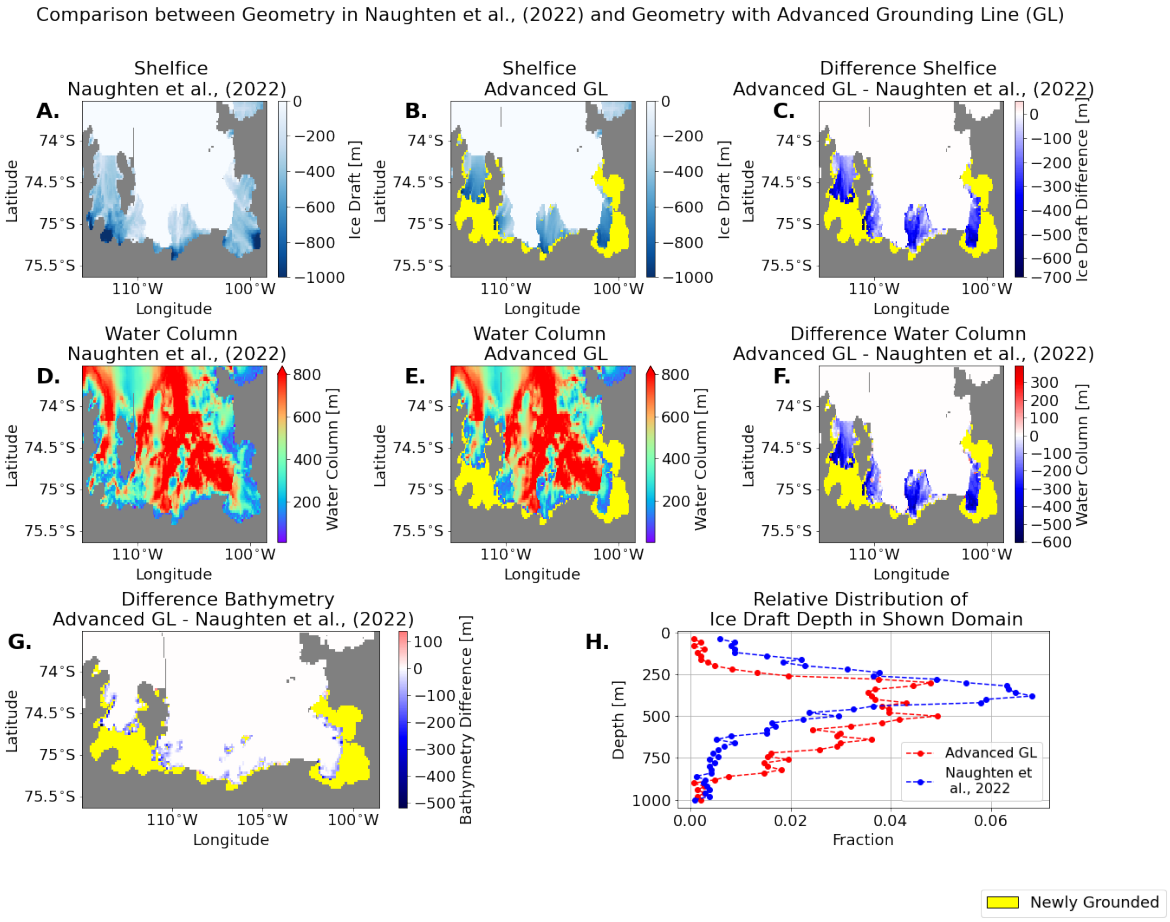

Figure 3: The difference between the geometry used by Naughten et al. (2022) and the new geometry with an advanced grounding Line (GL). A.) Ice raft used by Naughten et al., (2022). B.) Ice draft with advanced grounding line. C.) Difference between the ice drafts (subtracting old geometry from geometry with advanced GL) D.) Water column used by Naughten et al., (2022). E.) Water column with advanced grounding line. F.) Difference between the water columns. G.) Difference in bathymetry, due to digging when the water column is thinner than 3 cells. H.) Relative distribution of depth for ice drafts within the shown domain. Yellow areas indicate newly grounded ice.

For these new runs, 5 members were selected based on their melt response in the 1940-1942 compared to 1938-1940. Figure 4 present the selected members. Two members were chosen with increasing melt (members 6 and 10), complemented by two members with decreasing melt (members 11 and 12). One additional member was chosen to make the mean melt of these members more similar to the PACE ensemble-mean melt (member 4). The simulations were run with the same set-up as used by Naughten et al. (2022), but on a different machine because the old facility was replaced. This had negligible effect on the outcome (Kaitlin Naughten, personal communication).

The Python code which was used for this project can be found in Appendix C.

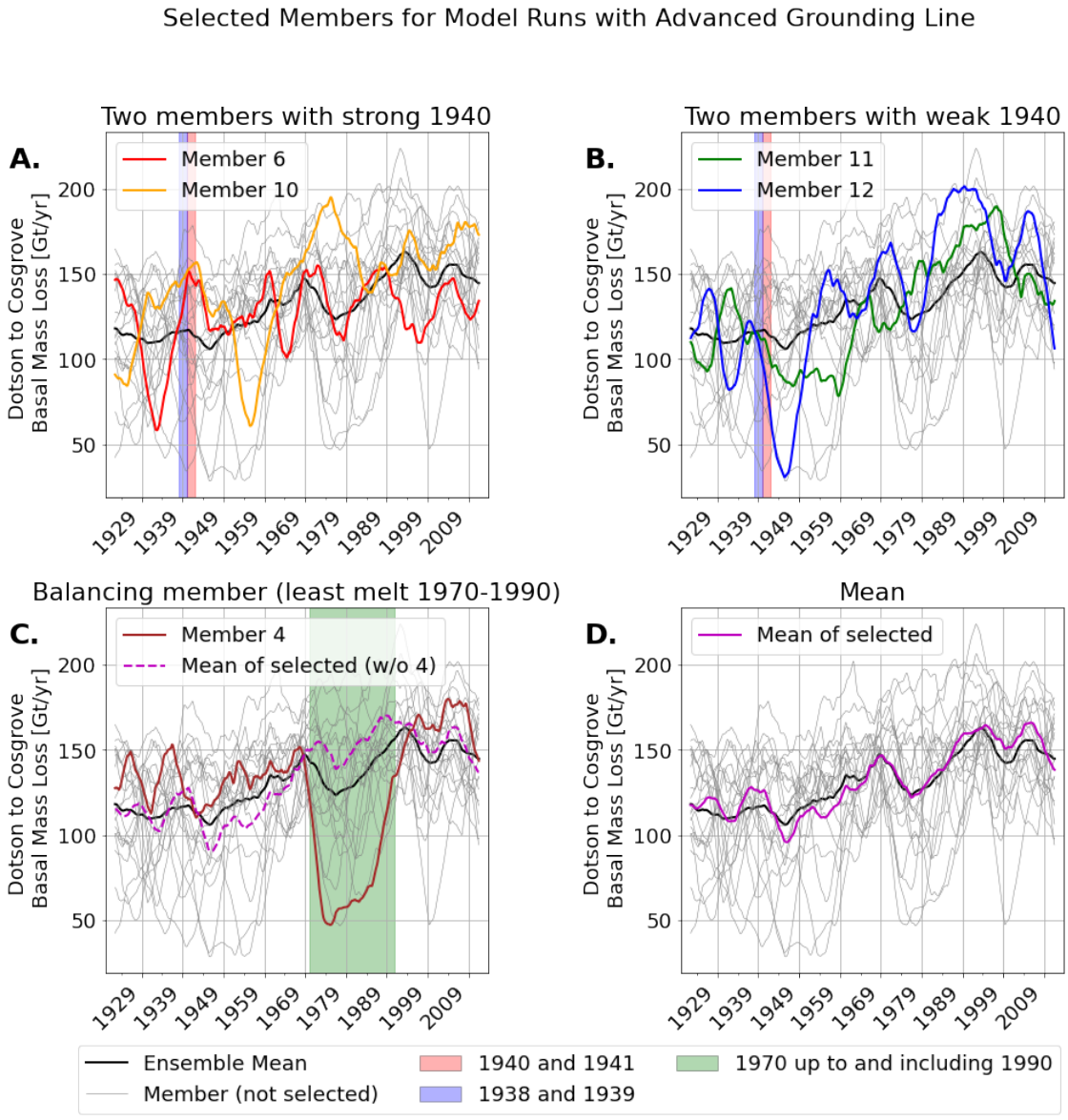

Figure 4: Selected members for the runs with a new geometry. All figures show the basal mass loss between Dotson and Cosgrove with a 60 month running mean. A.) Two members with high melt for the 1940s. B.) Two members with low melt in the 1940s. C.) Member used to improve the ensemble mean. D.) Comparison of the new and old ensemble mean.

3 The Mechanisms driving Decadal Variability in Ice Shelf Basal Mass Loss

Ice shelf basal mass loss shows strong decadal variability in the simulations, with large difference between members in timing and amplitude (compare Figure 4). In this section the focus is on reviewing the different theories described in the introduction for the decadal variability of ocean conditions and melt in the model. In section 3.1, the shelf break wind hypothesis is studied, followed by a discussion of baroclinicity and surface buoyancy in section 3.2.

3.1 Shelf Break Wind Hypothesis

The first theory that we discuss is the shelf break wind hypothesis. In this section, it is investigated if the model results are indeed consistent with the shelf break wind hypothesis. If previous literature is correct, strong links between ice shelf basal mass loss with flow at the shelf break and in the troughs (Kimura et al., 2017; Naughten et al., 2022; Silvano et al., submitted) as well as with the shelf break winds (Thoma et al., 2008; Dutrieux et al., 2014; Kimura et al., 2017; Naughten et al., 2022) are expected.

3.1.1 Heat Advection in Seabed Troughs

The initial focus is on establishing the role of CDW influx through the seabed troughs. Our results indeed show strong positive correlations between the horizontal heat advection in the lowest 100m of the water column and ice shelf basal mass loss (see Figure 5). Regions with particularly strong correlations (>0.8) include part of the shelf break (e.g. around 115 °W), the Pine Island Thwaites West (PITW) and East (PITE) inlets, the main PIT trough, as well as coastal regions. The Abbot trough also shows strong, but slightly weaker correlations (>0.5). The heat advection in the troughs leads the melt by a few months, which is also the case in some locations around the shelf break and near the coast in the eastern part of the basin. This agrees with the hypothesis that flow in the troughs is driving the melt. To the west of 110 °W, the heat advection mostly lags behind the melt. This could be related to the westward advection of the warm water anomaly by the coastal current, a possible later activation of the Dotson-Getz Trough or an ice shelf meltwater feedback (see Section 3.2).

Figure 5 only shows the correlation of the magnitude of heat advection, but not the direction of the flow. For this, composites of the flow during high and low melt are studied (see Figure 6). This shows that the main circulation at the bottom is clockwise, with an important role for the seabed troughs. During periods of strong melt, the eastward flow around the shelf break and southward flow in the PIT trough are strengthened. When melt is weak, the flow in both locations is reduced, but not reversed. Ocean speed is thus an important contributor to changes in heat advection.
In summary, the model results presented here are consistent with the idea that variability in influx of CDW within the seabed troughs is driving the ice shelf basal melt.

Observations indeed show on-shelf heat advection in the troughs, strong enough to explain most of the estimated melt (Walker et al., 2007). Furthermore, the spatial patterns are consistent with earlier modelling work. We show high correlations of heat advection with melt in the PITW and the Abbot trough, which are both proposed as inlets for the CDW (e.g.Thoma et al. (2008); Assmann et al. (2013); Jenkins et al. (2016)). Correlations of heat advection and the composites of velocity suggest the importance of the shelf break outside the troughs, consistent with ideas about the observed shelf break undercurrent (Walker et al., 2013). The strong difference in flow strength between times of high and low melt are in line with Assmann et al. (2013), who suggested that heat flux variability on the shelf is mainly driven by changes in velocity rather than CDW temperature. However, a limited number of observations showed only a weak connection between on-shelf velocities and temperature in Pine Island Bay, suggesting it is unlikely that interannual variability is driven by conditions in the troughs (Webber et al., 2017). Potential explanations for this discrepancy include the relatively short record of observations used, modelling issues or the time scales studied. However, even at shorter the time scales, the correlations in the troughs remain high (see Figure 28 in Appendix A).

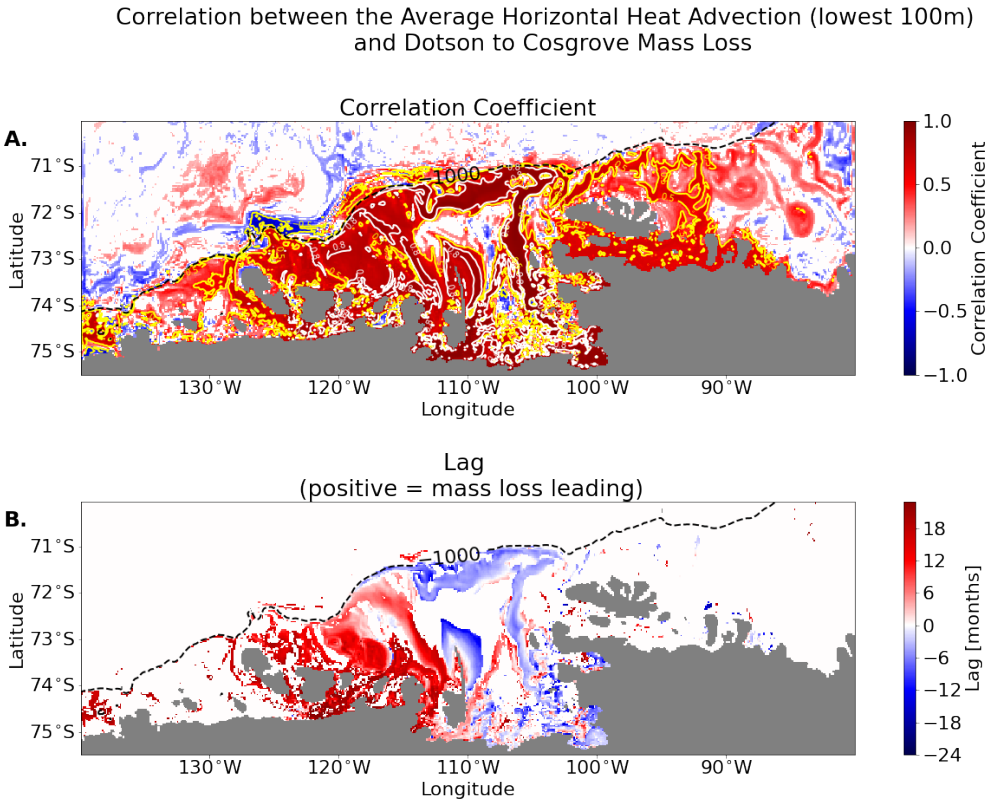

Figure 5: The correlation between local absolute horizontal heat advection in the bottom 100m and a time series of total basal melt over the Dotson to Cosgrove ice shelves, after applying a 60 month running mean. A.) The optimal correlation coefficient. Yellow and white contours indicate where the absolute correlation coefficient exceeds 0.5 and 0.8, respectively. White shaded regions indicate where the p value was larger than 0.05. B.) Lag corresponding to this optimal correlation coefficient. White shaded regions are where the standard deviation is larger than 8 months. For both panels, the black dotted line indicates the -1000m isobath and is an indication for the location of the shelf break.

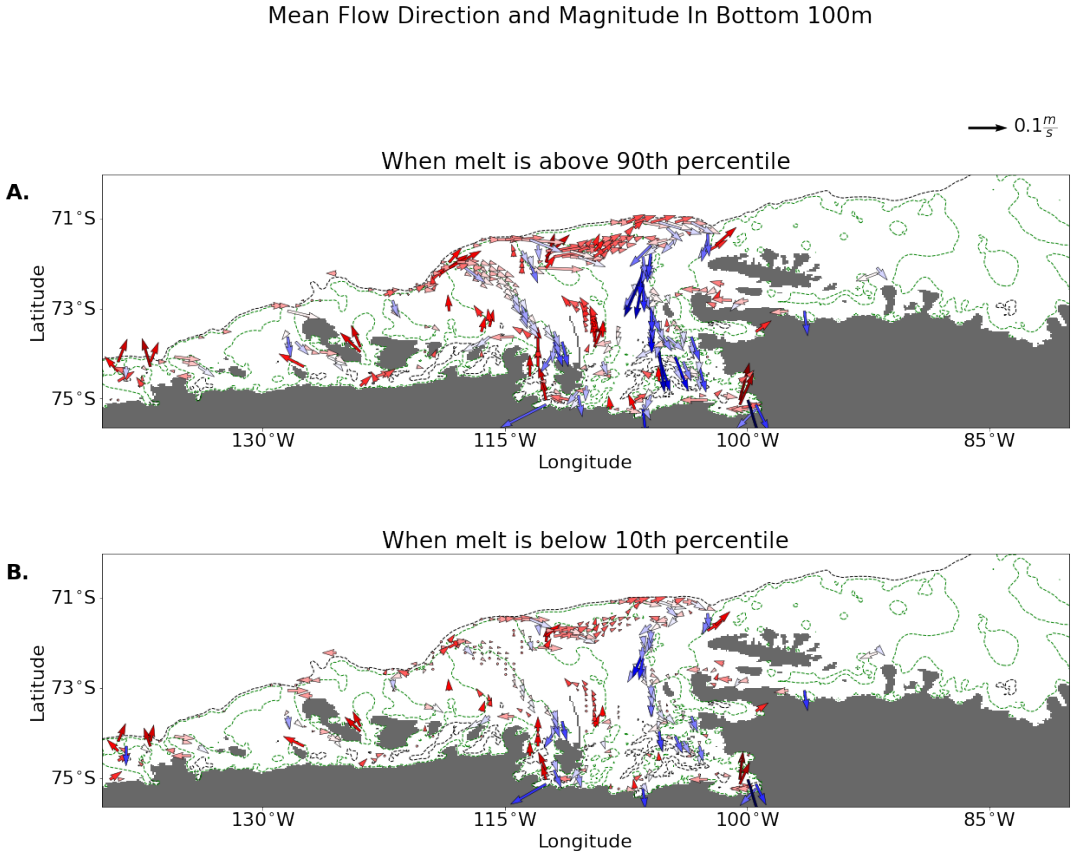

Figure 6: Composite showing the time-mean and ensemble-mean flow in the lowest 100m. A.) During strong basal melt during strong mass loss for the ice shelves between Dotson and Cosgrove (above the 90th percentile) B.) During weak basal mass loss (below the 10th percentile). Blue arrows indicate southward flow, red arrows indicate northward. Arrows are only shown when the difference in speed exceeds 0.01 m/s. The green and black dotted lines show the -500m and -1000m isobaths, respectively.

3.1.2 The Connection with the Wind

After having considered the role of heat advection in the troughs, the next step is to investigate the connection between the melt and the wind, which is hypothesized to be driving the flow of CDW through the seabed troughs towards the ice shelf.

Figure 7 shows the correlation between zonal shelf break winds and flow in the the bottom 100m. Contrary to expectations, the bottom 100m flow in the PITW inlet and along the shelf break is only weakly correlated with the shelf break zonal winds. More striking is that correlations are insignificant in parts of the PIT main trough. The best correlations are found in the eastern part of the basin. This is clearly different from the flow patterns related to ice shelf basal melt (compare Figures 5 and 11) and challenges the role of the zonal winds in driving this system.

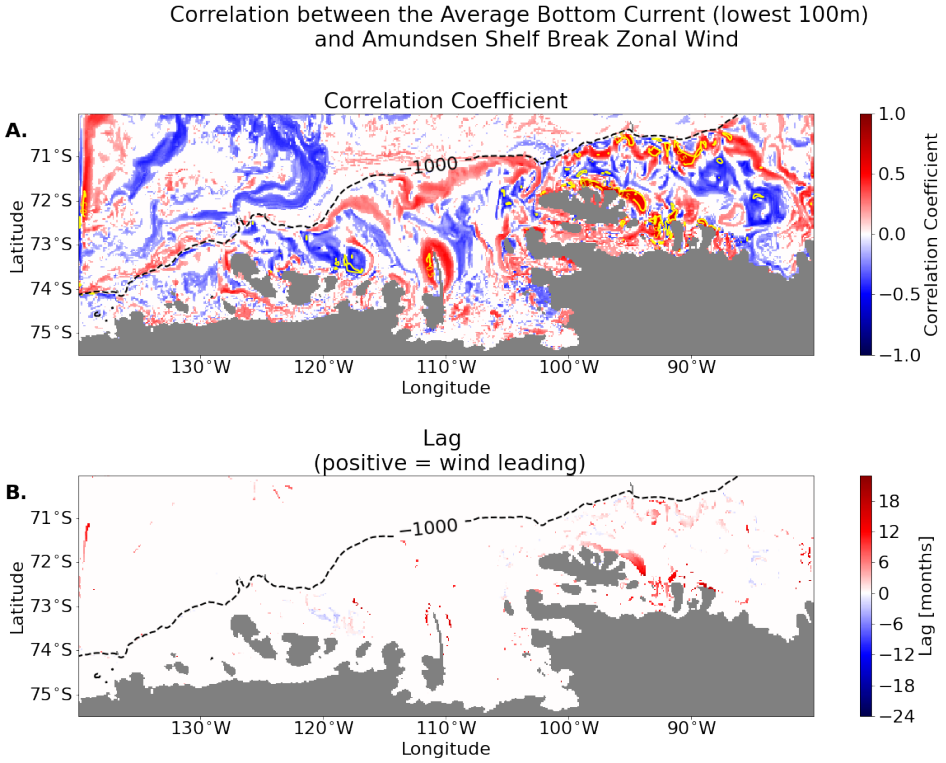

Figure 7: As for Figure 5, but showing the correlation and lag between local velocity in the lowest 100m and a time series for Amundsen shelf break zonal wind.

Possibly, the shelf break region is not the region that is relevant for melt. To study where winds are most important, Figure 8 shows spatial correlation of wind components with ice shelf basal mass loss. Correlations for the zonal wind are generally positive, but relatively weak (<0.5) (see Figure 8A). The zonal wind shows its best correlations over the shelf break and on the continental shelf in the east of the domain. Furthermore, there are negative correlations between the Thwaites and Crosson ice shelves. The meridional wind reveals weak negative correlations across most of the continental shelf, just exceeding -0.5 in front of Thwaites ice shelf (see Figure 8B). Cumulative winds show similar patterns (see Figure 8C and D), with weak positive correlations for the cumulative zonal wind around the shelf break, although there is a gap in the middle of the domain, and weak negative correlations on the continental shelf for the cumulative meridional wind.

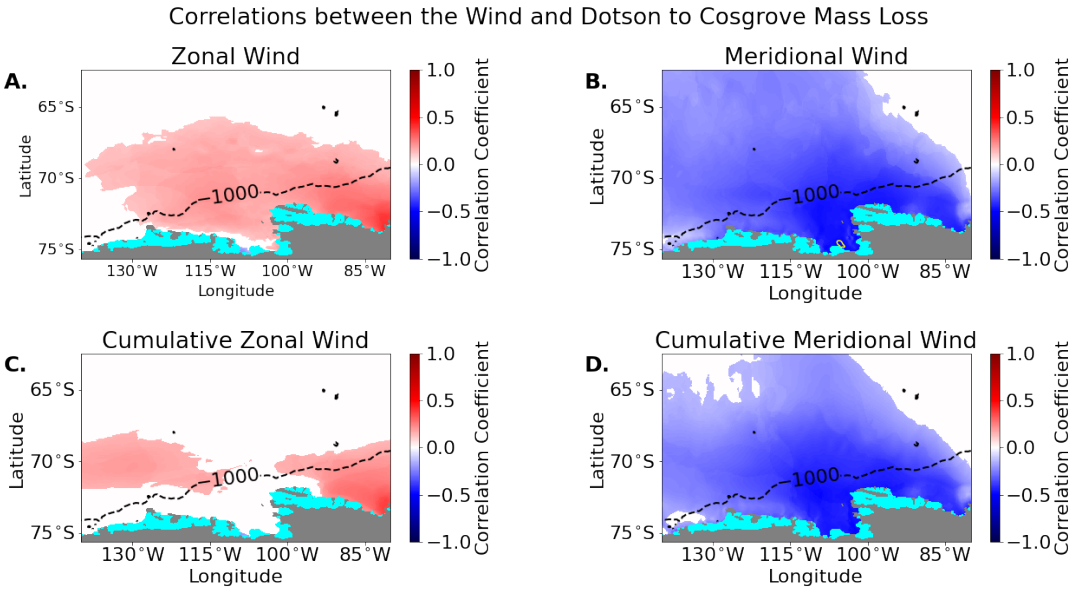

Figure 8: The correlation between different components of the local wind and a time series of basal melt between Dotson and Cosgrove. A.) Zonal wind. B.) Meridional wind. C.) Cumulative zonal wind. D.) Cumulative meridional wind. Description of the figures is the same as for Figure 5A. Winds were only correlated to be leading the melt, since the model is uncoupled and there is thus no feedback on the atmosphere.

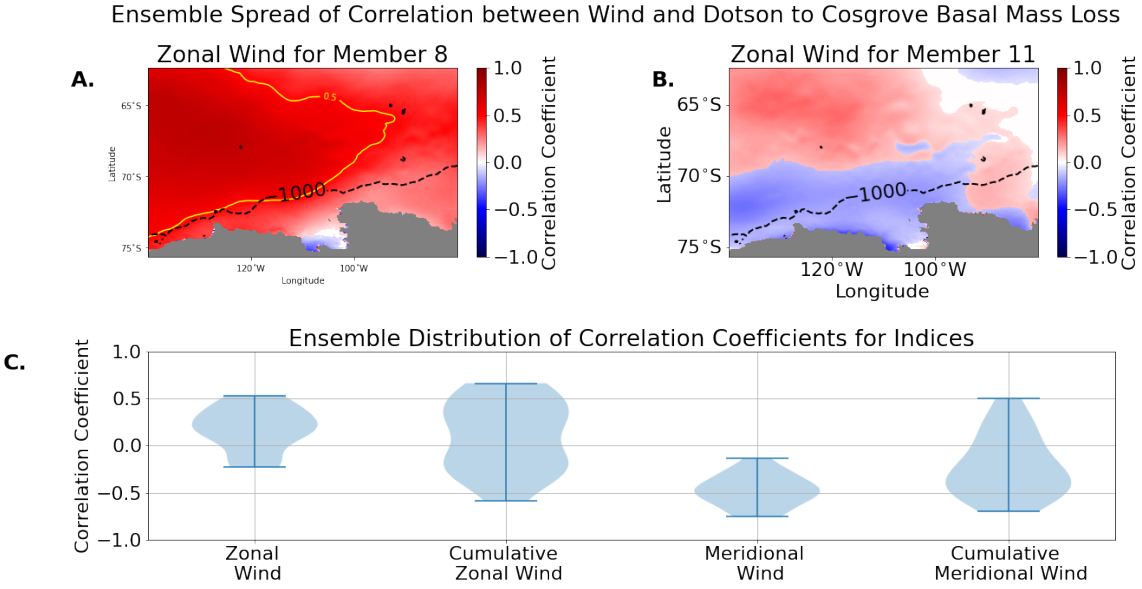

Figure 9: The spread within the ensemble for the correlation between wind and Dotson and Cosgrove basal mass loss. A.) Member 8, an example of a strong correlation. B.) Member 11, a member with a negative correlation. C.) The distribution of correlation coefficients, computed for indices for the normal and cumulative zonal shelf break wind and the normal and cumulative inner Amundsen Shelf meridional wind with ice shelf basal mass loss.

Underlying the weakness in the correlations is considerable ensemble spread. Figure 9 illustrates the differences between the members. Individual members of the zonal wind can show widely different patterns, including both strong positive and weak negative correlations. For the whole ensemble, the zonal winds show some ambiguity about the sign of the correlation, whereas meridional winds show more internal consistency (see Figure 9C).

To summarize, these results indicate that the shelf break wind hypothesis breaks down when looking at the connection between the wind and the ocean velocity. First, the Amundsen shelf break zonal wind, averaged over a region used in previous research (e.g. Holland et al. (2019); Naughten et al. (2022)), is not significantly correlated with the flow in the troughs. Second, even when zooming out to the model domain, there is indeed a significant correlation between the zonal wind and the ice shelf basal mass loss is present, but it remains relatively weak ($r<0.5$). There is considerable internal spread within the ensemble and the correlations do not improve substantially when looking at the cumulative zonal wind anomaly.

Zonal winds at the shelf break can thus explain part of the variation in the model, but their role is limited. Other factors are likely important: the effect of the zonal wind stress on the shelf could be mediated by smaller scale patterns in sea ice stress and meridional wind. Although this weakens the existing shelf-break wind theory, it is reflective of the often ambiguous literature, which finds both positive (Thoma et al., 2008; Kimura et al., 2017), negative (Silvano et al., submitted) as well as insignificant (Planchat et al., submitted) relationships between ice shelf melt and the shelf break winds.

Interestingly, there could be a role for on-shelf meridional winds, which show more internal consistency and generally stronger correlations. Their role will be further discussed in the following section.

3.2 Baroclinicity and Surface Buoyancy

Recent research suggests that variability in water composition and density gradients at the shelf break could affect ice shelf basal melt: surface processes or internal circulation could change the distribution of water, density gradients and baroclinicity in the undercurrent (Planchat et al., submitted; Silvano et al., submitted). This possibility will be discussed in more detail.

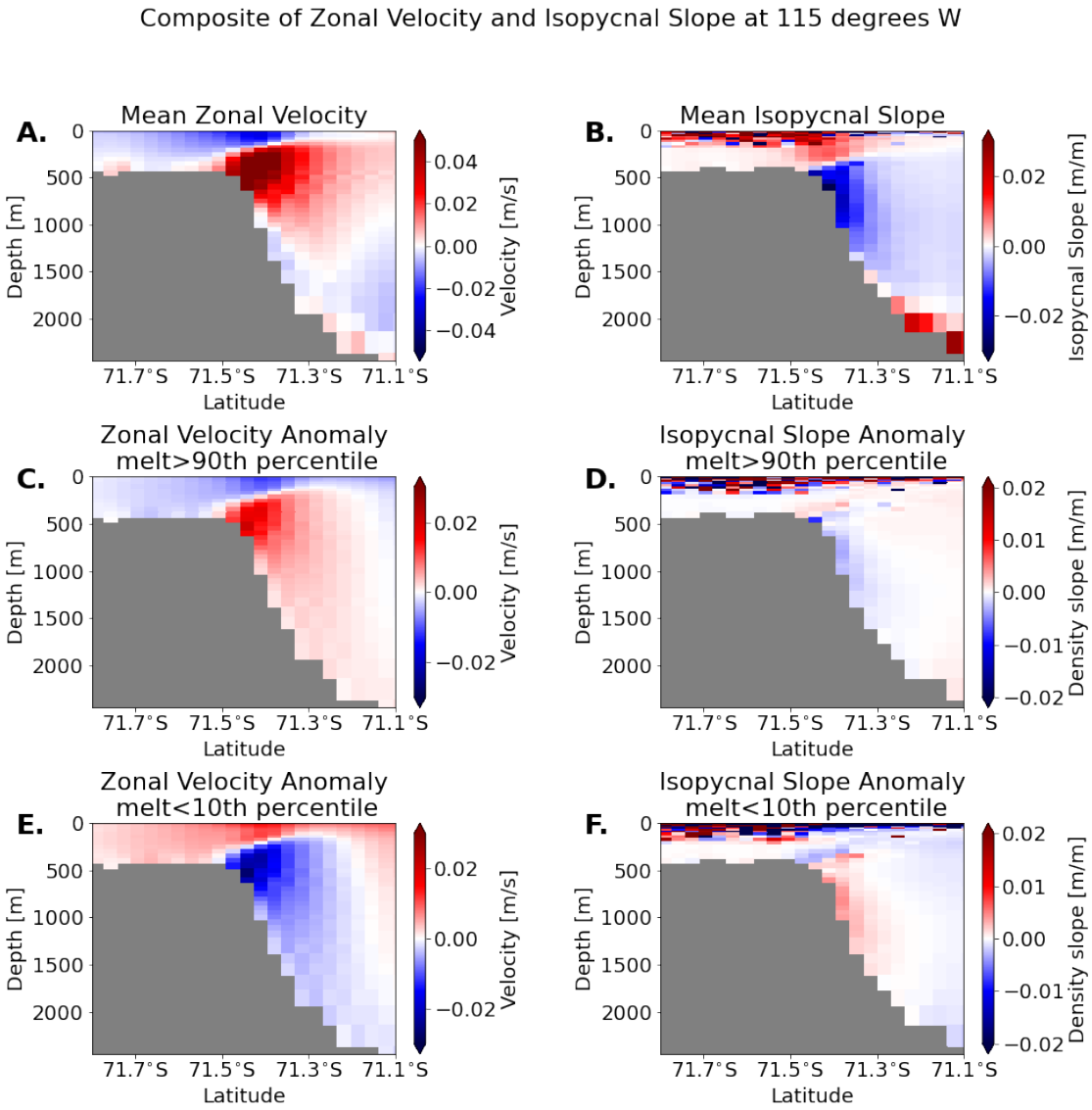

Figure 10: Composite showing the zonal velocity and isopycnal slopes at the shelf break at 115 °W. A.) Time-mean and ensemble-mean zonal velocity. B.) Time-mean and ensemble-mean isopycnal slope. The second row shows the anomalies during strong basal mass loss for the ice shelves between Dotson and Cosgrove (above the 90th percentile) (C. for zonal velocity, D. for isopycnal slope) and third row depicts anomalies during weak basal mass loss (below the 10th percentile) (E. for zonal velocity, F. for isopycnal slope).

The existence of a baroclinic component can be demonstrated by looking at cross sections with depth, which should display depth-dependent behaviour of the velocity. A cross section taken at 115 °W reveals the presence of an eastward undercurrent and a westward surface at the shelf break in the time-mean state (see Figure 10). They respond to changes in melt in opposite ways: during high melt, there is an eastward anomaly in the undercurrent and a westward anomaly in the surface current, and vice versa during low melt. This is similar to the results of Silvano et al. (submitted). The isopycnal slopes also change in accordance (steepen during high melt, flatten during low melt), further stressing that this is indeed a baroclinic feature.

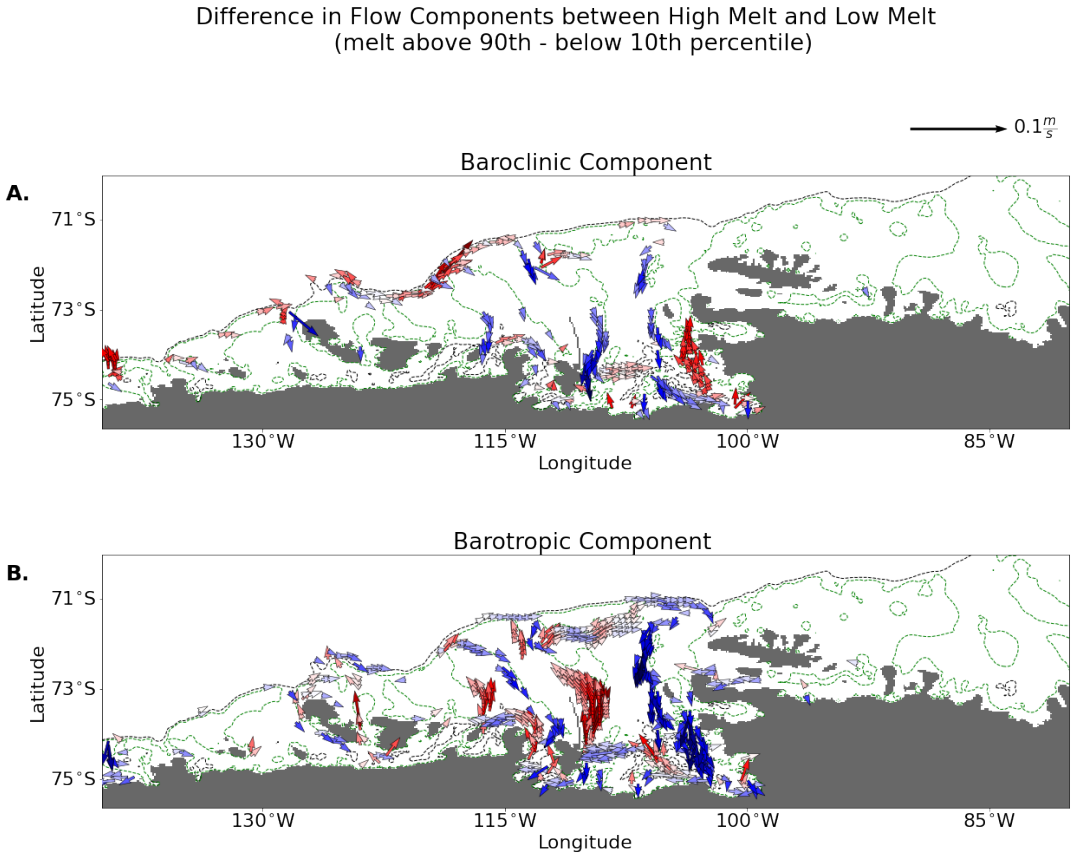

Figure 11: The difference for the velocity components between times with high (>90th percentile) and low (<10th percentile) ice shelf basal mass loss. A.) **Baroclinic** flow velocity (bottom 100m - depth averaged flow) B.) Depth averaged **barotropic** flow velocity. The black dotted line indicates the -1000m isobath. Green lines indicate the -500m isobath. Blue arrows indicate southward flow. For locations where the absolute difference in flow was smaller than 0.01 m/s between high melt and low melt, arrows are not shown.

Nevertheless, the total variability of the undercurrent is a complex mix of fast barotropic and slower baroclinic components (Planchat et al., submitted; Silvano et al., submitted). Figure 11 shows the difference between high and low melt for the baroclinic and barotropic component. Indeed, they have comparable spatial patterns. Both components strenghten along the shelf break, in the PITW inlet and in the PIT main trough during high melt.
There are however clear differences between the baroclinic and barotropic component: during high melt, the baroclinic flow shows stronger differences in the western part of the shelf break region near Russel Bay, whereas the difference in the PIT trough is strongest for the barotropic flow. We also find stronger northward flow on the shelf at 110 °W.

These results agree with Planchat et al. (submitted), who found a western fresh and an eastern more salty shelf, separated roughly around Russel Bay, and found that the undercurrent was mainly barotropic in the east, but had a stronger baroclinic component in the western fresh shelf.

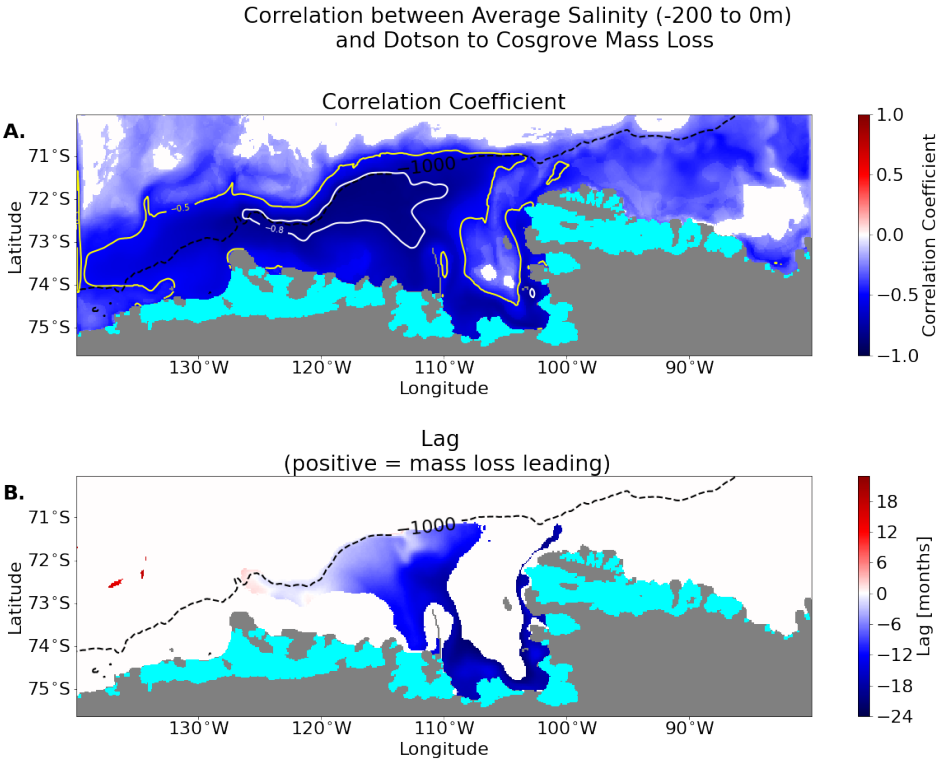

Figure 12: As for Figure 5, but for the correlation between salinity (averaged between 200m depth and the surface) and basal mass loss over the Dotson to Cosgrove ice shelves.

Baroclinic behaviour is mainly determined by horizontal density gradients. In cold climates, water density is less sensitive to temperature and is mainly controlled by salinity (Gill (1982) as cited by Bett et al. (2020)), which what this section focuses on. Figure 12 shows the correlation between salinity in the upper 200m with ice shelf basal mass loss. We find strong anti-correlations, especially close to the shelf break (<-0.8) and in the western part of the basin (<-0.5). Furthermore, the correlation map suggests that the salinity changes lead the melt. This could be affected by the applied 60 month running mean, but also with a 12 month running mean the salinity is still leading near the ice shelves and contemporaneous with basal mass loss at the shelf break (see Figure 29 in Appendix A). The salinity variability at the shelf break could influence melt via its effect on the baroclinic component of the undercurrent. Regions where the correlation is smaller than -0.8 coincide with regions where baroclinic currents co-vary strongly with the melt (see Figure 11).

The correlation between salinity and melt, in addition to the baroclinic component of the shelf break undercurrent, could be indicative both of a forcing or a feedback mechanism. They are schematically illustrated in Figure 13. An ice shelf meltwater feedback, as suggested by Bett et al. (2020), could be a positive feedback, in which ice shelf meltwater affects the density gradients near the shelf edge, which leads to more CDW input and more meltwater production. Furthermore, the effect of salinity could also be a forcing mechanism, since an important freshwater flux comes from sea ice growth and melt, which is correlated to wind forcing (Bett et al., 2020).

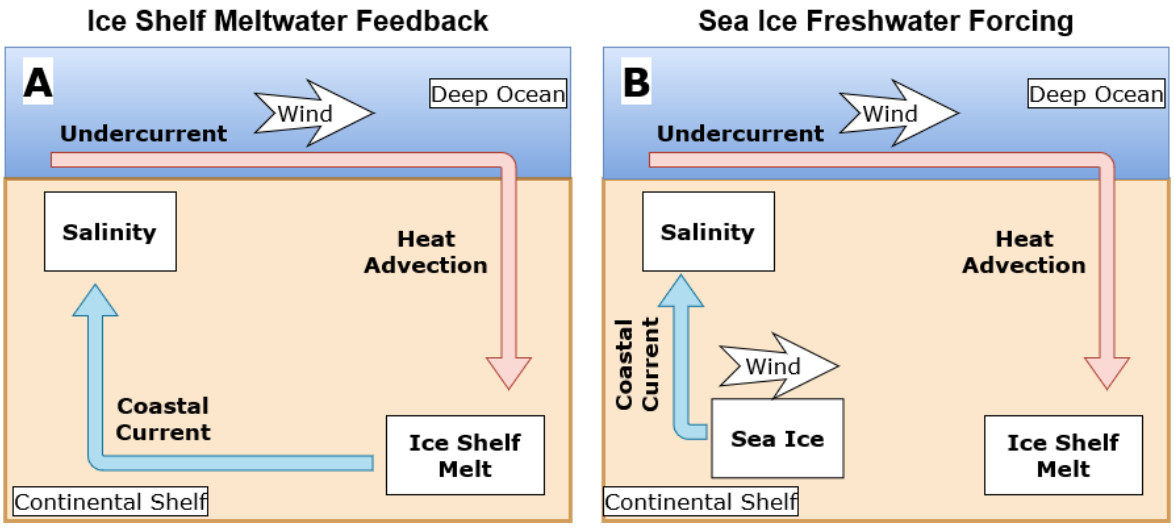

Figure 13: Schematic Illustration of Ice Shelf Meltwater Feedback (A.) and the Sea Ice Freshwater Forcing (B.).

It is difficult to separate these effects fully, but we can study the relative sizes of the freshwater fluxes in Figure 14. The contribution of ice shelf mass loss is roughly responsible for two thirds of both the total fluxes and the temporal variation. The net effect of sea ice freezing and melt is responsible for the last third and precipitation and evaporation have only a limited contribution (1-5 per cent). Through time, the contribution of ice shelf mass loss to the total flux grows slightly at the cost of sea ice fluxes (9 per cent points), but the amplitude of temporal variability remains constant. There is strong variability between ensemble members, both for the salinity and the freshwater fluxes. Finally, even though CDW influx is left out of the salinity balance, the ensemble mean freshwater flux and salinity show similar positively correlated variability towards the end of the time series, whereas in the beginning the coupling is less clear. These results are generally agreeing with Bett et al. (2020), who used a similar model and found that the sea ice and ice shelf fluxes are the largest freshwater fluxes, which also have the strongest interannual variability. The fact that ice shelf melt in our model is larger than the effects from sea ice would suggests that the melt feedback is stronger than the forced effect. However, sea ice effects are responsible for a third of the variation and can be important at different times than the ice shelf melt. Therefore,they could still be an important driver and can not be neglected.

Having established the potential for sea ice freshwater fluxes to be modulating trough activity, the relevant regions need to be found. Figure 15 illustrates where the surface freshwater flux correlates with ice shelf basal mass loss. Although the surface freshwater flux does include evaporation and precipitation, sea ice processes over the shelf are dominant (see Figure 14). The correlation map reveals the presence of regions near the ice front with strong positive correlations between surface freshwater flux and basal melt (>0.5). These regions are similar to regions found to relevant for the local surface buoyancy hypothesis (St-Laurent et al., 2015). The results indeed suggest that an increased freshwater flux, related to increased sea ice melt or decreased production, precedes high ice shelf melt. Still, the high correlations are weaker than those in the troughs, suggesting direct control of surface buoyancy on ice shelf melt is a secondary effect, mediating the exposure of the ice shelves to CDW.
Interestingly, these regions are also roughly in the locations where the salinity anomalies, but also convection, seem to originate from (see Figure 12). Water anomalies related to surface processes were found to be advected westward (St-Laurent et al., 2015). Furthermore, the region around Russel Bay shows a strong correlation (>0.5), additional evidence that this region might be sensitive to changes in salinity. The lags for the 60 month running mean plot show that the regions near the coast lead the melt, consistent with the idea of sea ice freshwater being a forcing mechanism, whereas the region near Russel Bay is lagging slightly.

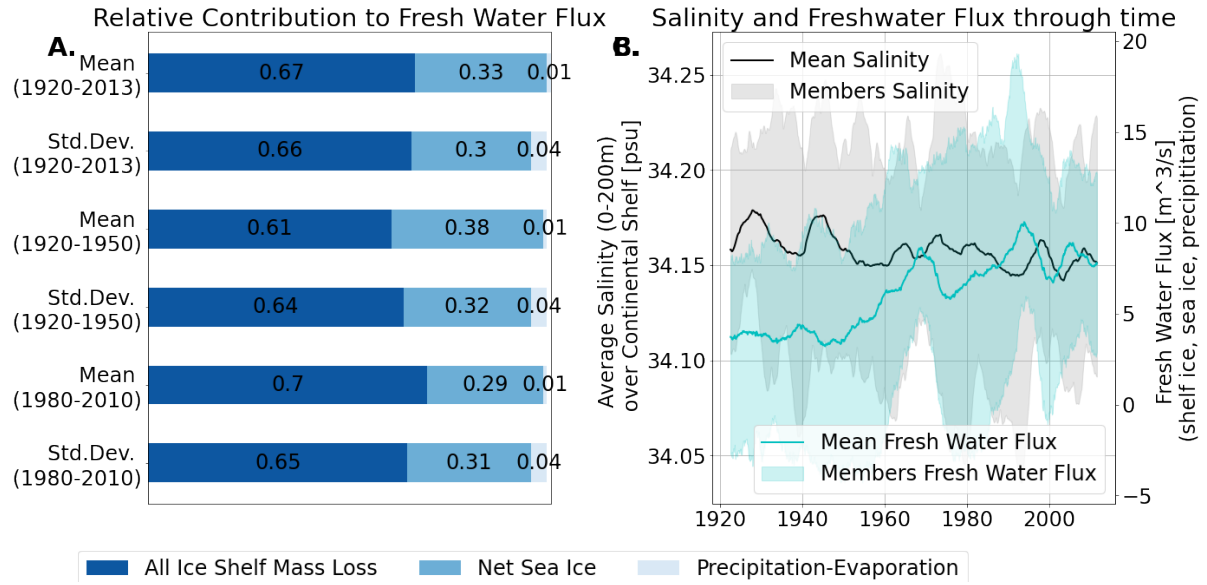

Figure 14: The influence of the freshwater fluxes on the salinity on the continental shelf. A.) The relative sizes of the absolute magnitudes of ice shelf mass loss, net sea ice and precipitation - evaporation. The mean and standard deviation are taken for individual members and then averaged over the ensemble. For the standard deviation, the data was detrended and a 60 month rolling mean was applied. B.) Time series of the total freshwater flux (from ice shelf, sea ice and precipitation and evaporation) (cyan) and the average salinity over the continental shelf at all depths (black). The shaded area indicate the range between the maximum and minimum of all ensemble members.

Sea ice freshwater fluxes arise from brine rejection during growth and freshwater release from melt and can thus both increase and decrease upper water column salinity. This could directly influence the ice shelves, but also indirectly via the baroclinic part of the mechanism as shown in the this chapter. The advected salinity would then affects the isopycnals at the shelf break, which in turn would control the undercurrent and the import of CDW on the continental shelf. The results are also consistent with wind patterns, since sea ice freshwater flux is promoted by southward wind anomalies (Bett et al., 2020). Surface buoyancy could thus be driving a meltwater feedback: a freshwater flux from sea ice in a sensitive region can increase local ice shelf melt via the surface buoyancy hypothesis, leading to a larger total freshwater flux that influences the shelf break currents. However, the growth of sea ice can lead to convection (Bett et al., 2020), since a weaker freshwater flux could lead to a less stable stratification. Although large convective events are not unrealistic, they have not been observed in the Amundsen Sea. The apparent predisposition of the model towards deep convection could mean that this effect might be weaker in reality than in the model, but an analysis where convection events are removed shows that the results are in a limited way affected by it. This increases the confidence in the realism of this part of the mechanism (see Appendix B).

In conclusion, the results in this section suggest that a baroclinic effect could play a role in influencing the undercurrent and thereby driving ice shelf basal melt variability. Furthermore, sea ice processes show a strong relation with ice shelf basal melt. Although the freshwater flux from ice shelf melt is stronger, the effect of sea ice formation on the salinity could influence the ice shelves directly by controlling the exposure to warm water, or indirectly via an effect on density gradients at the shelf break and the undercurrent. The sea ice freshwater flux could be connected to variability of meridional winds on the continental shelf, instead of zonal winds at the shelf break region. The potential bias of the model to convection might meant that the baroclinic mechanism is stronger in the model than in reality.

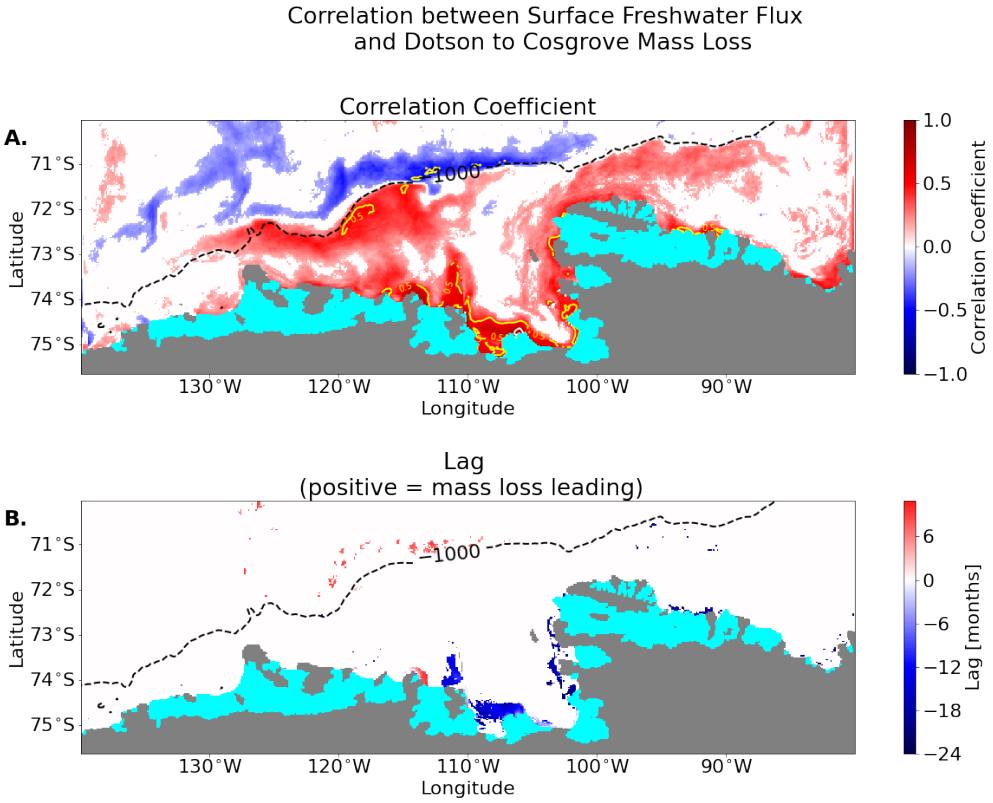

Figure 15: As for Figure 5, but with the correlation between surface freshwater flux and basal mass loss between Dotson and Cosgrove.

4 Far-Field Forcing of the Amundsen Sea

Earlier research identified a connection between the Amundsen Sea shelf break winds and the tropical Pacific (Steig et al., 2012; Holland et al., 2019). To investigate the role of remote processes, the focus is now shifted towards larger scale climatic processes in PACE and how these correlate with the output of the MITgcm model runs. This section is concerned with processes that affect the Amundsen Sea via the atmosphere only, since the usage of the climatology as a boundary condition in the ocean domain removes potential remote forcing via the ocean.

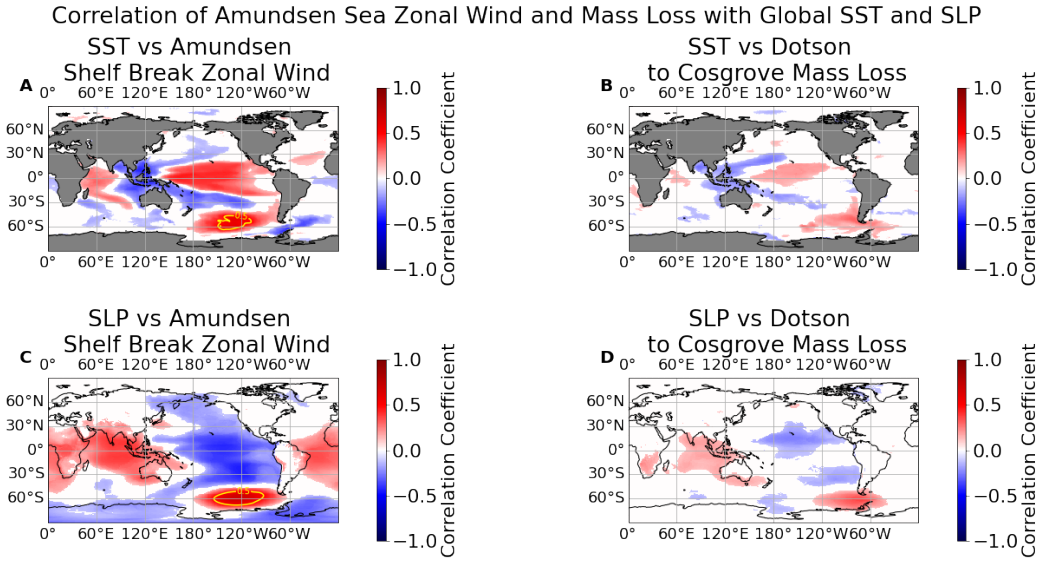

Figure 16: Correlation between between local variables in the Amundsen Sea and global values. A) SST with Amundsen Shelf Break Zonal Wind; B) SST with Dotson to Cosgrove Mass Loss; C) SLP with Amundsen Shelf Break Zonal Wind, D) SLP with Amundsen Shelf Break Zonal Winds. For description of subplots, see Figure 5A. The correlations are only performed with the SST and SLP leading; corresponding lags are shown in Appendix A in Figure 31.

Figure 16 compares how zonal shelf break winds and ice shelf basal mass loss correlate with global sea surface temperature (SST) and sea level pressure (SLP). Although the shelf break winds have stronger correlations than the ice shelf basal melt almost everywhere, the spatial patterns are similar.
For SST anomalies, the strongest correlations globally are found over the southern Pacific, close to the Amundsen Sea. SST changes in this region are related to tropical Pacific variability (Deser et al., 2010; Holland et al., submitted), but the strength suggests a large sensitivity to other local effects.
In the tropical Pacific, both the shelf break zonal winds and ice shelf basal mass loss show strong resemblance to patterns related to ENSO, with positive correlations around the equator and negative correlations in the subtropics. For the ice shelf basal melt, a remarkable difference with the ENSO pattern is an apparent westward shift. At the equator, the positive correlation is located in the central Pacific, but is not extended towards the eastern part of the basin. This shift agrees with ideas that tropical Pacific variability outside of ENSO is affecting the West-Antarctic climate (Ding et al., 2011; Thomas et al., 2015). However, since ENSO variability can be split up into different types, it could also be that basal mass loss is more related to the Central Pacific type (Kao & Yu, 2009).
Remarkably, there is no strong correlation to SSTs in the tropical Atlantic, whereas this also should affect the Amundsen Sea Low (ASL) (Li et al., 2015). The SSTs in the Indian Ocean shows an opposite east-west pattern when correlated with the winds, but this disappears when correlating with ice shelf basal mass loss.

When looking at SLP, both the shelf break zonal winds and ice shelf basal mass loss show positive correlations over the Indian Ocean. Negative correlations are found over most of the Pacific ocean for the zonal shelf break winds, whereas the ice shelf basal mass loss only shows slightly negative correlations over the subtropics in the central and eastern Pacific. There are additional negative correlations over the Ross Sea. The strongest correlations are found close to the Amundsen Sea, exceeding 0.5 for the winds and likely related to the ASL. These alternating positive and negative correlations could point to an atmospheric wave train, showing resemblance to patterns related to Pacific SST forcing (Ding et al., 2011; Holland et al., submitted).

To distinguish the different processes that affect the Amundsen Sea system, we study how well climatic indices in PACE correlate with variables in the MITgcm model (see Figure 17). The shelf break zonal winds have the best correlation with ENSO related indices like the IPO and SOI, as found by Holland et al. (2019). Furthermore, there is a strong correlation with the latitude of the ASL. Other aspects of the ASL show weaker correlations. Similar to Figure 16, the correlation coefficients of the ice shelf basal mass loss are weaker than those of the zonal shelf break wind: in all cases, the spread crosses the 0 line. For most indices, the sign of the mean value is preserved. This suggests that tropical Pacific variability affects the atmosphere in this region, but its effects are greatly weakened by local variability. A further analyses of combining different indices did not lead to a large improvement of correlations (not shown).

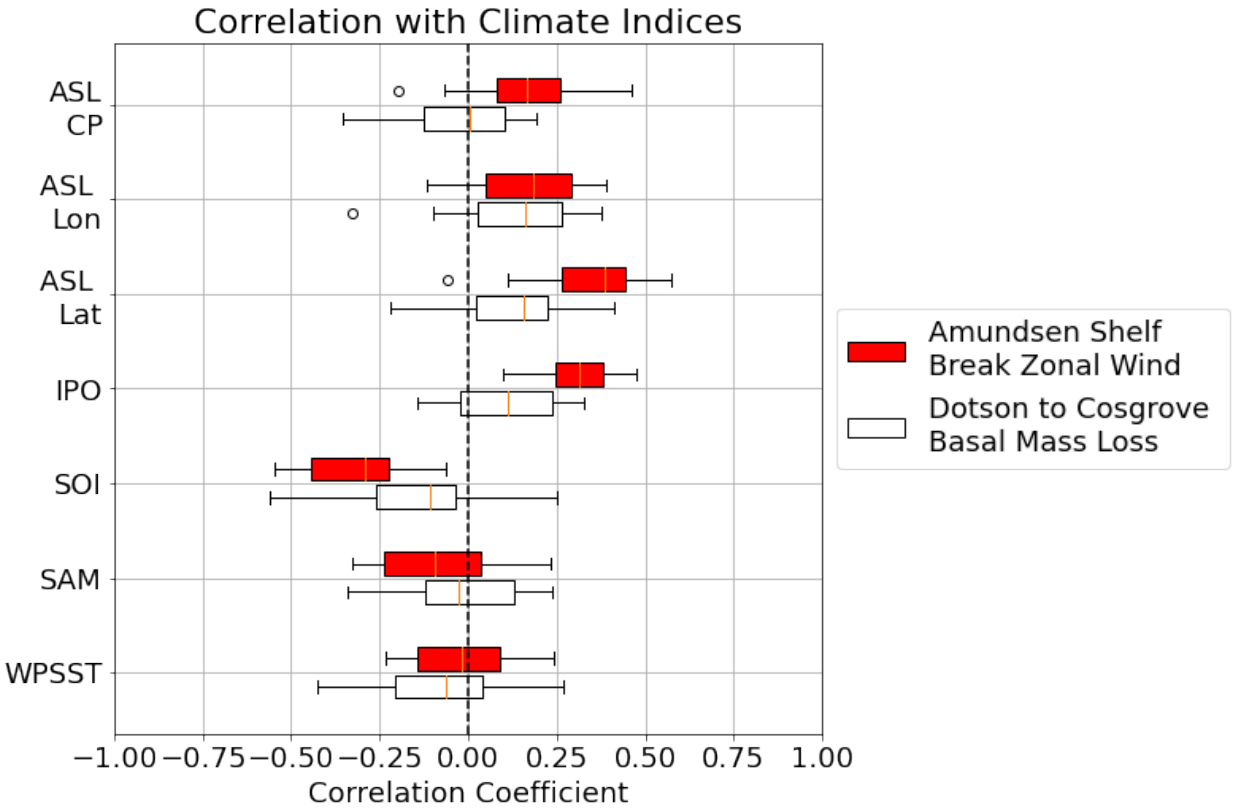

Figure 17: The correlation between different climatic indices with the Amundsen Shelf Break Zonal Wind (red boxes) and the Dotson to Cosgrove ice shelf mass loss (white boxes). The boxes indicate the spread between individual members: the edges of the box are the 1st and 3rd quartile, with the distance between them called the Inner Quartile Range (IQR). The yellow line indicates the median. The whiskers indicate minimum and maximum value of the data within a distance of 1.5 * IQR from the box. Anything outside of this range is an outlier and is indicated by white circles. The black dotted line shows where the correlation is 0.

The connection between the Amundsen shelf break winds and tropical Pacific and ENSO was already well-known in literature (e.g. Steig et al. (2012); Holland et al. (2019)). However, several studies have challenged the connection between the ENSO and ice shelf basal melt, showing no strong correlation (Planchat et al., submitted) or a negative correlation (Silvano et al., submitted) between ice shelf basal melt and the ENSO activity. Our results offer a possible explanation for this apparent discrepancy. They stress that connection between the winds and the ice shelf basal melt is not straightforward, as discussed in Section 3.1. The influence of tropical Pacific variability is clear for the shelf break zonal winds, but weaker for the ice shelf basal mass loss. The correlation maps shown in this section re-establish the connection with the tropical Pacific when looking at the full ensemble (see Figure 16), but there is still a wide spread between members: although most members correlate positively with the IPO, there are individual simulations that show an opposite sign (see Figure 17). A further reason for this can arise from the apparent westward shift of the pattern in the correlation of ice shelf basal melt with the SSTs. Some ENSO indices might not sample the relevant regions that here correlate with ice shelf basal melt, leading to lower correlations. West-Pacific SSTs, derived from a region that affected the Antarctic climate (Thomas et al., 2015), do not show a clear correlation with ice shelf basal mass loss (see Figure 17), so this has probably a minor effect.

In conclusion, this report confirms an influence of the tropical Pacific on the mass loss in the Amundsen Sea on decadal time scales. However, this relationship is relatively weak and the correlations are stronger in the central and western Pacific, thus showing a slightly different pattern than the ENSO.

5 The Influence of Cavity Geometry on Ocean Dynamics and Melt Variability

Ice shelves around the Amundsen Sea have retreated and thinned over the past decades (e.g. Shepherd et al. (2004); Jenkins et al. (2010); Smith et al. (2017)). Since meltwater production is affected by ice shelf geometry (De Rydt & Gudmundsson, 2016) and that ocean circulation is potentially sensitive to ice shelf melt as well (Jourdain et al., 2017; Bett et al., 2020), the present-day situation might not be representative for the early 20th century.

So far, the analysis has been performed on the output of Naughten et al. (2022), who used a model with a present day ice shelf configuration. In this section, new results from additional runs with a different ice shelf geometry are presented. This new geometry has much more advanced grounding line (GL) than the present-day situation. Since the geometry in the early 20th century is likely somewhere in between these two cases, the new runs are used to test the sensitivity of the results to ice shelf geometry and to bound the role that geometry played in influencing the results in the early 20th century. Note that in this section ensemble mean refers to the mean over the 5 members used for the new simulations.

We start by describing the differences in the time-mean state between the runs, followed by a short discussion of the implications for decadal variability. We hypothesize that the smaller ice cavities will lead to a reduction in ice shelf basal melt. Via the ice shelf meltwater feedback, this weakens the density gradients at the shelf break in Russel Bay and leads to a weaker undercurrent. Finally, the expectation is that this will change the periodicity and amplitudes of decadal variability.

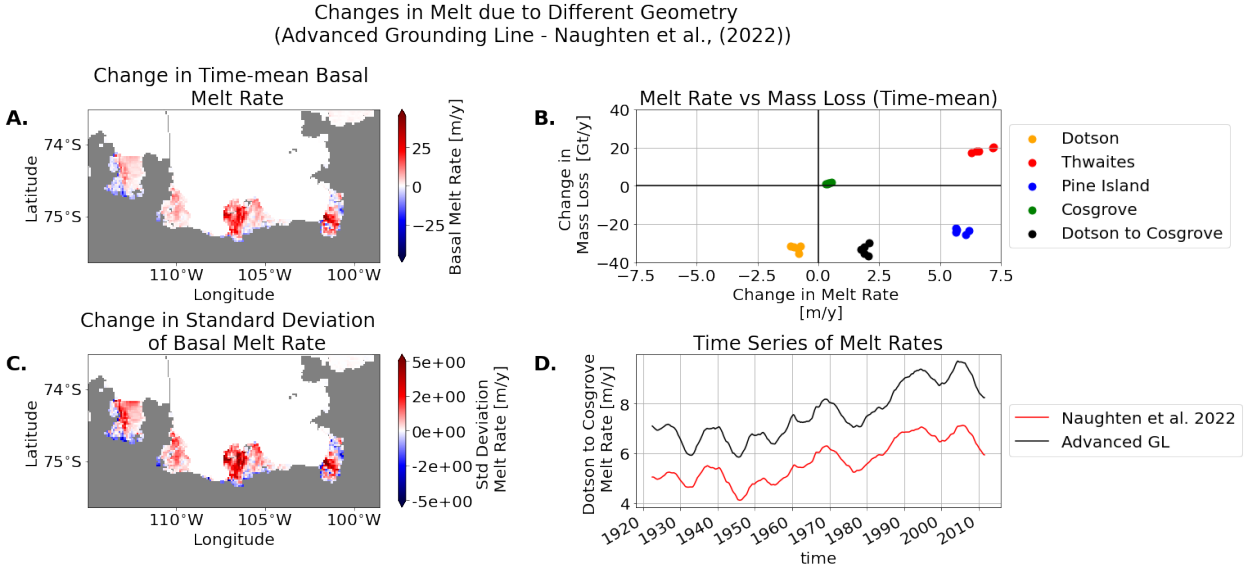

Figure 18: Melt in the simulations with an advanced GL minus those in Naughten et al. (2022). A. The spatial difference in time-mean and ensemble-mean ice shelf basal melt rate. B.) The time-mean change in melt rate vs the time-mean change in mass loss for each ensemble member and different ice shelves. C.) The standard deviation of the ice shelf basal melt rate when applying a 60 month running mean, averaged over the ensemble. D.) The difference in ensemble-mean melt rate for Dotson to Cosgrove through time.

5.1 The Effect on Basal Melt

Differences between the two sets of simulations should be related to the effect of geometry on basal melt or on circulation. Here, we describe how melt has changed.

Figure 18 shows the differences in ensemble-mean basal melt rates between the simulations. The geometry with an advanced GL leads to a higher time-mean melt rate for the Thwaites and Pine Island ice shelves, likely because deeper ice drafts are now exposed to warmer water (see Figure 3). This agrees with observations showing increased thinning for thicker ice shelves with warm bottom waters (Pritchard et al., 2012). The advanced GL reduces the area of the exposed ice shelf, which counteracts the effect of the increased melt rates on the mass loss. The reduction in total mass loss for Pine Island Glacier can likely be attributed to the latter effect dominating.
The Dotson ice shelf is the odd one out, showing both lower averaged melt rates and mass loss. A potential cause of this is the blocked cavity connection between the Dotson and Crosson ice shelves. Associated changes in circulation in the cavity might influence mass loss (Jacobs et al., 2011). Furthermore, it 'shelters' Dotson from what is happening in the eastern Amundsen Sea, potentially cutting off Dotson from the effects of the PIT trough.

The simulations with an advanced GL display slightly more variability in the ice shelf freshwater flux, but this effect is an order of magnitude smaller than the change in mean rates. Some ice that was exposed to cold water could now be within the range of the thermocline, where there might be more temperature variability. However, this effect is small. Around the GL the new simulations show less melt and a lower standard deviation, in contrast with the center of the ice shelves. Near the GL bathymetry was dug down, so these patterns might not be realistic (see Figure 3). Possibly, this deeper seabed leads to stagnation of the waters here.

To summarize, the response in melt rate and mass loss to the advanced GL differs between the individual ice shelves. The net effect is a reduced freshwater influx into the ocean.

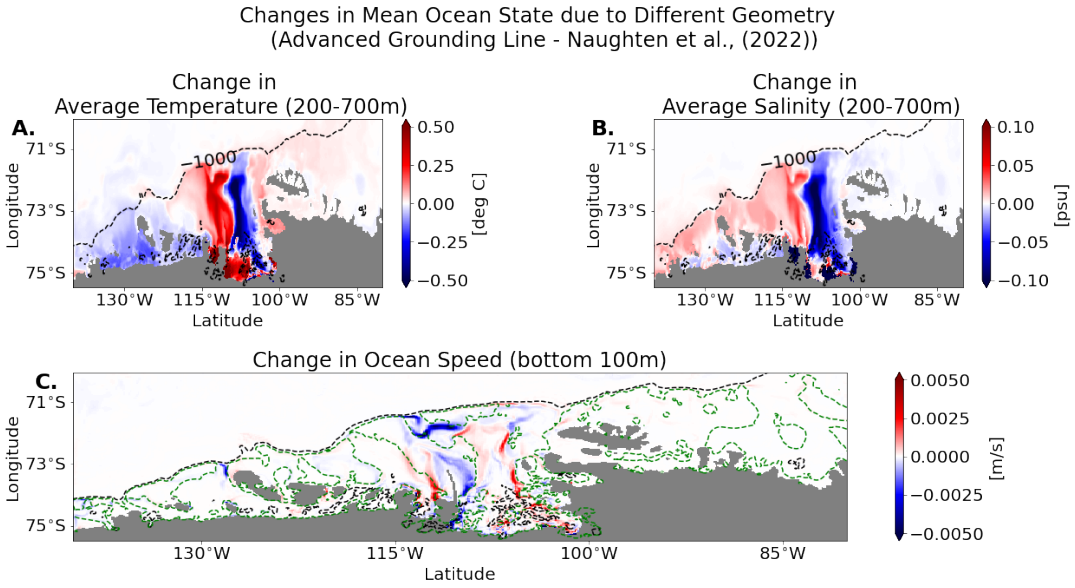

Figure 19: Difference in time-mean and ensemble-mean state of the ocean between runs with the advanced GL and the geometry in Naughten et al. (2022). A.) Change in the temperature averaged over 200-700m. B.) Change in salinity in the same depth range. C.) The difference in speed in the bottom 100m.

5.2 The Effect on Ocean Circulation

The previous section showed that glaciers show substantial changes in the time-mean basal mass loss and melt rates. The mean ocean circulation is likely affected by this reduced meltwater influx. Therefore, it can give us an indication of the importance the ice shelf melt feedback.

Figure 19 shows the spatial difference in mean state of the ocean between the new and old runs. The new geometry leads to a redistribution of the heat and salinity in the mean state. In the 200 to 700m depth range, the heat and salinity in the eastern part of the basin is greatly reduced. The opposite is true for the western part of the basin and around Russel Bay, which experiences increased salinity and increased temperature. Figure 20 shows cross sections taking over the continental shelf and illustrates that the reduced temperature in the eastern part of the basin is related to a decrease in CDW in the troughs. This is indicated by a drop in the 0 deg. C isotherm, a strong temperature decrease at depth and a general decrease in salinity.
The increase in salinity in the west of the basin is mainly contained at the surface. Together with the weaker northward velocities, this suggests that changes here are related to the reduced outflow of meltwater. The reduced meltwater outflow also raises temperatures, especially a bit lower in the water column.

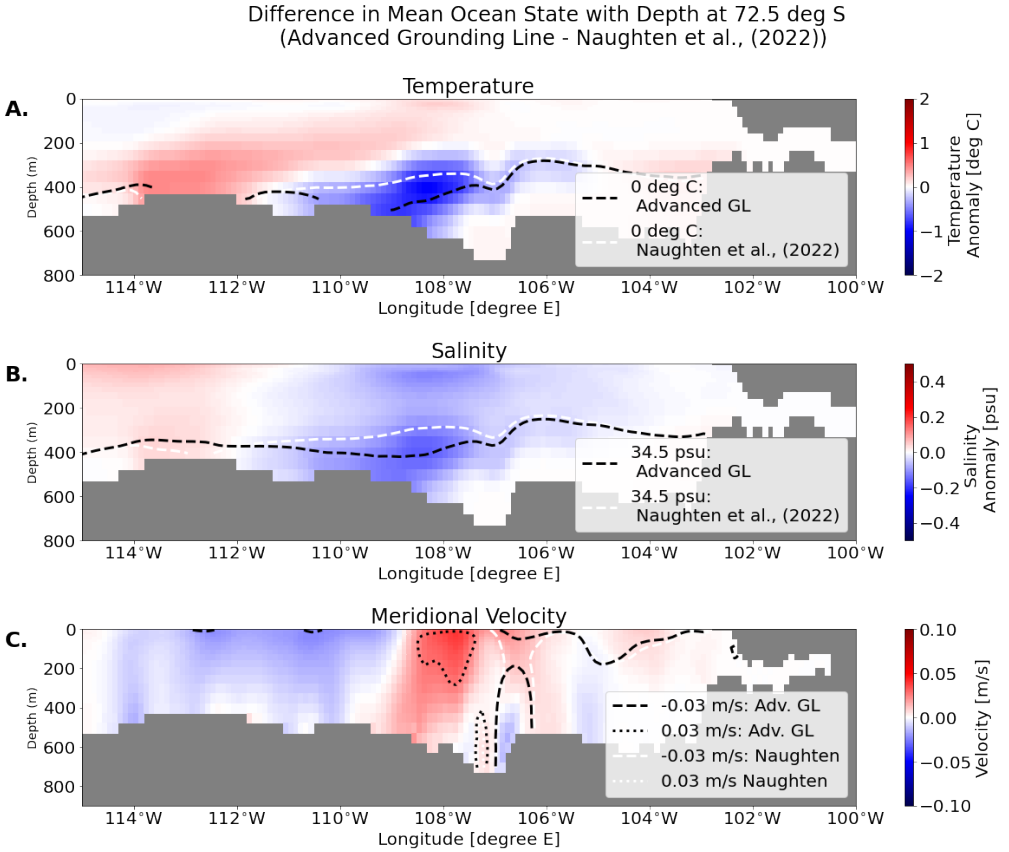

Figure 20: Cross section taken at 72.5 deg S for the time-mean and ensemble-mean state of the advanced GL simulations minus those from Naughten et al. (2022). A.) Temperature change (dashed line shows the new 0 deg C isotherm). B.) Salinity change (dashed lines shows the 34.5 psu line). C.) Change in meridional velocity (dashed lines show -0.03 m/s, dotted lines indicate 0.03 m/s). White lines indicate the mean state in Naughten et al. (2022), the black lines the mean state in the new geometry situation.

How is the large scale circulation affected by these changes? At the PITW inlet and the PITE inlet, the mean speed in the bottom 100m is reduced (Figure 19). This supports the hypothesis and can be attributed to the ice shelf meltwater feedback and associated changes in shelf composition. The strong connection with mass loss for both salinity and baroclinic flow in this region was already noted in Chapter 3 and the new runs show a positive shift in the mean state of salinity and temperature here. The affected horizontal density gradients have lead to weaker flow, which could also be an explanation for the reduced CDW on the continental shelf.

Interestingly, there are regions in the PIT main trough that do experience increased flow. The cross sections show that this could be related to increased baroclinicity (see Figure 20): the new geometry has a faster bottom flow, but a reduce flow around 200m depth in the troughs. This baroclinicity is likely related to the increased east west slope in the CDW (see the 0 deg C isotherm) and vertical shear related to new strong outflow of freshwater at 108 °W (around 200 m depth). This could be a new path for meltwater, but the water in this fresh flux is remarkably slightly warmer than in the old runs. Since there is less meltwater in total, it could also be that the temperature responds more rapidly to mixing with surrounding warmer water. However, an alternative explanation could be a changing cavity circulation. Higher ice shelf melt rates increase the pumping of CDW into the cavity, but only a small fraction of this heat is used for melting the ice (Jourdain et al., 2017). The rest is transported out of the cavity. This stronger cavity circulation would explain the strengthened northward flow at the surface, but also the locally stronger bottom flow in the troughs. Furthermore, Jourdain et al. (2017) demonstrated that it is leads to reductions in sea ice formation, which indeed shows a shift towards an increased freshwater flux (see Table 1).

Variable	**Change in Mean State (Advanced GL-Naughten et al. (2022)**	**Change expressed in Standard Deviations**
All Mass Loss	-42.69 [Gt/yr]	-0.491
Mean Salinity	-0.01547 [psu]	-1.252
Heat Content	1.538 [10^{10} GJ]	0.312
Mean Temperature (200-700m)	-0.007361 [deg K]	-0.048
Sea Ice Freshwater Flux	0.2092 [10^3 m^3/s]	0.223

Table 1: The change in time mean over the Amundsen Shelf for specific variables in the model between the runs with an advanced grounding line and the older runs of Naughten et al. (2022). Middle column shows the absolute change, the right columns shows this change expressed in standard deviations from the older runs when applying a 60 month running mean.

To summarize, the use of a protruded geometry has led to a new equilibrium with reduced meltwater input into the ocean, but possibly a stronger sub-cavity pump. Contrary to the expectations, this leads to a decrease in salinity on the shelf (see Table 1), because the influx CDW into the trough system via the undercurrent is reduced. Temperatures on the shelf in the range of the thermocline have decreased. The total heat content, which considers all depths, is increased, likely due to the reduction in meltwater. This section thus supports the existence of a ice shelf meltwater feedback and thus the sensitivity of the system to changes in salinity.

5.3 Changes in Decadal Variability

The mean circulation in the Amundsen Sea has changed because of the use of a new geometry, as indicated by the previous sections. Here we discuss the decadal variability. Since the atmospheric forcing has remained constant with respect to the old run, changes in the decadal variability can only be related to internal feedbacks within the ocean.

Figure 21 presents an overview of decadal variability in different variables for the old and new runs. Surprisingly, the mean decadal variability in the Amundsen Sea are hardly affected by the protruded geometry, suggesting only a minimal influence of the mean ocean state. Remarkably, this also holds for the sea ice freshwater flux. Although the mean sea ice freshwater flux is slightly increased because of the changed ocean conditions (see Table 1), sea ice variability is thus governed by atmospheric forcing, making it difficult to entangle atmospheric effects mediated by sea ice from direct wind effects.

The redistribution of salinity and temperature in the mean state has also not had an effect on their temporal variability. The variability in these two variables over the continental shelf hardly changes and the melt rate variations between Dotson and Cosgrove are likewise similar. However, this hides smaller scale spatial differences. The amplitude of melt variability in Thwaites and Pine Island Glacier increases in the runs with an advanced GL. This can be related to the ice draft now being in the range of thermocline variations, or because of a nonlinear of changes in cavity circulation to higher melt rates. Since decadal variability in total melt rates only shows a small change, the increase in amplitude of Thwaites and Pine Island Glacier has to be compensated by other glaciers. Part of this seems to be done by Dotson, which shows slightly weaker variability. Furthermore, the timing of maxima and minima appears to show a minor shift, with Pine Island in particular reaching some minima earlier than in the new runs.

In conclusion, although the geometry with an advanced GL has a clear effect on the mean state in the model, it barely influences the large scale decadal variability, contrary to our expectations. This suggests that the periodicity is purely atmospherically forced, which is surprising considering the many possible feedbacks in the domain. Why do we see ice shelf meltwater feedback affecting the mean state, but not in decadal time scale changes? A possible explanation can be a difference in timescale: the feedback can be too slow to respond to faster changes in the forcing, but it could also be too fast: the system could always be in balance with respect to longer term decadal forcing. The lack of large scale changes hide smaller scale local variability, with some ice shelves showing larger variability.

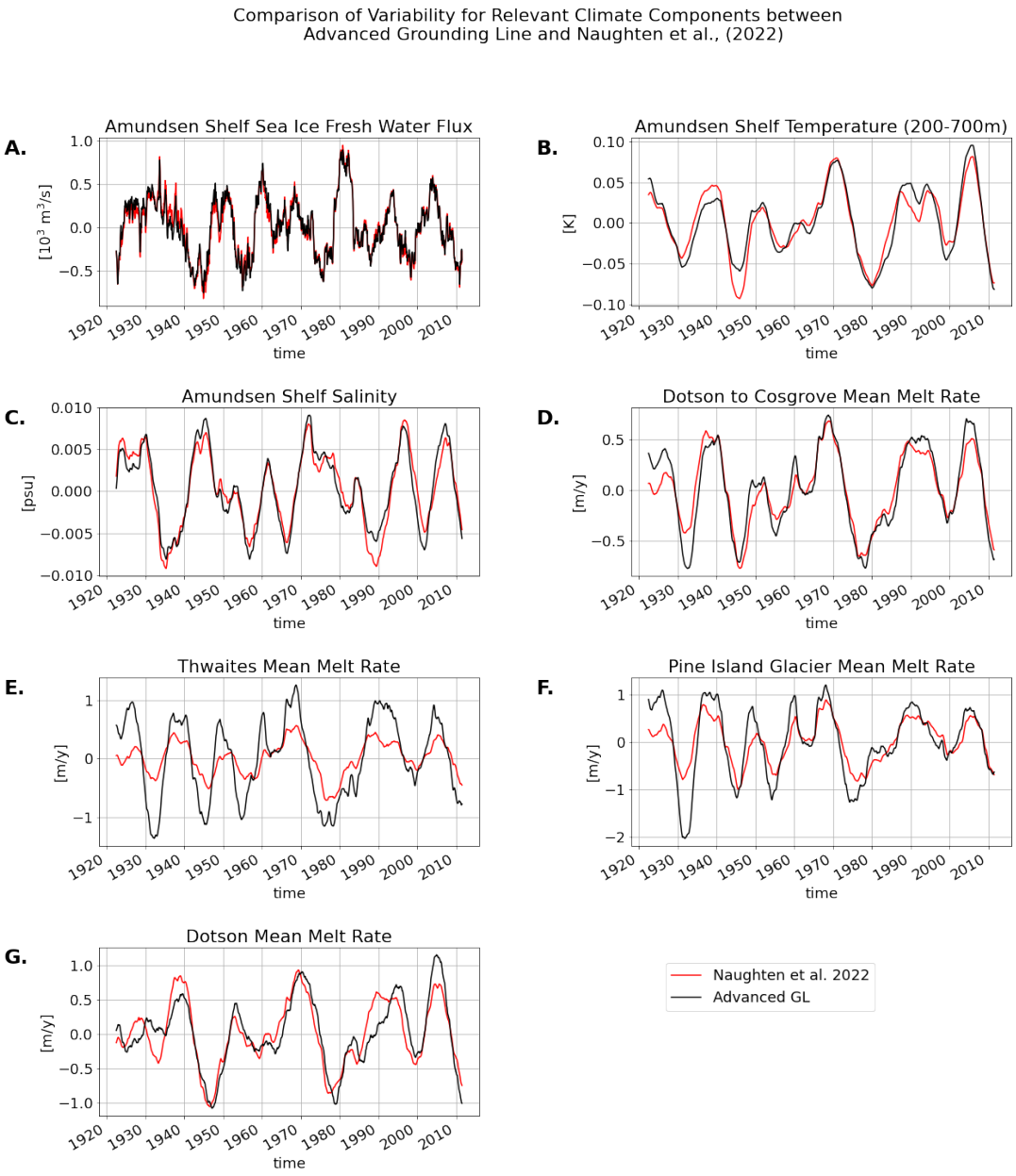

Figure 21: Detrended time series showing for different components the mean over the 5 members in the new geometry (black) and the old geometry (red). Everything is detrended and a 60 month running mean was applied. A.) Sea ice freshwater flux. B.) The average temperature over the Amundsen Shelf between 200-700m. C. The averaged salinity over the whole shelf. The last plots show the mean melt rate for Dotson to Cosgrove (D.), Thwaites (E.), Pine Island Glacier (F.) and Dotson (G.).

6 A Case Study of the 1940s

The early 1940s witnessed a strong El Niño event (Brönnimann et al., 2004). Observational evidence suggests that this could have had an impact on the Amundsen Sea (Schneider & Steig, 2008; Smith et al., 2017). Since the model run by Naughten et al. (2022) is constrained by historical external forcing and tropical Pacific SST anomalies, we can look at the output as a case study to investigate the potential for such a large scale melt event to occur.

In this section, we conduct a case study for the 1940s. The goal is two-fold: to describe how the mechanisms from the previous chapters affect the model spread through time and to see if there is a possibility for a strong 1940s ice shelf melting response.

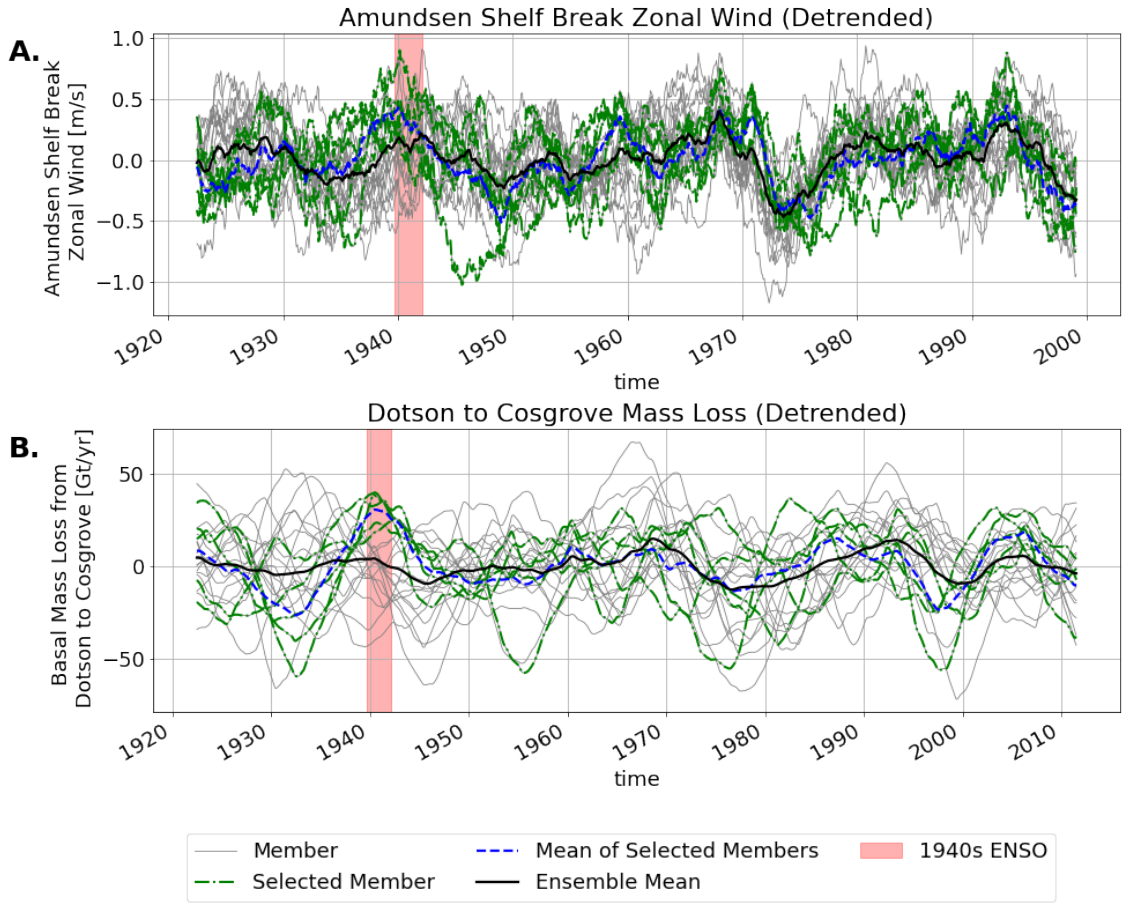

Figure 22: Detrended ensemble mean time series of zonal shelf break winds (A.) and basal mass loss from ice shelves between Dotson and Cosgrove (B.). The black line shows the ensemble mean. Gray lines show individual ensemble members. The blue lines are individual ensemble members selected based on a strong response in the 1940s, whereas the red line shows the mean of these selected members. A 60 months running mean was applied. The red shaded area shows the duration of the 1940-1942 El Niño event, showing the duration given by Brönnimann et al. (2004) (Autumn 1939- Spring 1942).

6.1 The Model Response in the Ensemble Mean

This section investigates how the ensemble mean of the model runs responded in the 1940s to see if it follows the shelf break wind hypothesis. Based on this mechanism, we expect that the strong ENSO event should have led to a strong positive zonal wind anomaly and a related positive ice shelf basal melt anomaly.

Figure 22 presents the anomalies in shelf break winds and basal mass loss for through time, both for individual members and for the ensemble mean. A small positive excursion in the zonal winds over the shelf break is indeed shown in the ensemble mean during the 1940s (see Figure 22A). This agrees with earlier findings of a positive correlation between the IPO and the PACE zonal shelf break winds (Holland et al., 2019). However, this positive excursion is not exceptionally large compared to other excursions in the record. Stronger positive excursions occur around 1970 and 1995. Furthermore, variability between members is large compared to the variability of the ensemble mean.

In contrast to the zonal winds, the ensemble mean of the ice shelf basal mass loss fails to show a melt anomaly in the 1940s, contrary to the expectations (see Figure 22B). The lack of a strong response in model melt and ocean heat content in the Amundsen Sea was already noted by Naughten et al. (2022). The ensemble-mean basal melt is smoother than the ensemble mean of the zonal winds and variability between members is clearly larger than the variability within the ensemble mean itself. The large variability between ensemble members suggests that the record is not dominated by the constrained tropical variability, but that natural variability and local differences are more important.

Similar to what we have seen with the zonal winds, the largest positive melt excursions occur not in the 1940s, but around 1970 and 1995. These latter two excursions are consistent with the historical record. Both satellite observations (Jenkins et al., 2010) and sediment cores (Smith et al., 2017) have suggested that Pine Island Glacier retreated from a submarine ridge in the early 1970s. Furthermore, satellite observations showed both strong thinning in the Amundsen Sea sector between 1992 and 2001 (Shepherd et al., 2004) as well as an acceleration of Pine Island Glacier in 1996 and 2000 with respect to 1992, but not between 1994 and 1992 (Joughin et al., 2003).

This apparent agreement with the observational record later in the century increases the confidence in the realism of the model, while at the same time making it more remarkable that the 1940s do not show a similar response. These recent cases thus support the shelf break wind hypothesis, but the 1940s do not.

6.2 Variability within the Ensemble for the Amundsen Sea

Although the ensemble mean fails to show a strong melt anomaly, there are individual members that do show a positive melting excursion in the 1940s (see Figure 22). Their response has to be mediated by other factors outside of the ENSO and in this section these high melt members (HMMs) are used to identify what other conditions have to be met to create a high melt response is.

In Figure 23, the mean of 5 high melt members (HMMs) is traced back to other components of the climate system and compared to the ensemble mean. Interestingly, in all time series there is a deviation from the ensemble mean around the 1940s event. First, we focus on the forcing. Both the normal and cumulative zonal shelf break winds show a further positive excursion for the HMMs, on top of the smaller anomaly in the ensemble mean. However, their timing is shifted, with the normal zonal shelf break wind reaching a maximum before the 1940s and the cumulative winds slightly later.
The inner shelf meridional winds show limited variability in the ensemble mean in the 1940s. The variability in the HMMs is stronger: in the 1930s, the meridional winds on the inner continental shelf experience a strong southward anomaly, slightly earlier than the eastward anomaly in the zonal winds. This leads to a minimum in the HMM cumulative meridional winds timed exactly during the 1940s event.

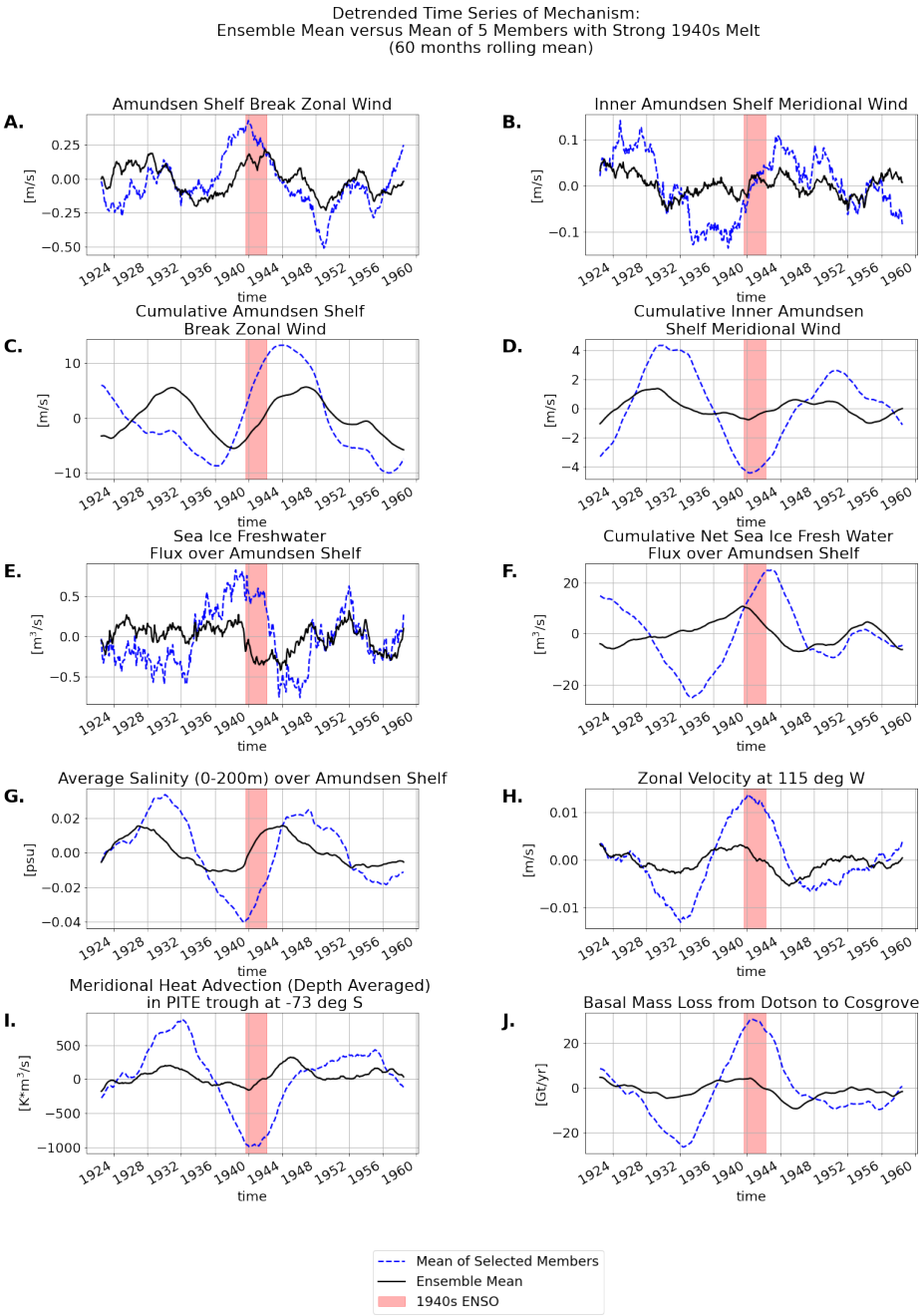

Figure 23: Detrended time series of variables that are indicative of the mechanism discussed in previous sections. Each time the ensemble mean is shown (continuous line) as well as the mean over the 5 members that show strongest 1940s response (blue dotted line). The red shaded area shows the duration of the 1940-1942 El Niño event, showing the duration given by Brönnimann et al. (2004) (Autumn 1939- Spring 1942). A 60 months running mean was applied to all time series. A.) Zonal winds averaged over the shelf break region; (B.) Meridional winds averaged over the inner Amundsen Sea continental shelf; C.) Cumulative anomaly in the zonal shelf break winds; D.) Cumulative meridional inner Amundsen Shelf winds; E.) Total freshwater flux on the Amundsen Sea continental shelf; F. Cumulative freshwater flux on the Amundsen Sea continental shelf; G.) Averaged salinity (0-200m) over the Amundsen Shelf; H.) Zonal undercurrent at 115 °W; I.) Meridional depth averaged heat advection in the PITE trough (note: negative is towards the south!); J.) Basal mass loss from ice shelves between Dotson and Cosgrove.

Having characterised the winds, the focus turns to the sea ice freshwater flux on the Amundsen Shelf. The ensemble mean shows a stark drop in the freshwater flux, exactly during the 1940s. The HMMs on the other hand show an increased flux, starting from the late 1930s, continuing until the end of the ENSO event. The HMM cumulative freshwater influx from sea ice also shows a positive anomaly, reaching its maximum sligthly after the ENSO event. The average salinity in the top 200m over the Amundsen Shelf shows a rise during the ENSO event. The HMMs show a similar pattern, but the minimum before the ENSO event is stronger. The anomaly remains negative until after the event. To summarize the last plots, the HMMs show a stronger undercurrent and more heat advection through the troughs compared to the ensemble mean. They both reach their maximum slightly earlier than the strong positive mass loss anomaly for the HMMs.

The observed patterns in this figure remain similar when studying the response of high melt members in the 1990s or after removal of convection, which is used as a second case study to illustrate that the mechanism do not only apply to the 1940s (see Figure **??** in Appendix A and see Appendix B).

These results contain elements of mechanisms discussed in previous chapters. In line with the shelf break wind hypothesis, the high melt members show an additional positive zonal wind excursion. This could suggest that the smaller anomaly in the ensemble mean is not strong enough to cause a large melt event by itself. Furthermore, the HMM zonal wind anomaly begins earlier than the anomaly in the ensemble mean. This shift in time could indicate that only one El Niño event is insufficient and that longer SST anomalies are important. This is likely affected by the use of a 5 year running mean, which is longer than individual El Niño events. Interestingly, a paleo-reconstruction seems to point to a long term zonal wind anomaly, but it is difficult to quantitatively compare this with our results (Holland et al., submitted).

There are also elements showing a potential role for surface buoyancy. Compared to the ensemble mean, the HMMs show an increase in the sea ice freshwater flux, which lasts throughout the 1940s event. Since sea ice is affected by meridional winds, the anomaly in the surface freshwater flux could be reated to the strong negative anomalies in the HMM meridional wind (Bett et al., 2020). Interestingly, the HMM cumulative meridional wind reaches a minimum exactly during the 1940s event. Contrary to the zonal winds, the meridional wind does not already show an anomaly in the ensemble mean. This new anomaly is thus a distinguishing factor for the HMMs.
Based on the increased ice shelf melt and sea ice freshwater flux, it is not surprising that the HMM salinity shows an additional negative excursion. However, the timing of this excursion before the 1940s event is remarkable. During the 1940s event, the HMM salinity increases, even though the ice shelf basal mass loss increases as well. The difference could be due to the increased CDW influx and associated internal mixing with shallower waters, which might be more important for salinity than the freshening from meltwater. The baroclinic mechanism could thus also be a negative feedback: before a high melt event, the water on the continental shelf is relatively fresh, which increases the baroclinic component of the undercurrent. This leads to more CDW import on the shelf, increasing both the melt and the surface salinity through mixing, which could again reduce the CDW influx.

Many anomalies in the HMMs for the 1940s are preceded by an anomaly with an opposite sign in the early 1930s. This effect is already present in the wind forcing and is not thus directly related to internal ocean circulation. Rather, it might mean that conditions with large melt are triggered by favourable conditions for low melt, 'forcing' a negative feedback response.

To conclude, the ENSO event and the ensemble mean zonal wind anomaly appear insufficient to cause a large scale melt event, contrary to our expectations. The strong excursions for the HMMs in other variables again suggest that the shelf break wind mechanism is likely heavily mediated by other processes, which are not directly affected by tropical Pacific variability in the model.

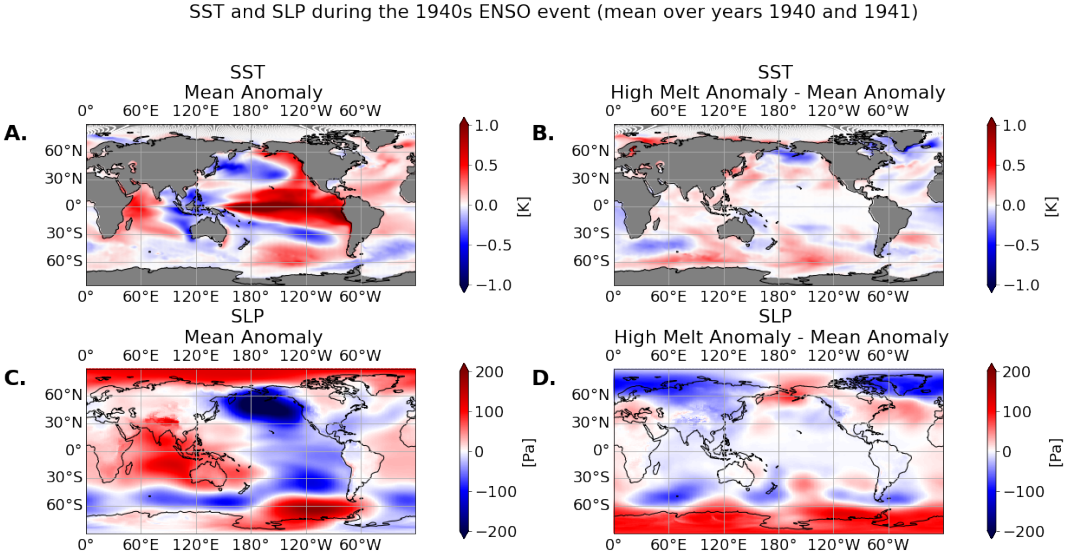

Figure 24: Sea surface temperatures (SST) and pressure at sea level (SLP) anomalies during the 1940 and 1941. A.) Ensemble mean SST anomaly. B.) SST anomaly in HMMs - ensemble mean anomaly. C.) Ensemble mean SLP anomaly. D.) SLP anomaly in HMMs - ensemble mean anomaly

6.3 Far Field Forcing in the 1940s

The previous chapters suggested that the Amundsen Sea sector is also influenced by larger scale and remote processes. In this section, their behaviour during the 1940s ENSO event is studied.

Figure 24 shows SST and SLP anomalies in the 1940-1941 and as expected, global climate is heavily influenced by a strong El Niño. Along the equator of the Pacific, strong positive SST anomalies can be found, whereas around the Maritime Continent and over the subtropical West-Pacific negative anomalies can be seen. The SLP shows higher pressures over the Indian Ocean and lower pressure in the Eastern Pacific. Furthermore, there is a positive SLP anomaly over the Amundsen and Bellinghausen Seas. Both the SST and SLP patterns are similar to the correlation maps in Figures 16. A clear difference is the strong negative SLP anomaly close to the Bering Strait.

To find an explanation for the differences between the individual members, the HMMs are again compared with the ensemble mean anomaly (see Figure 24B and D). By definition, SST anomalies in the eastern tropical Pacific remain the same. In the HMMs, the SSTs are slightly more positive than the ensemble mean over most of the Southern Ocean. Further weak positive anomalies are found around Indonesia, thus weakening the pattern in the ensemble mean. The SLP in the HMMs shows stronger deviations from the ensemble mean than the SST: the SLP is generally more negative over the Arctic, but especially more positive over Antarctica, resembling patterns of negative SAM (Fogt & Marshall, 2020). This also means that it contributes extra to the weakening of the ASL. Around 50 °S, there is an alternating pattern with positive and negative anomalies visible. This appears to be the pattern of an atmospheric feature called zonal wave 3, which influences sea ice in the Amundsen Sea (Raphael, 2007). In other regions, it seems to slightly counteract the ensemble mean patterns, such as over the Indian Ocean, the Bering Strait and the Northern Atlantic.

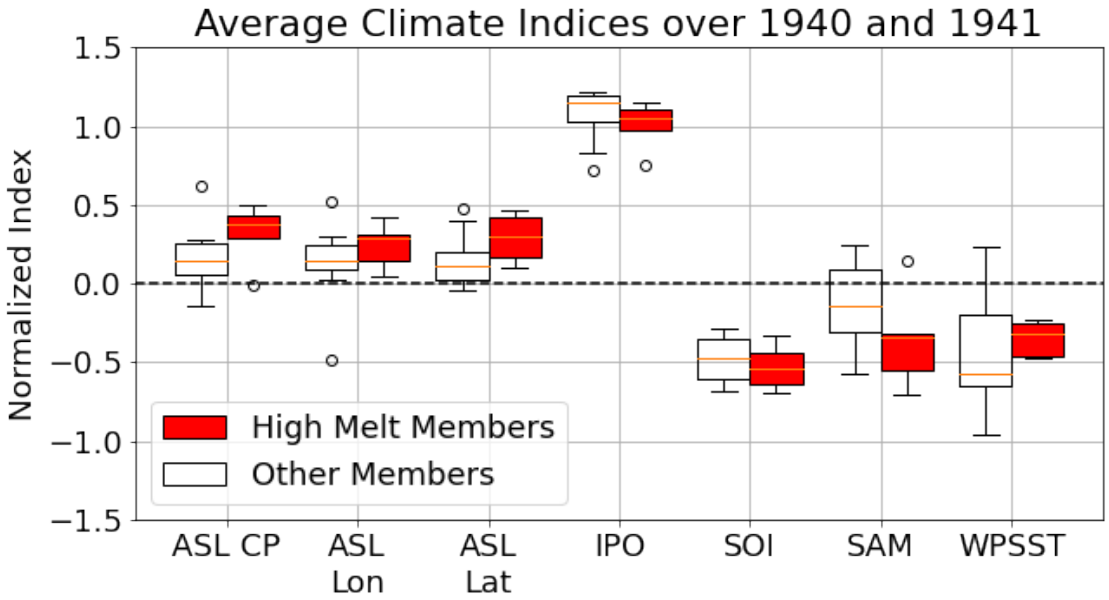

Figure 25: Distribution of climate indices between ensemble members, averaged over 1940 and 1941. Red boxes shows the 5 high melt members, white boxes show the other members. All indices are normalized by subtracting the time mean and dividing by the standard deviation. Meaning of the box sizes as in Figure 17.

Because of the pattern shown here, we expect that these HMMs also have different values for SAM and the ASL indices. Figure 25 shows the anomalies in climate indices for the 1940s. For the HMMs, the ASL has a higher central pressure than in the ensemble mean. The boxes and whiskers do not overlap, except for 2 outliers. The ASL is also slightly shifted north and east for the HMMs, but this is still within the range of the rest of the ensemble. The SAM of the HMMs is slightly more negative, but again still within the spread of the other members. However, the observed positive shifts in latitude and central pressure of the ASL could also be related to the lower SAM values (Turner et al., 2013).
ENSO indices such as the IPO and SOI do not show a clear anomaly. This is to be expected, since the SSTs were fixed between the members.

These findings indicate that the likelihood of the occurrence of a strong melt event in the 1940s is mainly mediated by regional atmospheric factors. Whereas the HMMs do not experience a strengthening of the ENSO pattern in the western Pacific, they do show further weakening of the ASL and further positive SLP anomalies over the Antarctica and SST anomalies over the Southern Ocean. The is corresponding with slight shifts within the ASL indices and the SAM. Interestingly, the anomalies in the HMMs show resemblance to a proxy-based reconstruction over the last century, which suggested that the 1940 likely did experience a negative SAM excursion and a positive pressure anomaly (O'Connor et al., 2021). Ice cores also provide evidence for strong anomalies in the regional Antarctic climate (Schneider & Steig, 2008), further increasing the likelihood of a large melt event in reality.

6.4 The Role of Ice Shelf Geometry in the 1940s

The ice shelf configuration in the 1940s was likely different from that of today. To study the role geometry could have played in the 1940s, we use the runs with the advanced grounding line as an extreme case. Figure 26 compares the HMMs and low melt members in these newer runs to their counterparts with the present-day configuration.

Although the new geometry hardly affects the mean heat content and the size of melt anomalies, the absolute melt rates are different for individual glaciers. For Thwaites and Pine Island Glacier, the difference made by the new geometry on the melt rate is so large that the low melt members still show higher melt rates than the high melt members in the old runs. For the Dotson ice shelf, the melt is reduced.

To the author's knowledge, the ice sheet response for the 1940s has only been reported for Pine Island Glacier (Smith et al., 2017). The results here show that this glacier in particular might have been more vulnerable, since an advanced grounding line leads to higher melt rates than at present. Furthermore, the amplitude of melt rate variability has generally increased for these glaciers compared to the old simulations (see Figure 21 in Section 5), although it is less clear for the 1940s. This would lead to an amplification of the response to temperature anomalies. Based on these results, it is plausible that Thwaites also showed a strong 1940s response.

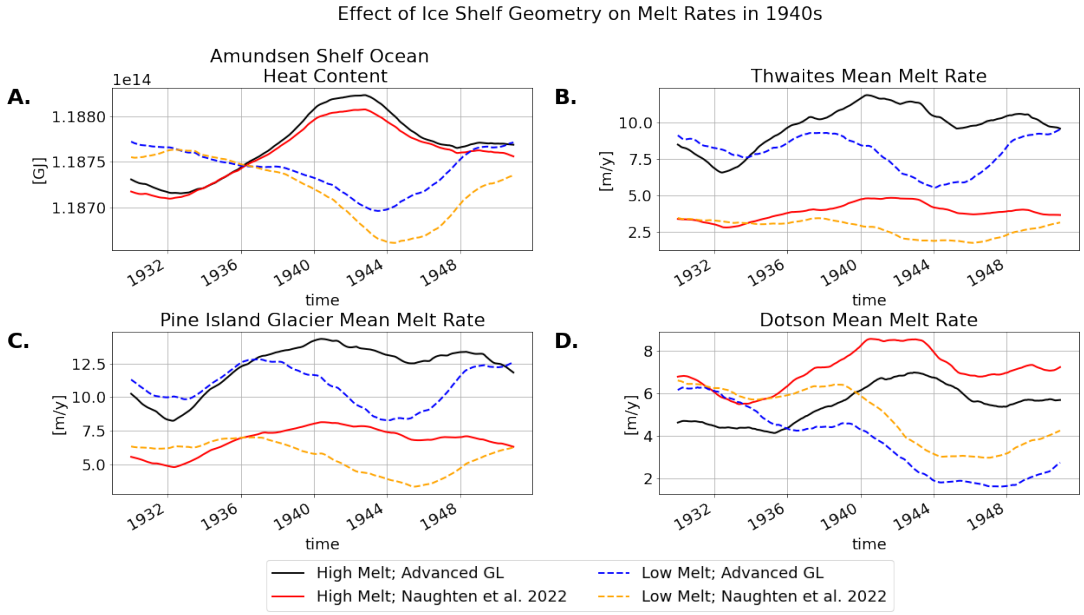

Figure 26: Melt rates and heat content compared between runs with new geometry and the old geometry from Naughten et al. (2022). A.) The ocean heat content, averaged over the Amundsen Shelf. B.) Mean melt rate of Thwaites. C.) Mean melt rate of Pine Island Glacier. D.) Mean melt rate of Dotson. Black continuous line shows the high melt members (6,10) of new run; red continuous line depicts the high melt members of Naughten et al. (2022); blue dashed line illustrate the low melt members (11,12) of new run; the low melt members of Naughten et al. (2022) are shown in orange dashed lines.

To summarize, the results in this chapter show that there is a possibility for a strong ice shelf melt event in the 1940s, but that it is not purely caused by the ENSO event itself. The members that do show this, have stronger zonal wind excursions, but these are mediated by regional and local conditions in the atmosphere and ocean. Some of these conditions appear to be in line with paleo-reconstructions, increasing the likelihood of a large melt event. In addition to this, Pine Island Glacier specifically might have been extra sensitive to such an event compared to the present-day situation.

7 Discussion

This study set out to identify the physical mechanisms controlling decadal variability in ice shelf basal melt for the Amundsen Sea. Previous chapters each dealt with a specific part of these. In this section, these separate components will be integrated, focusing on the wider implications of the results.

7.1 The Drivers of Ice Shelf Basal Melt

This study started by comparing several hypotheses in literature for controlling ice shelf basal melt, namely the shelf break wind hypothesis and the surface buoyancy hypothesis.

The first driving mechanism that was investigated was the shelf break wind hypothesis (see Section 3.1). The dominant narrative in literature suggests a positive connection of ice shelf basal melt with heat transport (e.g. Thoma et al. (2008); Kimura et al. (2017)) and with shelf break winds (e.g. Thoma et al. (2008); Dutrieux et al. (2014); Naughten et al. (2022)). However, several papers fail to find this last positive connection (Wåhlin et al., 2013; Silvano et al., submitted; Planchat et al., submitted). As expected, our simulations showed a strong relationship between heat advection in the troughs and ice shelf basal melt. Furthermore, there was also a statistically significant positive correlation between ice shelf basal mass loss and zonal shelf break winds when averaging over the ensemble. However, this correlation was relatively weak compared to the correlation with heat advection and individual members showed considerable deviations from the ensemble mean pattern, including even negative correlations over almost a century of simulation. The range in relationships for individual members shows similarity with the range of conclusions in publications. Furthermore, literature shows there is a positive correlation between ENSO and the Amundsen Shelf break winds (Steig et al., 2012; Holland et al., 2019). The connection between the ice shelf basal mass loss and ENSO thus hinges on the shelf break winds. It is therefore not surprising that conclusions about the connection between melt and the wind translate directly into the conclusions about melt and ENSO, both in the present study (see Section 4) and in literature (Steig et al., 2012; Planchat et al., submitted; Silvano et al., submitted).

Keeping these new results in mind, it is worth reflecting on conclusions drawn in earlier research. Most model runs in studies on the connection between wind and melt span only several decades (e.g. Thoma et al. (2008); Silvano et al. (submitted); Planchat et al. (submitted); Kimura et al. (2017)). This could mean that the low number of decadal oscillations affected the statistical significance for the conclusions. Our simulations, however, show that for a few ensemble members negative correlations persist even after nearly a century, indicating that this spread is not solely due to short time intervals. Rather, local factors are likely important, which either mediate the shelf break wind mechanism or happen to correlate with the winds, but are otherwise independent. An example of the latter could be the on-shelf meridional winds, since on a regional scale both zonal and meridional winds are affected by the longitude of the Amundsen Sea Low (Turner et al., 2013).

Our suggestion that it is not just the short time span leading to the spread in correlations also challenges longer term connections with the winds. Naughten et al. (2022) found statistical connections between long term trends in winds, undercurrent velocity and an associated thermocline rise and ice shelf basal melt increase. Based on the shelf break wind hypothesis, they inferred a causal relationship. However, they also found trends in other variables. Near the coast, the surface freshwater flux showed positive trends, leading to local surface salinity decrease. Furthermore, meridional winds had southward trends over parts of the continental shelf. These other processes all correlate with increased basal mass loss and could be affecting the trend in the melt. Although the shelf break wind connection was statistically significant, there might be some uncertainty about the implied causal relationship.

To summarize, it does not appear that the shelf break winds are the sole driver of decadal variability in ice shelf basal melt in our model. These results should warn researchers to be careful when using both the zonal winds and tropical indices as proxies for ice shelf melt in the Amundsen Sea region. It is important to use restraint when interpreting correlation as causation. The results also highlight the usefulness of model ensembles in addressing uncertainty when the observational record is short.

A second hypothesis that was investigated concerned the local role of surface buoyancy in destabilizing the water column, leading to erosion of the CDW layer. The surface freshwater flux in the model indeed correlated with ice shelf basal mass loss (see Figure 15 in Section 3.2), in agreement with earlier work on on-shelf surface processes (St-Laurent et al., 2015; Webber et al., 2017). However, this is likely not the main driver for mass loss, since the relationship with PIT heat advection is significantly stronger than with the surface freshwater fluxes. By controlling the exposure of the ice shelves to CDW, surface buoyancy can be a mediating factor and is likely most important on a local scale: both St-Laurent et al. (2015) and Webber et al. (2017) focused only on local effects on Pine Island Glacier. The role of surface freshwater fluxes could be inflated in the model by a potential bias towards deep convection. This could prioritise stable stratification of the water column as a precondition for basal mass loss. Still, the correlation patterns remain largely unchanged when removing periods of convection, suggesting this is not a dominant factor (see Appendix B).

Whereas this report downgrades the role of both the shelf break winds and the surface buoyancy in driving the melt, new emphasis is placed on the role of baroclinicity and the internal circulation in the Amundsen Sea (see Section 3.2). This study shows similarities to Planchat et al. (submitted). Both highlight the importance of salinity changes at the shelf break around Russel Bay and suggest that these are affected by on-shelf circulation. We suggest this leads to variability in the baroclinic component of the undercurrent in the western shelf break. The baroclinic component co-varies with ice shelf basal mass loss, similar to results from Silvano et al. (submitted).
The main differences between this report and the latter study can be found in the forcing. Silvano et al. (submitted) suggest that local winds are driving the baroclinic undercurrent. Although we find that local effects such as surface freshwater fluxes at Russel Bay can play a role, we suggest that density anomalies are mainly imported from the continental shelf.
Baroclinicity is thus sensitive to changes in ice shelf melt and might be more important as a feedback than as the driver of melt. Furthermore, decadal variability is not affected by changes in the ocean and thus appears to be controlled by the atmosphere (see Section 5).

If it is not the shelf break winds or the surface buoyancy, what else could be driving the ice shelf basal mass loss in the Amundsen Sea? The simulations can not provide a definitive answer, but allow us to speculate.

First, small scale variations in surface stress could be important. Large scale zonal wind is only one contributor to the surface stress, which is how the atmosphere physically drives ocean flow. Aside from the zonal wind, the surface stress is influenced by meridional wind and sea ice. Flow in the PIT trough appears to be better correlated to the total surface stress curl than to zonal winds, suggesting considerable influence of these latter processes (Kimura et al., 2017). Unfortunately, local surface stress curl is spatially heterogeneous, making it difficult to test this in observations. High resolution ocean models can contribute to our understanding of this process.

Second, a relatively small anomaly could trigger one of several internal feedbacks, such as those related to shelf break salinity and baroclinicity. Potential feedbacks include a positive ice shelf meltwater feedback, in which the ice shelf meltwater is advected to the shelf break, strengthens the meridional density gradients and increases the baroclinic component of the shelf break undercurrent, leading to an increased CDW influx. This effect, which depends on the total quantity of meltwater, could be further strengthened by the cavity pump, which depends on melt rates: higher melt rates lead to an additional import of CDW into the cavity Jourdain et al. (2017). The increased melt rates make it likely that the cavity pump plays a role in our runs with an advanced grounding line, but the ice shelf meltwater feedback related to decreased mass loss is probably present as well, making it difficult to separate the two effects (see Section 5). Negative feedbacks are also possible: we see that in the HMMs, salinity in the top 200m increases when mass loss increases (see Figure 23 in Section 6). Possibly, the increased pumping of CDW by the high melt rates could increase salinity in shallower waters over the continental shelf, either via internal mixing or via a shift in the location of fresh outflow currents, leaving relatively dense water behind. This water with an increased salinity could then weaken the meridional density gradients at the shelf break, decreasing the influx of CDW.

What kind of trigger could start these feedbacks? On-shelf processes such as sea-ice and meridional wind could be a possible candidate. Density anomalies from sea ice could be transported by the mean circulation,

which has been shown to happen locally (St-Laurent et al., 2015), but they could also influence local melt rates and the sub-cavity pump. Sea ice itself is again affected by changes in the cavity circulation, possibly amplifying its role (Jourdain et al., 2017).
Triggers for this system do not necessarily have to originate in the Amundsen Sea. Both the shelf break undercurrent and melt rates could also be triggered by the influx of temperature or salinity anomalies via the coastal current, possibly originating from the Bellinghausen Sea or even further away. For example, freshwater anomalies from the Antarctic Peninsula can affect the stratification and melt in the Amundsen Sea (Flexas et al., 2022). The coastal current can also provide a new connection to shelf break zonal winds, since they affect bottom flow in the Bellinghausen Sea (see Figure 7).

Finally, there might not be one clear driver of the ice shelf basal melt. Rather, different forcing and feedback mechanisms could play a role at the same time, sometimes resonating and causing strong melt. A large melt event in the 1940s could then arise from a 'perfect storm'. Still, the fact that decadal variability in our model does not change when using a different geometry suggests that the atmosphere is determining the pace of the melt, but this could be via the coupling of various elements in the climate system, namely the ocean, sea ice and ice shelves. Furthermore, in reality this does not have to be the case, since the model does not have a two-way coupling between ocean and atmosphere. Feedbacks with the atmosphere are thus not represented, which may inhibit the resonance that occurs in reality, so that a fully coupled model is needed to study all feedbacks. This and other limitations will be discussed in the following section.

7.2 Limitations and Further Research

This study identifies several limitations and open questions, which call for further research.

New insights could be gained from using different models. We find that intra-ensemble spread makes inferring conclusions from individual model runs difficult. We should also be wary of a potential spread between models: individual modelling choices can have large consequences. For example, the introduction of grounded ice bergs near Bear Ridge by Bett et al. (2020) likely influenced where the outflow of the eastern Amundsen Sea reaches the shelf break, thereby affecting the sensitivity to feedbacks. Replicating results with other models is thus important. For this, it might be problematic that most studies use similar models, often MITgcm (Assmann et al., 2013; Kimura et al., 2017; Bett et al., 2020; Naughten et al., 2022; Silvano et al., submitted) or Nucleus for European Modelling of the Ocean (NEMO) 3.6 (Jourdain et al., 2017; Planchat et al., submitted).

Our simulations suggest an important role for internal feedbacks, which calls for two main directions of further modelling research: the effect of specific drivers could be isolated and the processes involved in the feedbacks could be made more realistic.

First, there is a need for ice-ocean simulations with simple idealised forcing to isolate its effects on the Amundsen Sea. The present analysis based on correlations can not properly separate forcing from feedback and point to the actual driver. The relative timing of processes is crucial, but difficult to determine due to the substantial spread in lags (see Appendix A). An example of an idealised model run could be a simulation in which only a simple zonal wind anomaly is applied. However, the model itself should still be complex enough to incorporate necessary feedbacks.

Second, the representation of processes involved in feedbacks can be improved, for example related to sea ice and basal melt. The behaviour of sea ice could be improved by allowing ocean-atmosphere interaction. This has strong effects near the coast when sea ice is present (Jourdain et al., 2011). There are spatial differences in how sea ice responds to changes in ice shelf basal melt (Jourdain et al., 2017), which would likely affect the local atmosphere. Decadal variability might thus be more sensitive to changes in ice shelf geometry when using a coupled model.
The parametrization of basal melt could also affect the results, since most conclusions in this study were derived based on correlations with ice shelf basal mass loss. Although it seems that decadal melt variability is mainly governed by larger scale ocean variations, better incorporation of melt rates and cavity circulation could improve the results. For example, it appears that MITgcm might be underestimating melt rates near the grounding line (Lambert et al., submitted). In the runs with an advanced GL, melt decreases near the GL. This is likely related to the digging of the bathymetry to ensure a numerical connection, but could be

amplified by unrealistic melt patterns. Improvements could be made by downscaling the melt (Lambert et al., submitted).
Aside from new modelling studies, these internal feedbacks also require observational validation. Ideas regarding baroclinic variability and feedbacks are mainly based on model results. The presence of a baroclinic structure (Walker et al., 2013) and the existence of a fresher western shelf (Wåhlin et al., 2012) have already been observed, but data on temporal evolution is needed. Since undercurrent behaviour is dependent on the time scale (Silvano et al., submitted), a long term record is needed. Furthermore, the Fresh Water Boundary Index as suggested by Planchat et al. (submitted) looks promising, but its effectiveness is dependent on improvements of satellite altimetry.

Having discussed internal feedbacks, we now turn to larger scale forcing. In future studies additional interaction of the Amundsen Sea with surrounding seas and oceans could be interesting. Now, the influence of remote forcing on the model is limited because the boundary conditions only permit forcing through the atmosphere. However, ENSO also affects SSTs in the neighbouring southern Pacific (Deser et al., 2010), making an effect on the Amundsen Sea via the ocean not unlikely. For example, remote off-shelf temperature anomalies can find their way onto the Amundsen continental shelf (Nakayama et al., 2018). Furthermore, a role of baroclinicity makes ice shelves more sensitive to conditions on other Antarctic continental shelves than if wind stress was forcing a barotropic system. Amundsen shelf water characteristics can for example be influenced by the transport of meltwater from the Bellinghausen Sea via the coastal current (Schubert et al., 2021). To address these issues, ocean variables could be downscaled from PACE and applied at the model boundaries. However, this would still leave out two-way interactions between the Amundsen Sea and the surrounding oceans: for example, although the Bellinghausen Sea can influence the Amundsen Sea, there might also be an influence in the other direction (Drijfhout et al., submitted). Two-way effects can only be properly addressed using a circum-Antarctic domain.

Finally, the representation of historical melt events can be improved. For example, the case study for the 1940s is dependent on how well PACE captures the relevant dynamics in the Pacific, which is questionable. Earlier work by Thomas et al. (2015) and Ding et al. (2011) already suggested that the West-Antarctic climate is mainly affected by changes in the western Pacific. This present study adds that that this is perhaps even more true for ice shelf basal melt. Since PACE is created by fixing the historical SST anomalies in the eastern to central part of the Pacific (Schneider & Deser, 2018), it potentially leaves out relevant SSTs in the western Pacific. Potentially, this could affect the number of members that show a strong 1940s event. To improve this, repeating some of the simulations with the CESM2 pacemaker ensemble from NCAR CVCWG (Jeong et al., 2022a,b) could be interesting. In this ensemble the area of fixed Pacific SSTs in PACE is extended towards the west. However, the CESM2 pacemaker ensemble still does not contain most of the areas around the Maritime Continent, which are also correlated with basal mass loss.

7.3 Implications for the Evolution of the Amundsen Sea

The findings presented in this report have implications for the projected changes of the Amundsen Sea in the future. It seems difficult to use changes in the large scale circulation, such as the likely strengthening of zonal winds (Goyal et al., 2021), as proxies for ice shelf melt. To start, not all relevant wind trends are clear and some might not rise above internal variability (Hosking et al., 2016; Holland et al., submitted). An additional problem is that decadal variability is related to small scale circulation in our simulations, which may not be resolved in global climate models. In particular, resolving internal feedbacks is necessary, since the system could show different behaviour in the future. For example, there is a nonlinear relationship between ocean temperatures and ice shelf melt (Jenkins et al., 2018). The same temperature anomaly in a warmer ocean might lead to more ice shelf melt than at present, potentially shifting changing feedbacks related to meltwater. Furthermore, the system is likely sensitive to ice shelf retreat, which would not only affect the freshwater balance, but also the available area for sea ice formation and potentially wind patterns. There is thus a need for coupled ice-ocean models to study the sensitivity of ice shelves to anomalies in ocean temperature, both for the past, as well as for the future.

All in all, the results in this report suggest that future conditions in the Amundsen Sea depend on more variables than just the wind alone. Together with the large internal variability between the members, it is difficult to estimate when potential tipping points for ice sheet instability are surpassed. The future evolution of the Amundsen Sea sector thus remains uncertain, but also that of other regions considering the role of the Amundsen Sea in affecting CDW conditions on other Antarctic continental shelves (Drijfhout et al., submitted).

8 Conclusion

The rapid mass loss of ice sheets in the Amundsen Sea region plays a major part in the contribution of Antarctica to global sea level rise. Since ocean warming is an important driver, accurate projections for the future depend on a thorough understanding of ocean variability and associated forcing.

The presented ice-ocean simulations show that decadal variability of ice shelf basal mass loss is mainly determined by the advection of warm waters through seabed trough towards the ice shelves, but that this is only weakly related to shelf break zonal winds. Rather, it is driven by a complicated mix of wind, sea ice and internal ocean dynamics. The substantial differences between individual simulations illustrate the importance of using an ensemble of model runs together with long time intervals when modelling this system.

The model shows that tropical variability in the Pacific does have a slight but significant effect on the ice shelf melt. However, it is heavily modulated by regional climate variability such as the Amundsen Sea Low, but also by local conditions. Internal feedbacks related to baroclinicity at the shelf break appear to play an important role in the model, as do polynyas near the coast. The results show that only when multiple factors work together a strong response to remote forcing is realised, such as is hypothesized for the 1940s.

More research into this topic is needed. As of now, a baroclinic feedback is still in need of validation by observations. The importance of sea ice processes and salinity would likely benefit from more interactive models, such as coupled ice-ocean or atmosphere-ocean models. A further limitation of the present study is that the internal feedbacks make it difficult to isolate the impacts of a specific forcing. A natural next step would therefore be to use new model runs with a simplified forcing to better characterise the associated impact.

These results imply increased difficulty in inferring the impacts of climate change on ice shelf basal melt. Large scale atmospheric forcing appears to be insufficient as a proxy for ice shelf basal melt. Furthermore, processes affecting decadal melt variability can have an individual response to climate change, changing feedbacks and making the behaviour of the system as a whole less predictable. Low resolution output of global climate models thus needs to be downscaled to regional ice-ocean models when studying the impacts of climate change on the Amundsen Sea. As of now, the strong decadal variability, combined with the potentially sensitivity of glaciers to tipping points, makes it likely that the uncertainty clouding the contribution of the Amundsen Sea region to sea level rise will remain.

References

Assmann, K., Jenkins, A., Shoosmith, D., Walker, D., Jacobs, S., & Nicholls, K. (2013). Variability of Circumpolar Deep Water transport onto the Amundsen Sea continental shelf through a shelf break trough. *Journal of Geophysical Research: Oceans*, *118*(12), 6603–6620.

Bett, D. T., Holland, P. R., Naveira Garabato, A. C., Jenkins, A., Dutrieux, P., Kimura, S., & Fleming, A. (2020). The impact of the Amundsen Sea freshwater balance on ocean melting of the West Antarctic Ice Sheet. *Journal of Geophysical Research: Oceans*, *125*(9), e2020JC016305.

Brönnimann, S., Luterbacher, J., Staehelin, J., Svendby, T., Hansen, G., & Svenøe, T. (2004). Extreme climate of the global troposphere and stratosphere in 1940–42 related to El Niño. *Nature*, *431*(7011), 971–974.

Bulthuis, K., Arnst, M., Sun, S., & Pattyn, F. (2019). Uncertainty quantification of the multi-centennial response of the Antarctic ice sheet to climate change. *The Cryosphere*, *13*(4), 1349–1380.

Copernicus Climate Change Service. (2017). ERA5: Fifth generation of ECMWF atmospheric reanalyses of the global climate.
(Retrieved from `https://cds.climate.copernicus.eu/cdsapp`)

De Rydt, J., & Gudmundsson, G. H. (2016). Coupled ice shelf-ocean modeling and complex grounding line retreat from a seabed ridge. *Journal of Geophysical Research: Earth Surface*, *121*(5), 865–880.

Deser, C., Alexander, M. A., Xie, S.-P., Phillips, A. S., et al. (2010). Sea surface temperature variability: Patterns and mechanisms. *Annu. Rev. Mar. Sci*, *2*(1), 115–143.

Ding, Q., Steig, E. J., Battisti, D. S., & Küttel, M. (2011). Winter warming in West Antarctica caused by central tropical Pacific warming. *Nature Geoscience*, *4*(6), 398–403.

Dotto, T. S., Naveira Garabato, A. C., Wåhlin, A. K., Bacon, S., Holland, P. R., Kimura, S., ... Jenkins, A. (2020). Control of the oceanic heat content of the Getz-Dotson Trough, Antarctica, by the Amundsen Sea Low. *Journal of Geophysical Research: Oceans*, *125*(8), e2020JC016113.

Drijfhout, A. C., Sybren S. Naveira Garabato, Holland, P. R., Bull, C. Y., Jenkins, A., Hewitt, H., & Mathiot, P. (submitted). An Amundsen Sea source of decadal temperature changes on the Antarctic continental shelf.

Dutrieux, P., De Rydt, J., Jenkins, A., Holland, P. R., Ha, H. K., Lee, S. H., ... Schröder, M. (2014). Strong sensitivity of Pine Island ice-shelf melting to climatic variability. *Science*, *343*(6167), 174–178.

Flexas, M. M., Thompson, A. F., Schodlok, M. P., Zhang, H., & Speer, K. (2022). Antarctic Peninsula warming triggers enhanced basal melt rates throughout West Antarctica. *Science Advances*, *8*(31), eabj9134.

Fogt, R. L., & Marshall, G. J. (2020). The Southern Annular Mode: variability, trends, and climate impacts across the Southern Hemisphere. *Wiley Interdisciplinary Reviews: Climate Change*, *11*(4), e652.

Fretwell, P., Pritchard, H. D., Vaughan, D. G., Bamber, J. L., Barrand, N. E., Bell, R., ... others (2013). Bedmap2: improved ice bed, surface and thickness datasets for Antarctica. *The Cryosphere*, *7*(1), 375–393.

Gill, A. (1982). Atmospheric-ocean dynamics. *Int. Geophys. Ser.*, *30*, 662.

Gong, D., & Wang, S. (1999). Definition of Antarctic oscillation index. *Geophysical research letters*, *26*(4), 459–462.

Goyal, R., Sen Gupta, A., Jucker, M., & England, M. H. (2021). Historical and projected changes in the Southern Hemisphere surface westerlies. *Geophysical Research Letters*, *48*(4), e2020GL090849.

Gudmundsson, G., Krug, J., Durand, G., Favier, L., & Gagliardini, O. (2012). The stability of grounding lines on retrograde slopes. *The Cryosphere*, *6*(6), 1497–1505.

Harrison, D., & Larkin, N. K. (1996). The COADS sea level pressure signal: A near-global El Niño composite and time series view, 1946–1993. *Journal of Climate*, *9*(12), 3025–3055.

Hellmer, H. H., & Olbers, D. J. (1989). A two-dimensional model for the thermohaline circulation under an ice shelf. *Antarctic Science*, *1*(4), 325–336.

Henley, B. J., Gergis, J., Karoly, D. J., Power, S., Kennedy, J., & Folland, C. K. (2015). A tripole index for the interdecadal Pacific oscillation. *Climate Dynamics*, *45*(11), 3077–3090.

Holland, P. R., Bracegirdle, T. J., Dutrieux, P., Jenkins, A., & Steig, E. J. (2019). West Antarctic ice loss influenced by internal climate variability and anthropogenic forcing. *Nature Geoscience*, *12*(9), 718–724.

Holland, P. R., O'Connor, G. K., Bracegirdle, T. J., Dutrieux, P., Naughten, K. A., Steig, E. J., ... Smith, J. A. (submitted). Anthropogenic and internal drivers of wind changes over the Amundsen Sea, West Antarctica, during the 20th and 21st centuries.

Hosking, J. S., Orr, A., Bracegirdle, T. J., & Turner, J. (2016). Future circulation changes off West Antarctica: Sensitivity of the Amundsen Sea Low to projected anthropogenic forcing. *Geophysical Research Letters*, *43*(1), 367–376.

Jacobs, S. S., Hellmer, H. H., & Jenkins, A. (1996). Antarctic ice sheet melting in the Southeast Pacific. *Geophysical Research Letters*, *23*(9), 957–960.

Jacobs, S. S., Jenkins, A., Giulivi, C. F., & Dutrieux, P. (2011). Stronger ocean circulation and increased melting under Pine Island Glacier ice shelf. *Nature Geoscience*, *4*(8), 519–523.

Jenkins, A., Dutrieux, P., Jacobs, S., Steig, E. J., Gudmundsson, G. H., Smith, J., & Heywood, K. J. (2016). Decadal ocean forcing and Antarctic ice sheet response: Lessons from the Amundsen Sea. *Oceanography*, *29*(4), 106–117.

Jenkins, A., Dutrieux, P., Jacobs, S. S., McPhail, S. D., Perrett, J. R., Webb, A. T., & White, D. (2010). Observations beneath Pine Island Glacier in West Antarctica and implications for its retreat. *Nature Geoscience*, *3*(7), 468–472.

Jenkins, A., Hellmer, H. H., & Holland, D. M. (2001). The role of meltwater advection in the formulation of conservative boundary conditions at an ice–ocean interface. *Journal of Physical Oceanography*, *31*(1), 285–296.

Jenkins, A., Shoosmith, D., Dutrieux, P., Jacobs, S., Kim, T. W., Lee, S. H., ... Stammerjohn, S. (2018). West Antarctic Ice Sheet retreat in the Amundsen Sea driven by decadal oceanic variability. *Nature Geoscience*, *11*(10), 733–738.

Jeong, H., Park, H.-S., Stuecker, M. F., & Yeh, S.-W. (2022a). Distinct impacts of major El Niño events on Arctic temperatures due to differences in eastern tropical Pacific sea surface temperatures. *Science Advances*, *8*(4), eabl8278.

Jeong, H., Park, H.-S., Stuecker, M. F., & Yeh, S.-W. (2022b). Record low Arctic sea ice extent in 2012 linked to two-year La Niña-driven sea surface temperature pattern. *Geophysical Research Letters*, e2022GL098385.

Joughin, I., Rignot, E., Rosanova, C. E., Lucchitta, B. K., & Bohlander, J. (2003). Timing of recent accelerations of Pine Island glacier, Antarctica. *Geophysical Research Letters*, *30*(13).

Jourdain, N. C., Mathiot, P., Gallée, H., & Barnier, B. (2011). Influence of coupling on atmosphere, sea ice and ocean regional models in the Ross Sea sector, Antarctica. *Climate Dynamics*, *36*(7), 1523–1543.

Jourdain, N. C., Mathiot, P., Merino, N., Durand, G., Le Sommer, J., Spence, P., ... Madec, G. (2017). Ocean circulation and sea-ice thinning induced by melting ice shelves in the Amundsen Sea. *Journal of Geophysical Research: Oceans*, *122*(3), 2550–2573.

Kao, H.-Y., & Yu, J.-Y. (2009). Contrasting eastern-Pacific and central-Pacific types of ENSO. *Journal of Climate*, *22*(3), 615–632.

Kimura, S., Jenkins, A., Regan, H., Holland, P. R., Assmann, K. M., Whitt, D. B., ... Dutrieux, P. (2017). Oceanographic controls on the variability of ice-shelf basal melting and circulation of glacial meltwater in the Amundsen Sea Embayment, Antarctica. *Journal of Geophysical Research: Oceans*, *122*(12), 10131–10155.

Lambert, E., Jueling, A., van de Wal, R. S., & Holland, P. R. (submitted). Modeling sub-kilometer resolution Antarctic ice shelf basal melt rates using LADDIE.

Li, X., Holland, D. M., Gerber, E. P., & Yoo, C. (2015). Rossby waves mediate impacts of tropical oceans on West Antarctic atmospheric circulation in austral winter. *Journal of Climate*, *28*(20), 8151–8164.

Locarnini, M., Mishonov, A., Baranova, O., Boyer, T., Zweng, M., Garcia, H., ... others (2018). *World Ocean Atlas 2018, Volume 1: Temperature* (Tech. Rep.). Retrieved from `https://archimer.ifremer.fr/doc/00651/76338/`

Losch, M. (2008). Modeling ice shelf cavities in az coordinate ocean general circulation model. *Journal of Geophysical Research: Oceans*, *113*(C8).

Losch, M., Menemenlis, D., Campin, J.-M., Heimbach, P., & Hill, C. (2010). On the formulation of sea-ice models. Part 1: Effects of different solver implementations and parameterizations. *Ocean Modelling*, *33*(1-2), 129–144.

Marshall, J., Adcroft, A., Hill, C., Perelman, L., & Heisey, C. (1997). A finite-volume, incompressible Navier Stokes model for studies of the ocean on parallel computers. *Journal of Geophysical Research: Oceans*, *102*(C3), 5753–5766.

McDougall, T. J., Jackett, D. R., Wright, D. G., & Feistel, R. (2003). Accurate and computationally efficient algorithms for potential temperature and density of seawater. *Journal of Atmospheric and Oceanic Technology*, *20*(5), 730–741.

Morlighem, M. (2020). *MEaSUREs BedMachine Antarctica, Version 2, NASA National Snow and Ice Data Center Distributed Active Archive Center, Boulder, Colorado USA [data set].*

Morlighem, M., Rignot, E., Binder, T., Blankenship, D., Drews, R., Eagles, G., ... others (2020). Deep glacial troughs and stabilizing ridges unveiled beneath the margins of the Antarctic ice sheet. *Nature Geoscience*, *13*(2), 132–137.

Nakayama, Y., Menemenlis, D., Zhang, H., Schodlok, M., & Rignot, E. (2018). Origin of Circumpolar Deep Water intruding onto the Amundsen and Bellingshausen Sea continental shelves. *Nature Communications*, *9*(1), 1–9.

National Centers for Environmental Information. (n.d.). *Southern Oscillation Index.* Retrieved 2022-11-07, from `https://www.ncei.noaa.gov/access/monitoring/enso/soi#calculation-of-soi`

Naughten, K. A., Holland, P. R., Dutrieux, P., Kimura, S., Bett, D. T., & Jenkins, A. (2022). Simulated Twentieth-Century Ocean Warming in the Amundsen Sea, West Antarctica. *Geophysical Research Letters*, *49*(5), e2021GL094566.

O'Connor, G. K., Steig, E. J., & Hakim, G. J. (2021). Strengthening Southern Hemisphere Westerlies and Amundsen Sea Low Deepening Over the 20th Century Revealed by Proxy-Data Assimilation. *Geophysical Research Letters*, *48*(24), e2021GL095999.

Physical Sciences Laboratory. (n.d.). *20CR Climate Indices: Southern Annular Mode (SAM).* Retrieved 2022-11-07, from `https://psl.noaa.gov/data/20thC_Rean/timeseries/monthly/SAM/`

Planchat, A., Jourdain, N. C., & Dutrieux, P. (submitted). Spatio-temporal variability of ocean currents at the Amundsen Sea shelf break and their link to CDW inflow and ice-shelf melt.

Pritchard, H., Ligtenberg, S. R., Fricker, H. A., Vaughan, D. G., van den Broeke, M. R., & Padman, L. (2012). Antarctic ice-sheet loss driven by basal melting of ice shelves. *Nature*, *484*(7395), 502–505.

Raphael, M. N. (2007). The influence of atmospheric zonal wave three on Antarctic sea ice variability. *Journal of Geophysical Research: Atmospheres*, *112*(D12).

Rignot, E., Mouginot, J., Morlighem, M., Seroussi, H., & Scheuchl, B. (2014). Widespread, rapid grounding line retreat of Pine Island, Thwaites, Smith, and Kohler glaciers, West Antarctica, from 1992 to 2011. *Geophysical Research Letters*, *41*(10), 3502–3509.

Rignot, E., Mouginot, J., Scheuchl, B., Van Den Broeke, M., Van Wessem, M. J., & Morlighem, M. (2019). Four decades of Antarctic Ice Sheet mass balance from 1979–2017. *Proceedings of the National Academy of Sciences*, *116*(4), 1095–1103.

Schneider, D. P., & Deser, C. (2018). Tropically driven and externally forced patterns of Antarctic sea ice change: Reconciling observed and modeled trends. *Climate Dynamics*, *50*(11), 4599–4618.

Schneider, D. P., & Steig, E. J. (2008). Ice cores record significant 1940s Antarctic warmth related to tropical climate variability. *Proceedings of the National Academy of Sciences*, *105*(34), 12154–12158.

Schubert, R., Thompson, A. F., Speer, K., Schulze Chretien, L., & Bebieva, Y. (2021). The Antarctic coastal current in the Bellingshausen Sea. *The Cryosphere*, *15*(9), 4179–4199.

Seroussi, H., Nowicki, S., Payne, A. J., Goelzer, H., Lipscomb, W. H., Abe-Ouchi, A., ... others (2020). ISMIP6 Antarctica: a multi-model ensemble of the Antarctic ice sheet evolution over the 21st century. *The Cryosphere*, *14*(9), 3033–3070.

Shepherd, A., Ivins, E., Rignot, E., Smith, B., van den Broeke, M., Velicogna, I., ... others (2018). Mass balance of the antarctic ice sheet from 1992 to 2017. *Nature*, *558*(7709), 219–+.

Shepherd, A., Wingham, D., & Rignot, E. (2004). Warm ocean is eroding West Antarctic ice sheet. *Geophysical Research Letters*, *31*(23).

Silvano, A., Holland, P. R., Naughten, K. A., Dragomir, O., Dutrieux, P., Jenkins, A., ... Naveira Garabato, A. C. (submitted). Baroclinic ocean response to climate forcing regulates decadal variability of ice-shelf melting in the Amundsen Sea.

Smith, J. A., Andersen, T., Shortt, M., Gaffney, A., Truffer, M., Stanton, T. P., ... others (2017). Sub-ice-shelf sediments record history of twentieth-century retreat of Pine Island Glacier. *Nature*, *541*(7635), 77–80.

Steig, E. J., Ding, Q., Battisti, D., & Jenkins, A. (2012). Tropical forcing of Circumpolar Deep Water inflow and outlet glacier thinning in the Amundsen Sea Embayment, West Antarctica. *Annals of Glaciology*, *53*(60), 19–28.

St-Laurent, P., Klinck, J., & Dinniman, M. (2015). Impact of local winter cooling on the melt of Pine Island Glacier, Antarctica. *Journal of Geophysical Research: Oceans*, *120*(10), 6718–6732.

Thoma, M., Jenkins, A., Holland, D., & Jacobs, S. (2008). Modelling circumpolar deep water intrusions on the Amundsen Sea continental shelf, Antarctica. *Geophysical Research Letters*, *35*(18).

Thomas, E. R., Hosking, J. S., Tuckwell, R. R., Warren, R., & Ludlow, E. (2015). Twentieth century increase in snowfall in coastal West Antarctica. *Geophysical Research Letters*, *42*(21), 9387–9393.

Turner, J., Phillips, T., Hosking, J. S., Marshall, G. J., & Orr, A. (2013). The Amundsen Sea low. *International Journal of Climatology*, *33*(7), 1818–1829.

Verdy, A., & Mazloff, M. R. (2017). A data assimilating model for estimating Southern Ocean biogeochemistry. *Journal of Geophysical Research: Oceans*, *122*(9), 6968–6988.

Wåhlin, A., Kalén, O., Arneborg, L., Björk, G., Carvajal, G., Ha, H. K., ... Stranne, C. (2013). Variability of warm deep water inflow in a submarine trough on the Amundsen Sea shelf. *Journal of Physical Oceanography*, *43*(10), 2054–2070.

Wåhlin, A., Muench, R., Arneborg, L., Björk, G., Ha, H., Lee, S., & Alsén, H. (2012). Some implications of Ekman layer dynamics for cross-shelf exchange in the Amundsen Sea. *Journal of Physical Oceanography*, *42*(9), 1461–1474.

Walker, D. P., Brandon, M. A., Jenkins, A., Allen, J. T., Dowdeswell, J. A., & Evans, J. (2007). Oceanic heat transport onto the Amundsen Sea shelf through a submarine glacial trough. *Geophysical Research Letters*, *34*(2).

Walker, D. P., Jenkins, A., Assmann, K. M., Shoosmith, D. R., & Brandon, M. A. (2013). Oceanographic observations at the shelf break of the Amundsen Sea, Antarctica. *Journal of Geophysical Research: Oceans*, *118*(6), 2906–2918.

Webber, B. G., Heywood, K. J., Stevens, D. P., & Assmann, K. M. (2019). The impact of overturning and horizontal circulation in Pine Island Trough on ice shelf melt in the eastern Amundsen Sea. *Journal of Physical Oceanography*, *49*(1), 63–83.

Webber, B. G., Heywood, K. J., Stevens, D. P., Dutrieux, P., Abrahamsen, E. P., Jenkins, A., ... Kim, T. W. (2017). Mechanisms driving variability in the ocean forcing of Pine Island Glacier. *Nature Communications*, *8*(1), 1–8.

Zweng, M., Seidov, D., Boyer, T., Locarnini, M., Garcia, H., Mishonov, A., ... others (2019). *World Ocean Atlas 2018, Volume 2: Salinity* (Tech. Rep.). Retrieved from `https://archimer.ifremer.fr/doc/00651/76339/`

A Extra Figures

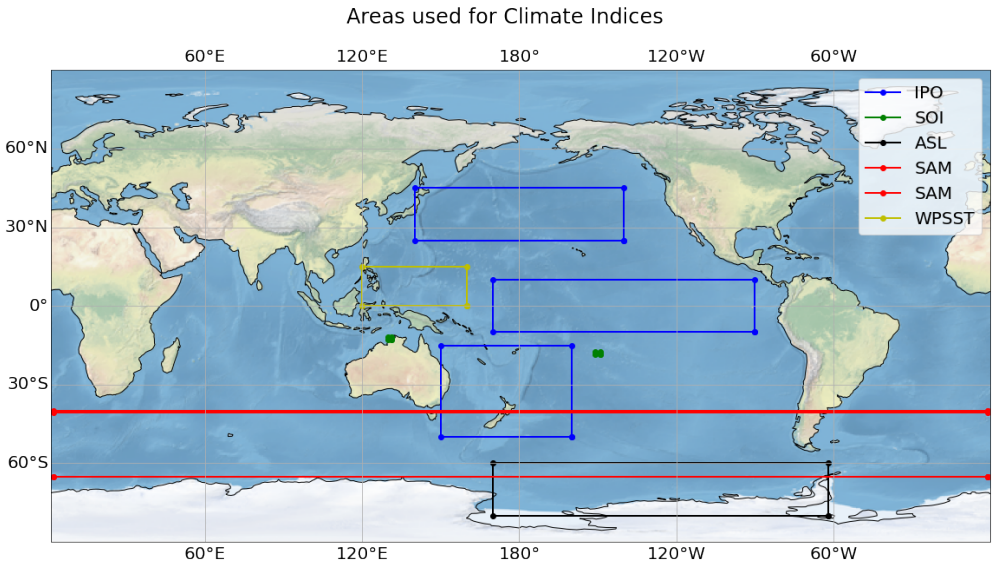

Figure 27: The areas used to compute the climate indices. IPO=Interdecadal Pacific Oscillation; SOI=Souther Oscillation Index; ASL=Amundsen Sea Low; SAM=Southern Annular Mode; WPSST=West Pacific Sea Surface Temperature index.

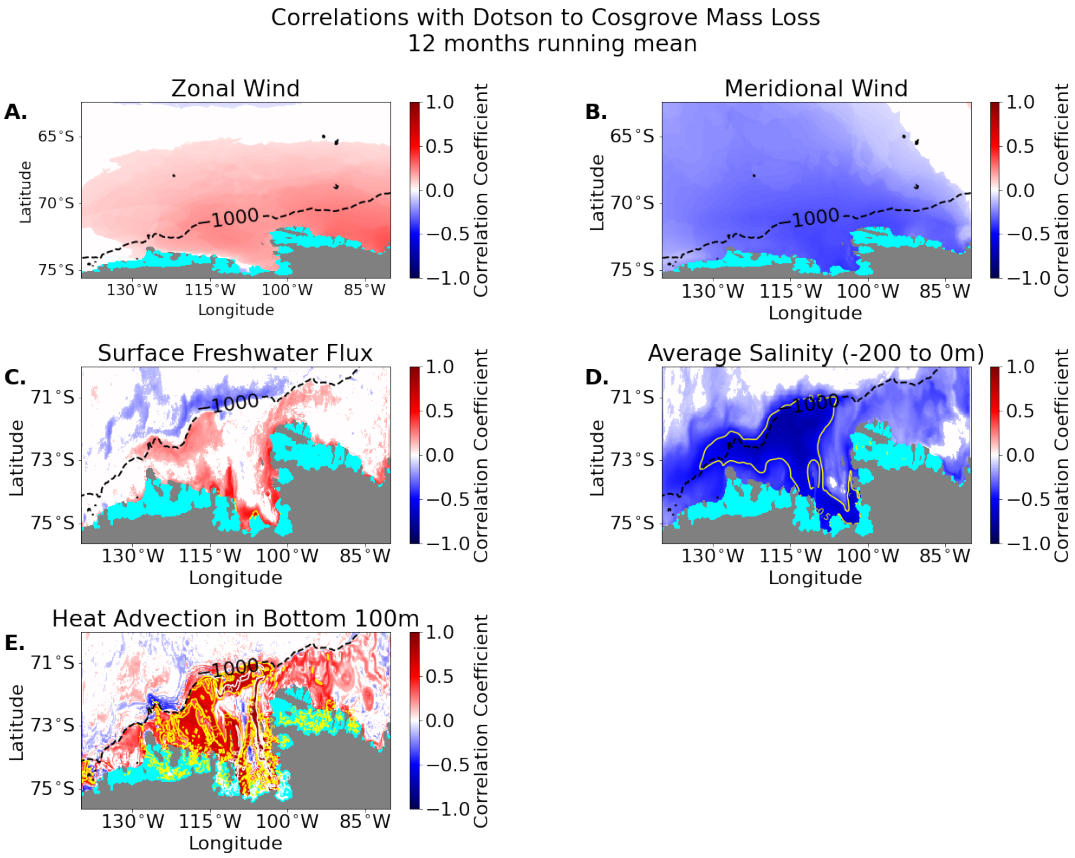

Figure 28: Each subplot as for Figure 5A, but with the correlation of different variables with ice shelf basal mass loss when applying a 12 month running mean. A.) Zonal wind, B.) Meridional wind, C.) Surface fresh water flux, D.) Salinity in the top 200m, E.) Horizontal heat advection in the bottom 100m.

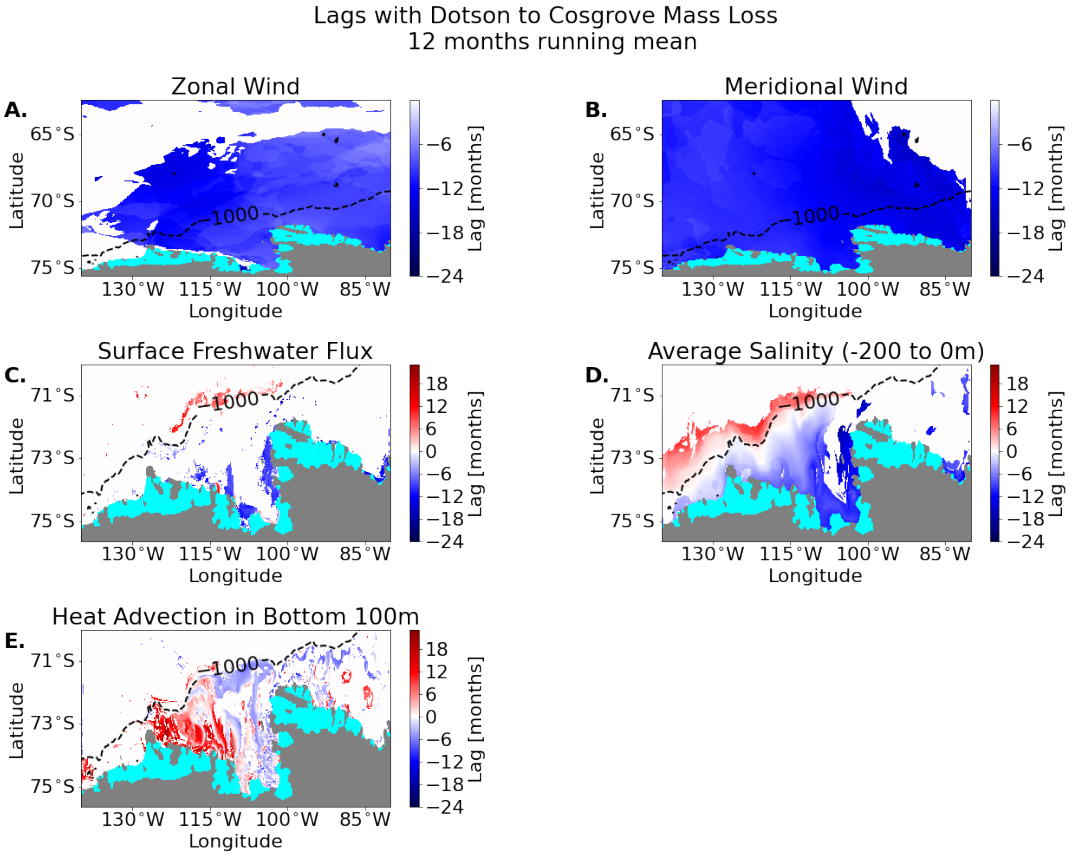

Figure 29: The lags with ice shelf basal mass loss when applying a 12 month running mean. Subplots as for Figure 28 and description following Figure 5B.

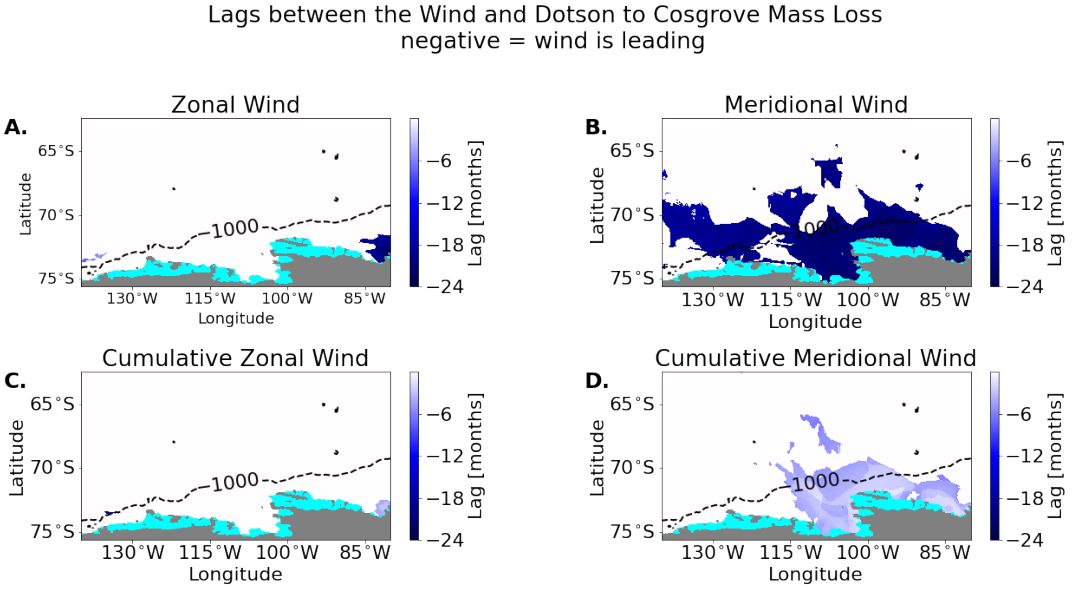

Figure 30: Lags between the winds and Dotson to Cosgrove mass loss at a 60 month runnning mean, associated with Figure 8. Subplots as in that figure, description of subplots as in Figure 5B.

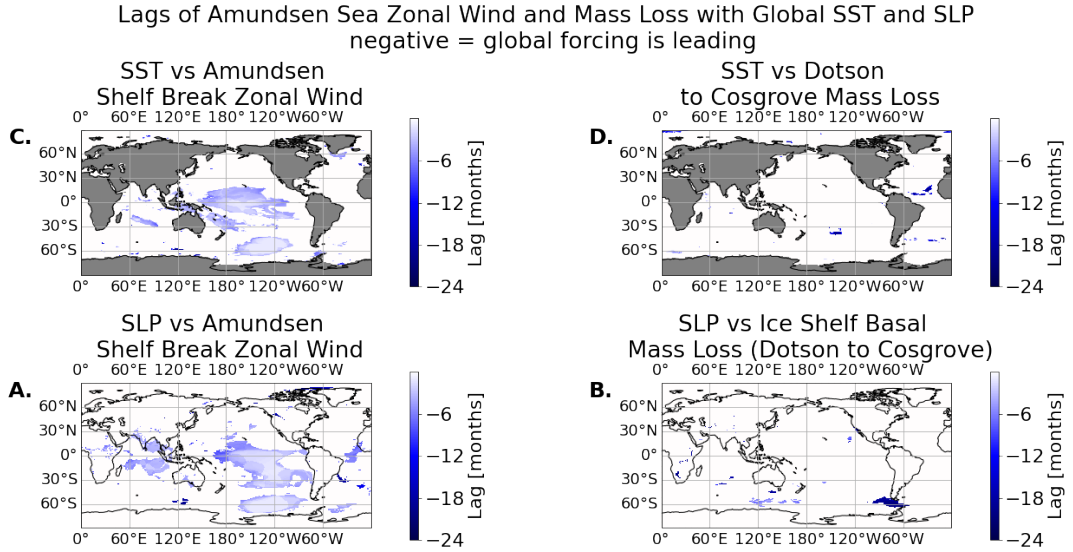

Figure 31: Lags between global and Amundsen Sea variables, corresponding to 16. Subplots as in that figure, description of subplots as in Figure 5B.

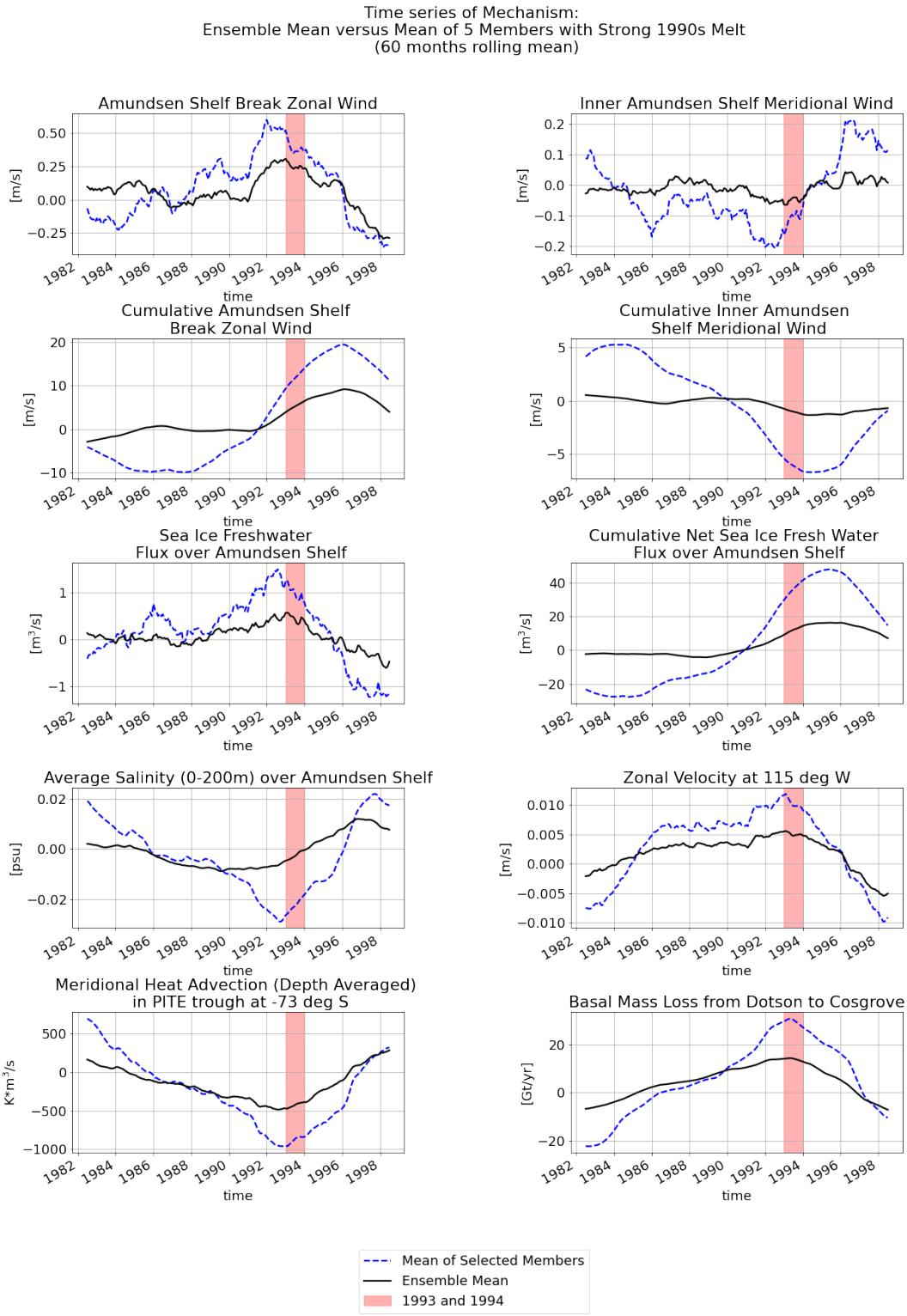

Figure 32: As for Figure 23 in Chapter 6, but for the 1990s. High melt members were selected similarly as for the 1940s, but then based on melt anomaly in 1993 and 1994, which is also the period that is highlighted.

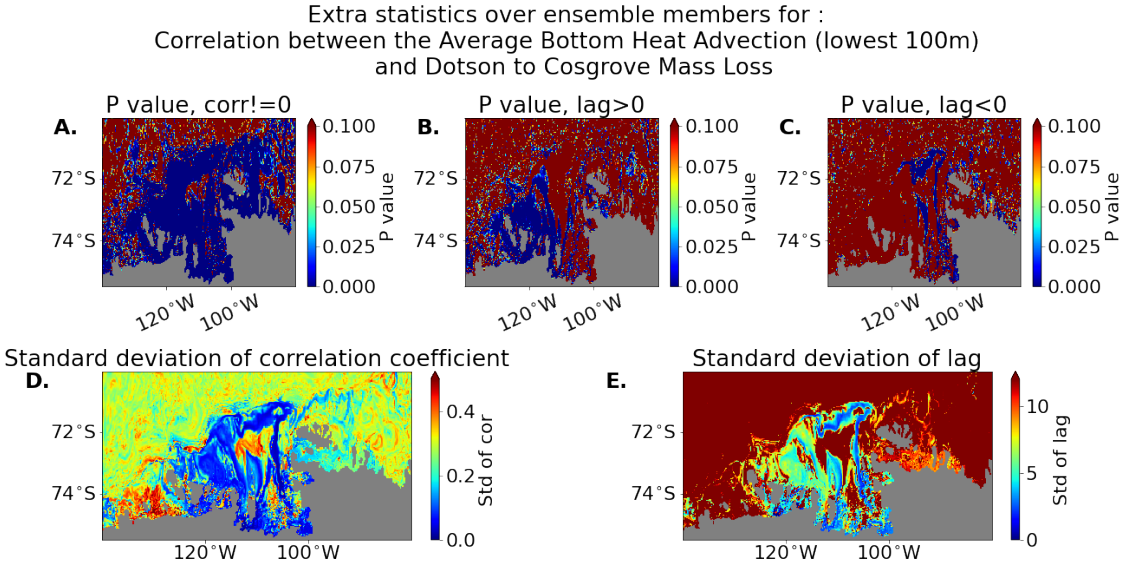

Figure 33: Extra statistics for Figure 5. A.) P value of test if correlation coefficient is different from 0. B.) P value of tests to see if lags are significantly larger than 0. C.) P value for test if the mean lag is smaller than 0. D.) Standard deviation of the correlation coefficients between the members. E.) Standard deviation of the lag.

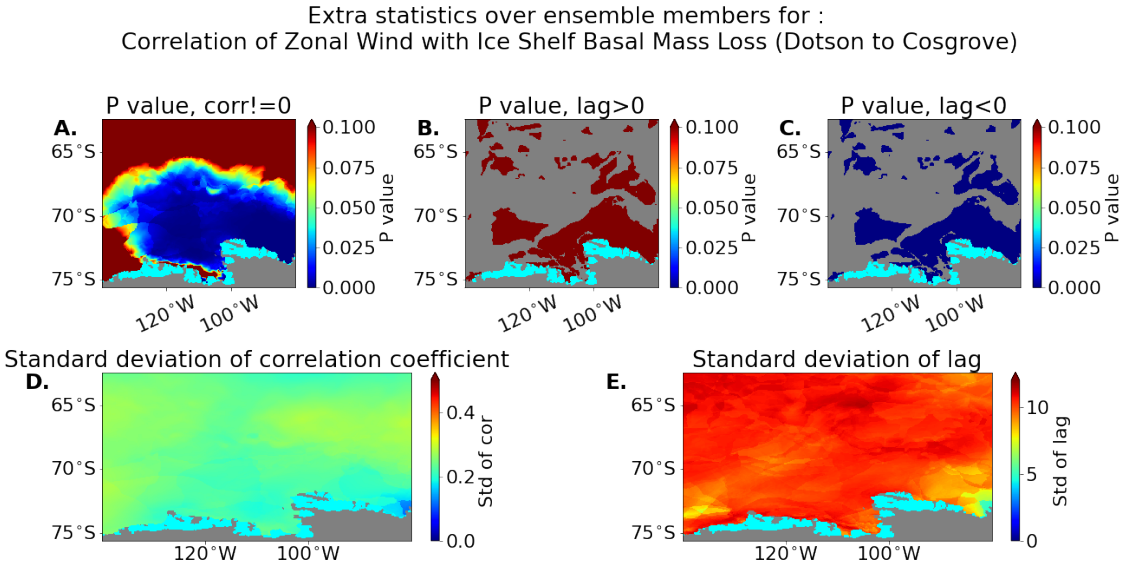

Figure 34: Extra statistics for Figure 8A. Description of plots in caption of 33. Note: p-values of lags can not be computed is the correlation is insignificant, which is the case for individual members of the winds.

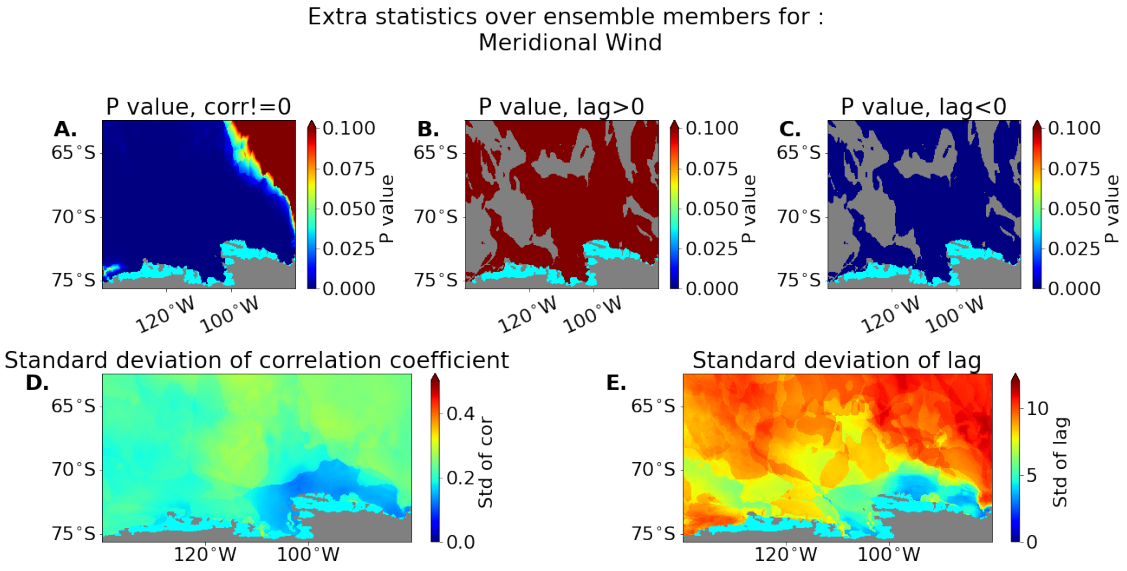

Figure 35: Extra statistics for Figure 8B. Description of plots in caption of 33. Note: p-values of lags can not be computed is the correlation is insignificant, which is the case for individual members of the winds.

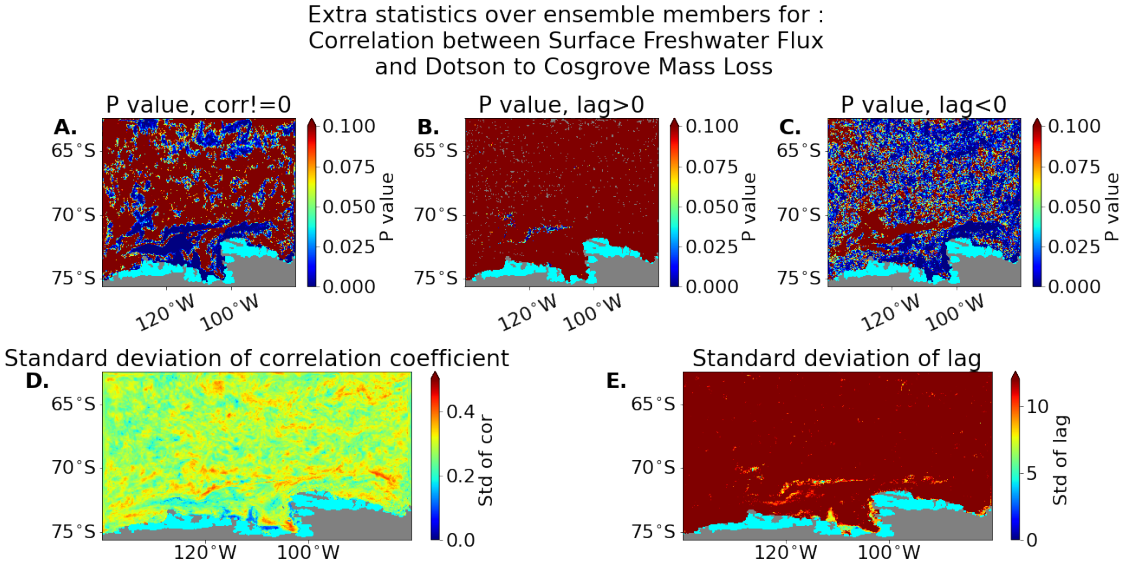

Figure 36: Extra statistics for Figure 15. Description of plots in caption of 33.

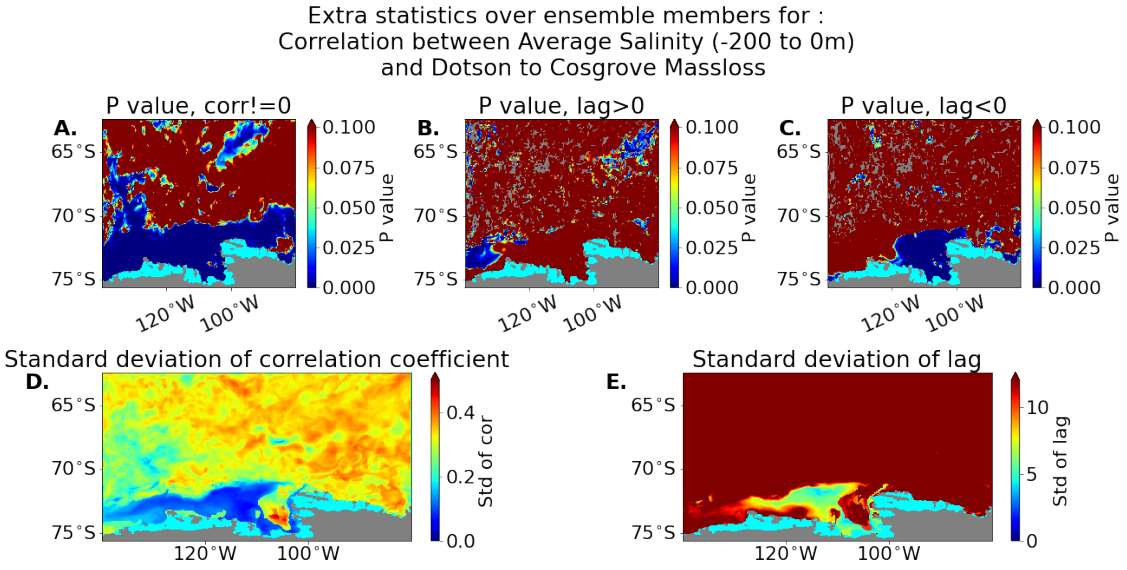

Figure 37: Extra statistics for Figure 12. Description of plots in caption of 33.

B Analysis of Convection

During the validation experiments performed by Naughten et al. (2022), it was found that the model might have a bias towards convection in the Amundsen Sea. In this section, the sensitivity of some of the results presented here to this potential bias is discussed.

Naughten et al. (2022) created three conditions to define a convective event, which were created to select for the unrealistic event that occurred in their reanalysis-forced simulation. They used three separate conditions, but in the present report a deep convection event is thought to occur when all three need are met:

1. Averaged over the Amundsen Shelf region, the 2-year running mean time series of the 0.5 C degree isotherm has to drop below 440m
2. Averaged over the Pine Island Bay region, the 0 degree C isotherm (2-year running mean) has to drop below 470m
3. In front of Dotson Ice Shelf, the -1 degree C isotherm (2-year running mean) has to drop below 430m

Using this definition, it turns out that most ensemble members show multiple convective events during the simulation (see Figure 38). However, there are a handful of members that do not show any event between 1920 and 2013.

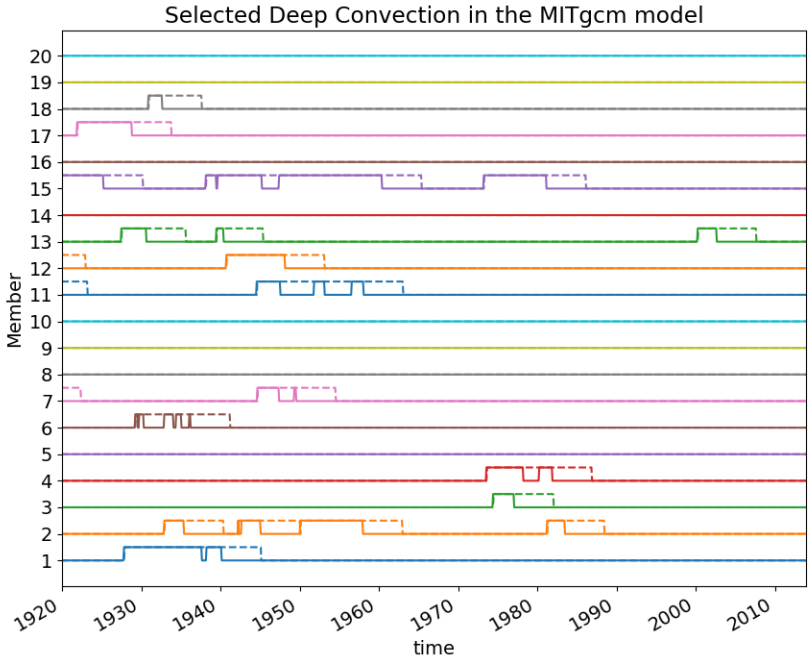

Figure 38: Deep convection events in the MITgcm model. Each line shows a member, as indicated on the y-axis. When a line is raised, this means that a convective event is detected here. The dotted line indicate the times that are removed from the correlation, which is the duration of the deep convection event plus a recovery time of 5 years.

In order to check if our results still hold without convection, the same correlation maps as in the main text are created, after removing the convective events themselves and a recovery period defined as the 5 following years, similar to Naughten et al. (2022). The times that are removed are indicated in Figure 38,

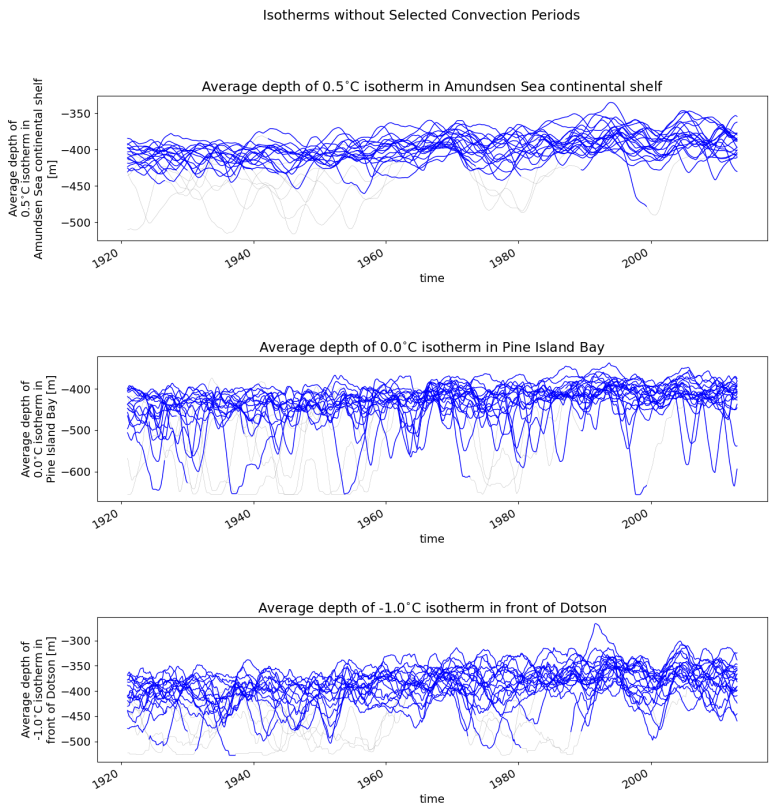

Figure 39: Isotherms, indicating which times are removed from the analysis without convection. Blue lines indicates when a line is used for the analysis, grey lines indicate when it is not. Upper panel shows 0.5 degree C isotherm averaged over the Amundsen Sea Continental Shelf; Middle panel shows the 0 degree C isotherm over Pine Island Bay; Bottom panel shows the -1 deg C isotherm in front of Dotson Bay.

whereas the behaviour of the isotherms in the selected periods are shown in Figure 39. Almost all moments that the 0.5 degree isotherm drops below 450m are removed, suggesting that no large scale convective events are used in the ensemble. It has to be noted that Dotson and especially Pine Island Bay still shows several local convective events, although their number is reduced.

The new correlation maps show a very strong resemblance to the old maps 40. Area's of high correlation largely remain the same. The same holds for the lags, as can be seen in Figure 41. For the sea ice flux, the areas that have a lags with a standard deviation smaller than 8 are reduced.

To conclude, it seems that in the results only affected in a very limited way by deep convective events. An analysis with only the members that do not show any deep convective events led to a similar conclusion (not shown).

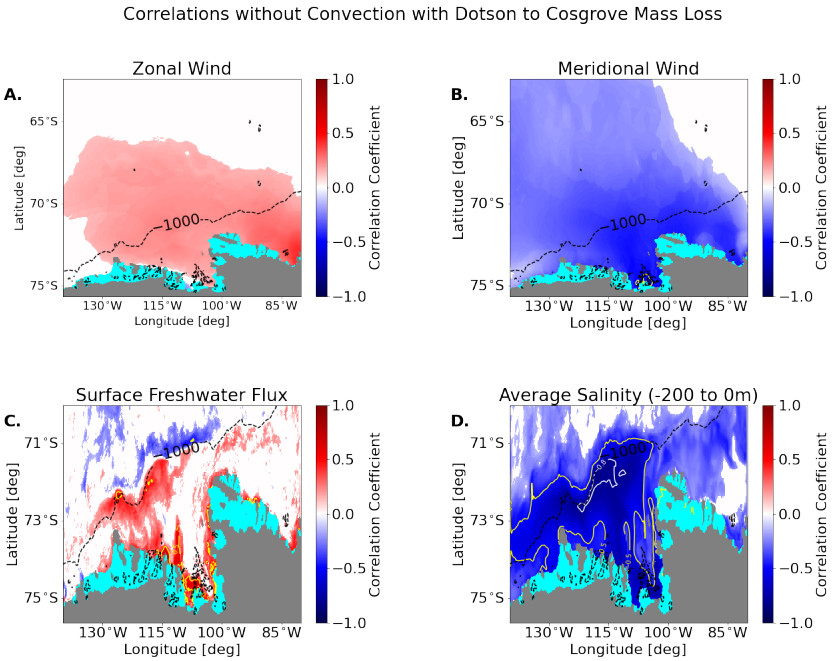

Figure 40: Correlations without convection between different variables and Dotson to Cosgrove Mass Loss. Description of each subplot as for Figure 5A. A.) Zonal wind; B.) Meridional wind; C.) Surface freshwater flux; D.) Salinity averaged over the top 200m.

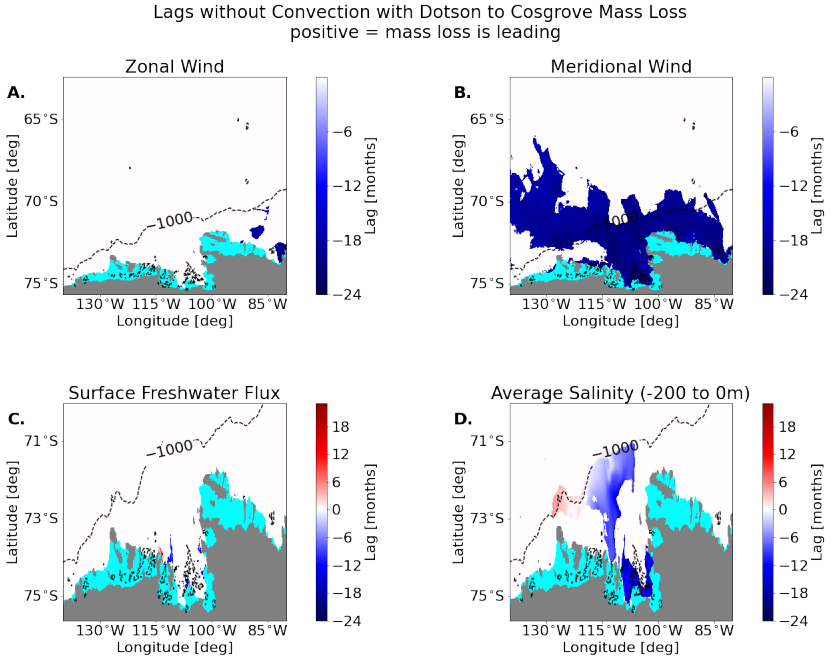

Figure 41: Lags without convection between different variables and Dotson to Cosgrove Mass Loss. Corresponding to Figure 40, with the description following Figure 5B.

C Code Access

The code used in this study will be made available in a public GitHub repository: `https://github.com/Joren1996/Amundsen_Sea_Project.git`

Furthermore, this study used code by Kaitlin Naughten. This can also be found on GitHub:

- General functions for the analysis of the MITgcm output are found here: `https://github.com/knaughten/mitgcm_python`
- An example on running the MITgcm model on Archer2 can be found here: `https://github.com/knaughten/UaMITgcm/tree/archer2/example/PAS_999`

Some of the Matlab code is based on code provided by Paul Holland (BAS), this is available on reasonable request to the author: `gjanzing@mailfence.com`.